DEVELOPMENT OF PARAMETERIZED SURGE RESPONSE FUNCTIONS FOR COASTAL BAYS

A Thesis

by

RAJAT KATYAL

Submitted to the Office of Graduate Studies of
Texas A&M University
in partial fulfillment of the requirements for the degree of

MASTER OF SCIENCE

December 2009

Major Subject: Ocean Engineering

DEVELOPMENT OF PARAMETERIZED SURGE RESPONSE FUNCTIONS FOR COASTAL BAYS

A Thesis

by

RAJAT KATYAL

Submitted to the Office of Graduate Studies of
Texas A&M University
in partial fulfillment of the requirements for the degree of

MASTER OF SCIENCE

Approved by:

Chair of Committee, Jennifer L. Irish
Committee Members, David Brooks
Scott A. Socolofsky
Head of Department, John Niedzwecki

December 2009

Major Subject: Ocean Engineering

ABSTRACT

Development of Parameterized Surge Response Functions for Coastal Bays.

(December 2009)

Rajat Katyal, B.E., Punjab Engineering College, Chandigarh, India

Chair of Advisory Committee: Dr Jennifer L. Irish

In the past few years, there has been an increase in the number of hurricanes hitting the Gulf of Mexico coastline. These hurricanes have caused damage in the billions of dollars, and hundreds of people have been killed during these events. The damage from hurricanes is caused by four main factors: storm surges, waves, strong winds and rain. At the coast, the damage due to the storm surge and waves is dominant. Numerical simulation models like ADCIRC are available for estimating storm surge, but high computational time makes it impossible to use them for evacuation planning purposes. Public perception of storm surge hazard is based upon the Saffir Simpson scale. As demonstrated by Hurricanes Katrina and Ike, the Saffir Simpson scale does not work well for surge prediction.

The accurate and timely prediction of storm surge is very important. For this purpose, dimensionless Surge Response Functions (SRFs) for the open coast of Texas has been developed (Irish et.al 2008a and Song, 2009). The surge inside bays tends to be different from that at the open coast due to local geometric factors like shape, center of gravity, and characteristic size of the bay. To predict accurately the surge levels inside the bay, scaling laws are developed based upon the above mentioned factors. These scaling laws

are used along with SRFs for the open coast (Irish et. al. 2009) to develop dimensionless SRFs for bays. The SRFs for 3 bays, Matagorda, Galveston and Corpus Christi have been explored. Results have shown that the Surge Response method works reasonably well for Matagorda, Corpus Christi and Galveston Bay. For these bays the dimensionless surge lies within the 95% confidence interval of Surge Response Functions.

ACKNOWLEDGEMENTS

I would like to thank Dr. Jennifer Irish, my advisor, for guiding me and improving my professional and technical skills throughout my studies and research at Texas A&M University. I would also like to thank my other members of committee, Dr David Brooks and Dr. Scott A. Socolofsky for reviewing my thesis and for their help in completing my master's program.

I would also like to thank my family and friends who have motivated me to attend graduate school and giving me the support to complete my master's degree.

I would also like to thank Texas General Land Office, who has provided the funds for this work to be completed.

TABLE OF CONTENTS

CHAPTER Page

LIST OF FIGURES

Page

Page

Page

Page

Page

LIST OF TABLES

Page

CHAPTER I

INTRODUCTION

According to Federal Emergency Management Agency (FEMA 2009), in the region of Atlantic Ocean, Caribbean Sea or Gulf of Mexico every year approximately ten tropical storms develop. Most of these storms dissipate over ocean and only few develop into hurricane and hit United States coastal areas. Every three years, five hurricanes have the probability of hitting the United States coastline. Two out of these five hurricanes have the probability of developing into a category 3 hurricanes as defined on the Saffir-Simpson scale. These storms cause damage in millions of dollars. Hurricanes cause damage mainly by two phenomena, first being the direct wind damage and second being the damage caused by storm surge. As hurricanes approach coast, rotating wind pushes the water at coast and generate storm surge. Storm surge is the major cause of damage at the coast and inside coastal bays.

Historically, hurricane surge had been considered to be primarily dependent upon its intensity, as represented by the Saffir-Simpson scale. But Saffir-Simpson scale fails to describe storm surge induced damage caused by hurricanes like Rita, Katrina and Ike. Thus for accurate and timely prediction of hurricane damage potential, storm surge due to various hurricane conditions should be predicted.

This thesis follows the style of *Composites of Construction.*

Various numerical models are available for predicting storm surge, but storm simulation with high resolution numerical models is highly computationally intensive with each simulation requiring of the order of 1000 hours of CPU time. Thus, use of these numerical models for planning purpose is limited. To predict hurricane surge accurately and quickly, the development of parameterized, dimensionless SRFs for Texas coastal bays (Galveston, Matagorda, and Corpus Christi) have been explored. SRFs (SRF, Irish and Resio., 2009) are parameterized dimensionless functions for defining continuous surge response surface. The SRF method for the open coast has been developed by identifying the relationship between the peak surge at station and the meteorological and geometrical parameters such as size, intensity and landfall location of storm. It has been shown that when SRFs approach is applied to open coast, error in surge prediction is 30 cm, which is comparable with the expected error in numerical simulations.

However, the relevant parameters influencing the form of SRFs inside coastal bays tends to differ from those along the open coast due to various local parameters related to bay configuration, including the center of gravity of bay, horizontal bay dimensions, relative position of the hurricane eye with respect to bay, mean water depth, and shoreline irregularities. Research results presented in this thesis show that the surge inside Matagorda, Galveston and Corpus Christi Bays can indeed be described in terms of these parameters by introducing additional physical scaling laws which account for bay geometry. Thus, these new parameters can be integrated with the open coast surge response to efficiently predict the storm surge inside the bay.

In the following sections first background and literature review for the work will be presented, then the study area will be described and finally the methodology and general form of SRFs developed for the bays will be presented along with its applications.

CHAPTER II

BACKGROUND AND LITERATURE REVIEW

2.1 Hurricanes

Hurricanes are defined as a weather system which has maximum wind speed of approximately 120 km/h or higher, is accompanied by thunderstorms and have well defined surface circulation system.

Historically hurricanes are categorized according to the Saffir-Simpson scale (Table 1) based upon their intensity and wind speed. But Hurricanes Katrina, Ike have demonstrated that intensity alone cannot be used to categorize hurricanes for predicting their damage potential.

Table 1 Saffir-Simpson Scale

Type	Maximum Wind Speed (km/h)	Pressure (mb)
Depression	<24.2	--
Tropical Strom	24.2-45.4	--
Category 1	46-59	>980
Category 2	59.6-68.3	965-980
Category 3	68.9-80.7	945-965
Category 4	81.4-96.3	920-965
Category 5	>96.3	<920

The main hazards associated with tropical cyclones and especially hurricanes are storm surge, high winds, heavy rain, and flooding. Parameters like hurricane forward speed and path are very difficult to predict, because these parameters depend upon the

interaction between storm circulations, earth's atmosphere, and constantly changing region of high and low pressure system. Based upon these complex interactions, some hurricanes follow a straight path, while other wavers along the path. Typically, the forward speeds of hurricanes are in range of 24 to 32 km/h.

2.2 Governing Equations for Storm Surge

Physics behind storm surge generation is very complex, particularly the interaction between the storms parameters and the geometric characteristics. Earlier surge prediction was based upon the historical surge data (Resio and Wasterink, 2008). But due to low frequency of these events, the extent of data available was not enough to characterize the geometrical and metrological parameters. Thus use of such inadequate data leads to inaccurate prediction of storm surge.

Storm surge is generated by rotating wind and pressure deficit on its surface, which cause the water to pile up at coastline (NOAA 2009). Thus physics behind the storm surge is completely described by the 3-dimensional equations for mass and momentum conservation. Based upon these equations physics based numerical models were developed which consider both geometric and meteorological conditions for surge prediction.

Based upon the assumption that the water density in shallow water can be considered to be a constant and for storm surge generation horizontal scale is much more important than vertical scale. The 3-dimensional equations of mass and momentum conservation

can be integrated over depth to generate 2-dimensional shallow water equations (Pritchard 1971). The mass conservation is represented as

$$\frac{\partial H}{\partial t} + \nabla_h(H\vec{u}) = 0 \tag{2.1}$$

and momentum conservation as

$$\frac{\partial \vec{u}}{\partial t} + (\vec{u}.\nabla_h)\vec{u} + g\nabla h\xi + f\,\hat{k}\times\vec{u} + \tau_b\vec{u} = \psi \tag{2.2}$$

where

H is total fluid depth,

U is vertically averaged horizontal velocity,

ξ is elevation above the mean sea level

f is the Coriolis parameter,

τ is bottom stress parameter,

∇_h is the horizontal gradient operator, and

$\hat{k}$ is the vertical unit vector,

ψ is a forcing term.

The forcing for storm surge is due to the pressure difference and the wind stress (τ_s) produced at the surface of the water along with the other forces like the coriolis force, wave radiation stress, etc. The wind stress is defined as (Dean and Dalrymple, 2002)

$$\tau_S = \rho_a C_f U^2 \tag{2.3}$$

Where,

τ_s is wind stress,

ρa is density of air,

C_f is friction coefficient,

U is wind speed.

In deep water the rise in water level is contributed mainly by the pressure deficit at the center of the storm. The storm surge caused by the pressure deficit can be calculated (Dean and Dalrymple 2002) by

$$\xi_b = \frac{\Delta p}{\gamma} \tag{2.4}$$

where,

ξ_b is set up of surface water due to the barometric pressure deficit.

γ is the specific weight of water.

As mentioned earlier, storm surge in coastal area depends upon the interaction of meteorological parameters and coastal geometrical characteristics. The simplified storm surge at steady state near open coast can be represented as (Resio and Westerink 2008)

$$\xi_c = \left(\frac{\tau}{gh}\right) W \tag{2.5}$$

Where, ξ_c is storm surge at the coast

τ is hurricane induced wind and barometric pressure

h is depth of water

W is continental shelf width

g is the acceleration due to gravity

The dependence of surge on the characteristics like water depth and the shelf width is one of the reason for variation in surge generation from location to location for similar metrological conditions.

2.3 Numerical Studies

Accuracy of numerical models used is very important for this study. Thus it becomes very important to use a numerical model which gives result with sufficient accuracy. Provost et al. (1994) has investigated the feasibility of using a Finite Element Model (FEM) as an alternative to the Finite Difference method usually developed for high resolution large scale ocean circulation model and concluded that the Finite Element technique can be used as an alternative to more commonly used Finite Difference technique for ocean circulation models.

The effect of grid refinement on storm surge prediction was studied by Westerink et al. (1991). He found that to accurately simulate the interaction between the storm parameters and the geometrical parameters a high resolution grid is required near coastal regions. He also compared two grids, one with uniform nodal density and other with varying nodal density. He found that both grids gave similar results for storm surge prediction. Thus by adopting the finer grid in coastal regions and coarser grid in the offshore areas, computational time can be saved.

The effect of domain size on the surge prediction had been investigated by Westerink et al (1994), and it was found that the large domain containing the Western North Atlantic Ocean, the Caribbean Sea, and the Gulf of Mexico along with the boundary condition at a sufficiently offshore location gave surge predictions more accurately as compared to those obtained from computation using smaller grid domains. Regarding variable

density, Older (1981) have found that smoother and slower change in resolution helps in better prediction. Also the resolution should vary with the flow rather than across it.

2.4 Wind Models

The accuracy of storm surge prediction by any numerical model depends upon the accuracy of the wind and pressure inputs. Numerical models require specification of the surface wind, or the surface wind stress itself at high resolution throughout the life of the storm. Earlier surge model applications use simplified parametric models for atmospheric forcing while the response of the ocean is predicted based upon numerical models. In the simplest form, parametric atmospheric models use the relation between the maximum surface winds (V_{max}) and pressure drop across the storm (Δp) (Thompson and Cardone. 1996). The relationship general form can be represented as:

$$\mathrm{V_{max}} = a(\Delta \mathrm{p^b}) \tag{2.6}$$

Where a, b are constant and Δp is the difference in P_{far} and Pcentral.

Parametric approaches for atmospheric forcing are simplified representations of complicated processes in the atmosphere. Thus, these approaches does not always represent the wind and pressure profiles accurately, and the error induced at this stage gets carried over to the ocean response numerical models, which uses these wind and pressure fields as input. The tropical cyclone wind field can also be calculated by analysis of observation. But this approach requires large amount of measured data. Most of the measured data available for tropical storms is for coastal areas, which does not correctly represent the data at the offshore locations.

Vortex boundary layer models based upon the primitive equations of motions have also been used for representing the tropical wind fields. The U.S Army Corps of Engineers vortex model was extensively used for storm surge modeling (Mark and Scheffner 1993). The model is based upon the concept that the tropical storm changes its structure relatively slowly. Thus, the tropical cyclone is represented by a small number of snapshots representing the different phase of storms and the intermediate transition between these storms. The model is based upon the equation of horizontal motion vertically averaged through the depth of the Planetary Boundary Layer (PBL) (Chow 1971, Cardone et al. 1992). The final form of equation represents the balance between the Coriolis force, the pressure gradient force and the frictional force at the outermost boundary

$$fK \times (V - V_g) = -\frac{1}{\rho}\nabla P_c - \frac{C_D}{h}|V + V_c|(V + V_c) \tag{2.7}$$

The simplest pressure field is defined by the exponential pressure law and is of the form

$$P_c(r) = Po + \Delta pe^{(-\frac{\bar{R}_p}{r})} \tag{2.8}$$

These equations are solved over a grid which is a system of rectangular nests, with the very fine spacing near the hurricane center and relatively coarse spacing in the outer regions. Chow (1971) provides the detail of the grid and the computational scheme followed in the model. The limitation of the horizontal spatial resolution was addresses in Cardone et al. (1994) in which the horizontal computational nests were increased from five to seven. The option has provided an increase in the spatial resolution around the

centre of storm and also extends the computational nests which allow better application of far field boundary condition.

The wind model used for this study is PBL model (Thompson and Cardone 1996). Detailed description of model and its interaction with the numerical model is provided in Chapter IV.

2.5 Surge Response Functions (Open Coast)

To predict potential damage due to hurricanes, agencies like National Ocean and Atmospheric Administration (NOAA) and Federal Emergency Management System (FEMA) uses the Saffir Simpson scale. But damage caused by Hurricane Katrina, which was a Category 3 storm (NOAA) at landfall, cannot be explained by the Saffir-Simpson scale. Irish and Resio (2008b) have shown that the storm size plays a key role in generating the surge in coastal areas. They have concluded that for a given intensity, storm surge varies by 30% for reasonable variation in storm size. SRFs for the open coast were developed by Irish and Resio (2009). It showed that the surge response surfaces changes continuously with the meteorological parameters like size, intensity of storm along with geometrical parameters like landfall location of storm and station location of interest. They investigated the surge response surfaces for the four tracks as shown in Figure 1 and gave relationship between the distance between the peak surge, the landfall location and the size of the storm. They represented this relationship as

$$X_{\xi peak} - X_O \cong \lambda R_p \tag{2.10}$$

Based upon this, they proposed the dimensionless distance in the form of

$$X' = \frac{X - Xo}{R_p} - \boldsymbol{\lambda} \tag{2.11}$$

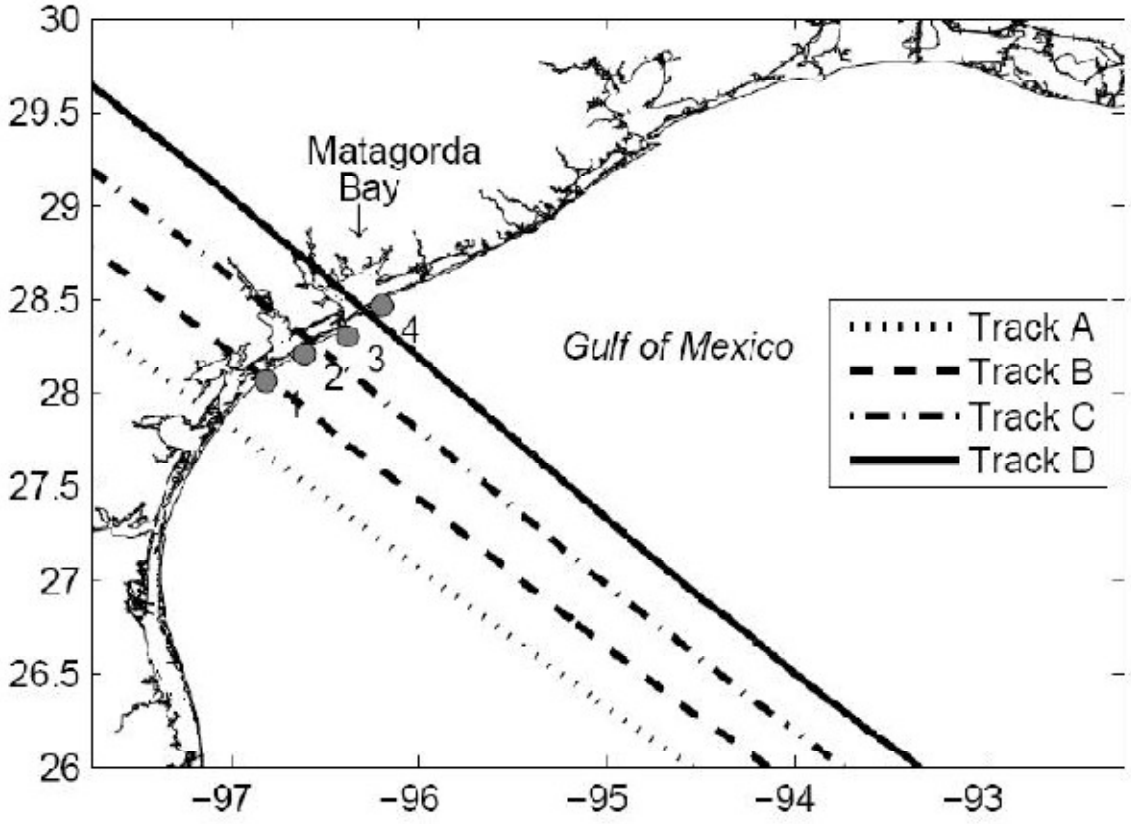

Figure 1 Matagorda Tracks for open coast SRF (from Irish and Resio 2009)

After performing linear regression analysis on the numerical simulation results for the four tracks, they have found the slope (λ) to be 0.87. More recently, the values of λ along the Texas coastline have been shown to vary (Song 2009) based upon the variation of the continental shelf width along Texas coastline**.** Irish and Resio(2009) define a dimensionless surge (ξ') as a function of peak surge at the station and the pressure deficit:

$$\xi' = \frac{\gamma\xi}{\Delta p} + m_x \Delta p \tag{2.12}$$

where, m_χ is a constant determined by linear regression analysis at each station.

Δp = (Difference in far field pressure and central pressure)

and, γ is specific weight of water.

To account for secondary effect related to storms of size less than the threshold size($R_{thres} = 25km$), alongshore distance ($X_2{}'$) was modified to a form

$$X_2{}' = X' - F(1 - R')H(1 - R') \tag{2.13}$$

Where R' is a dimensionless storm size defined as

$$R' = \frac{R_p}{R_{thres}} \tag{2.14}$$

R_{thres} = Threshold size of storm=25 km.

$H(1 - R')$ is a heaviside function defined as

$$H(1 - R') = \begin{matrix} 1 & for\ x \geq 0, \\ 0 & for\ x < 0. \end{matrix} \tag{2.15}$$

$F(1 - R')$ is a Ramp function defined as

$$F(1 - R') = \begin{matrix} a_1(1 - R') + b_1, & -\lambda \leq x' \leq 0, \\ a_2(1 - R') + b_2, & 0 < x' \leq \lambda, \\ 0, & \lambda < |x'|. \end{matrix} \tag{2.16}$$

The coefficients *a* and *b* for Texas coast were determined by linear regression to be

a_1 = -1.04, b_1 = 0.16, and

a_2 = 3.29, b_2 = -0.67.

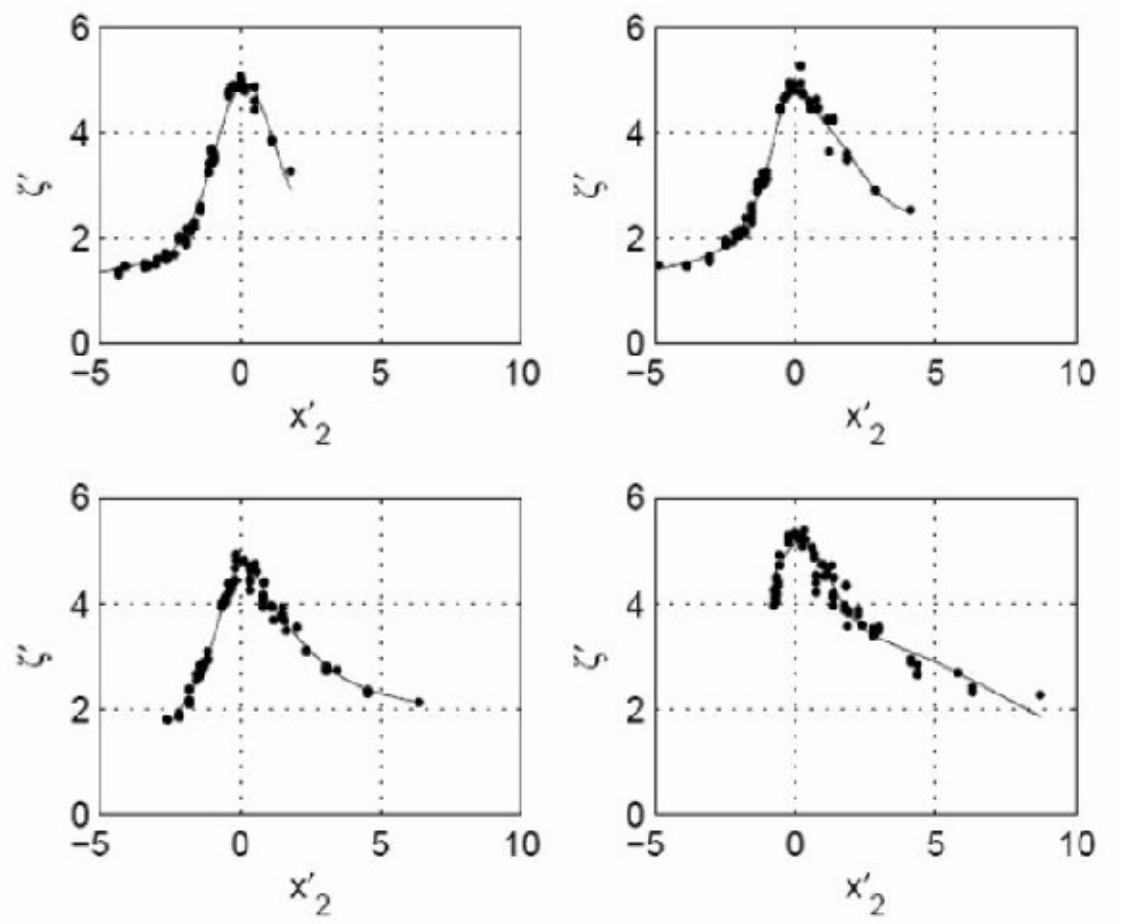

Figure 2 Open coast SRF (from Irish and Resio 2009)

They have found that the Gaussian 3 term distribution represents non-dimensional data at most stations. The R-square value for fit at these stations is above 0.9 for Gaussian 3 term fit. The coefficients for Gaussian fit at these locations were determined based upon linear regression analysis. Figure 2 shows the SRFs predicted at four locations near the Matagorda Bay. At all of these locations the mean of error between the simulated surge

values and the predicted surge values was in range of 13 to 24 cm, which is comparable to the accuracy of numerical models for storm simulations. Irish and Resio (2009) also showed, that the SRFs work well for limited data sets.

CHAPTER III

STUDY AREA

3.1 Introduction

For the purpose of this study, three bays (Matagorda, Galveston and Corpus Christi Bay) have been selected along the Texas coastline. Hypothetical storms have been simulated and the peak surge values have been extracted at the various stations inside the bays for these simulations. Analysis at these stations is performed to extend the SRF method (Irish and Resio 2009) for application inside the bays.

3.2 Matagorda Bay

Matagorda Bay is located between Calhoun and Matagorda counties on Texas coast. The bay has three inlets through which it interacts with the Gulf of Mexico. The average depth inside the bay is around 2.5 m with respect to geoid. On the west side of bay there is a deep shipping channel with a depth of 17m. The center of gravity of bay is shown in appendix A.

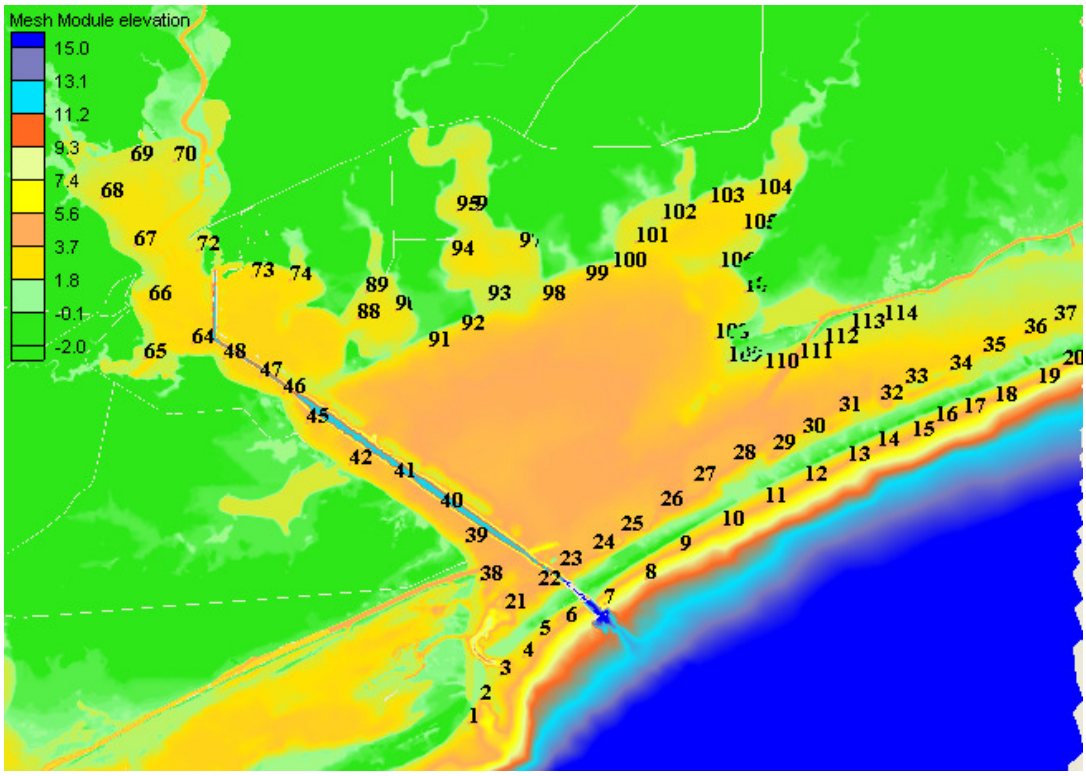

Figure 3 Matagorda contour and stations locations

For the purpose of development of SRFs, a total of 128 stations were selected inside the bay as shown in Figure 3. The details of the station location have been attached in appendix A.

3.3 Galveston Bay

The Galveston Bay is the largest estuary on the Texas Coast (Gulf Base 2009). It consists of six sub bays systems. The bay covers approximately 1,500 km², and is 50 km long and 27 km wide. The average depth of Galveston Bay is 2.0m with respect to the geoid. The bay has three inlets at the Gulf of Mexico. Like Matagorda Bay, Galveston

also has a deep shipping channel on the west side of the bay. In Galveston Bay a total of 159 stations were selected for SRFs development as shown below in Figure 4.

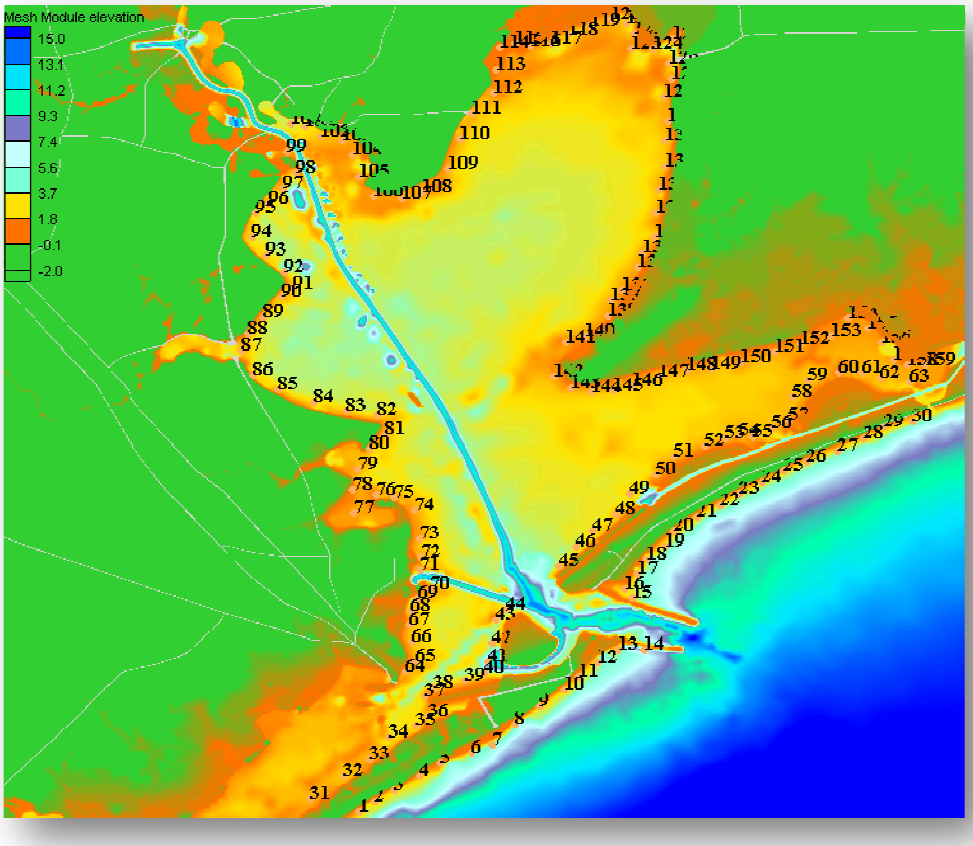

Figure 4 Galveston contour map and station locations

The details for the station locations (Latitude and Longitude) and Center of Gravity of bay are attached given in appendix A.

3.4 Corpus Christi Bay

Corpus Christi is located in the southern Texas coast. The bay is 15km long and 22 km wide. The average depth of the bay is 3.0 m with respect to geoid.

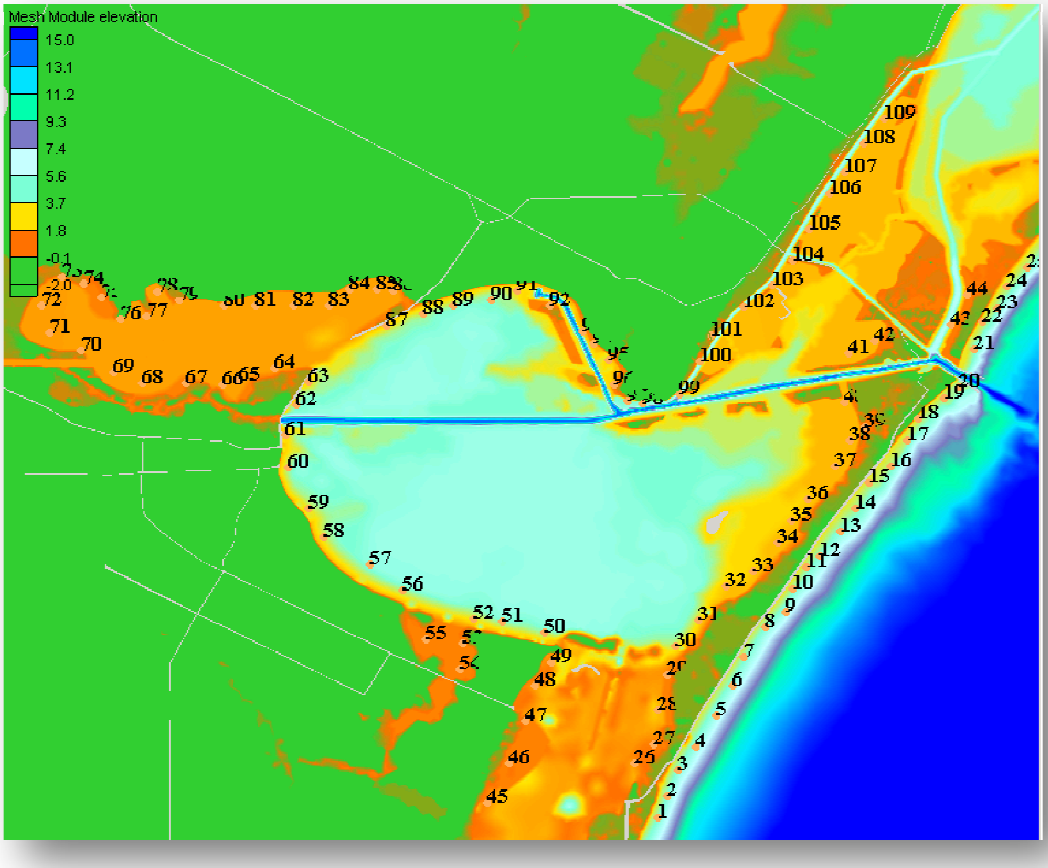

Figure 5 Corpus Christi Bay contour map and stations location

The Figure 5 shows the contour map for the Corpus Christi Bay and the locations of 109 stations which are selected for SRF's analysis. The details of station locations (Latitude and Longitude) and Center of Gravity of bay are attached in appendix A.

CHAPTER IV

NUMERICAL SIMULATIONS

The interaction between hurricane wind forcing and bay parameters like bathymetry, shape and size of a bay are very complex and needs to be understood for defining SRFs inside bays. To understand the response of bays to a hurricane wind forcing, sufficient amount of storm surge data is required in the area of interest. In this section, the numerical model used for simulations, model domain, wind model, and the storms parameters used for simulations are described.

4.1 ADCIRC Hydrodynamic Model

For accurate prediction of surge inside bays, the hydrodynamic numerical model needs to have a high resolution in area of interest and large domain size. A large domain helps in specifying the boundary conditions at offshore locations which reduces the errors caused by the boundary conditions. The variable grid density is required for more refined grid near coastal location as this helps in saving the computational time with less dense grid in offshore locations compared to coastal areas. For these reasons ADCIRC (Luettich et al., 1991 and 1994; Westerink et al, 1992) which is an advanced hydrodynamic model and uses a finite element scheme in space and finite different method in time to solve the Generalized Wave Continuity Equation (GWCE) (4.1) is chosen for simulating storm surge in area of interest. The GWCE is derived by differentiating continuity equation with respect to time and by spatially differentiating

the conservation of momentum equation. The GWCE in cartesian coordinates is as follows:

$$\frac{\partial^2\xi}{\partial t^2}+\tau_o\frac{\partial\xi}{\partial t}+\frac{\partial}{\partial x}\{U\frac{\partial\xi}{\partial t}-UH\frac{\partial U}{\partial x}-VH\frac{\partial V}{\partial x}+fVH-H\frac{\partial}{\partial x}\left[\frac{P_S}{p_o}+g(\xi-\alpha\eta)\right]$$
$$-E_{h_2}\frac{\partial^2\xi}{\partial x\partial t}+\frac{\tau_{sx}}{\rho_o}-(\tau_*-\tau_o)UH\}+\frac{\partial}{\partial y}\{V\frac{\partial\xi}{\partial t}-UH\frac{\partial V}{\partial x}$$
$$-VH\frac{\partial V}{\partial y}-fUH-H\frac{\partial}{\partial y}\left[\frac{P_S}{p_o}+g(\xi-\alpha\eta)\right]-E_{h_2}\frac{\partial^2\xi}{\partial y\partial t}+\frac{\tau_{sy}}{\rho_o}$$
$$-(\tau_*-\tau_o)VH\}=0 \qquad 4.1$$

ADCIRC-2DDI is a two dimensional depth integrated model which uses depth integrated mass and momentum equations subjected to incompressibility, Boussinesq and hydrostatic pressure approximations as its basis.

$$\frac{\partial H}{\partial t}+\frac{\partial UH}{\partial x}+\frac{\partial VH}{\partial y}=0 \qquad 4.2$$

$$\frac{\partial U}{\partial t}+U\frac{\partial U}{\partial x}+V\frac{\partial V}{\partial x}-fv=-\frac{\partial}{\partial x}\left[\frac{P_S}{p_o}+g(\xi-\alpha\eta)\right]+\frac{1}{H}M_x+\frac{\tau_{sx}}{\rho_{oH}}-\tau_*U \qquad 4.3$$

$$\frac{\partial V}{\partial t}+U\frac{\partial V}{\partial x}+V\frac{\partial V}{\partial x}+fU=-\frac{\partial}{\partial y}\left[\frac{P_S}{p_o}+g(\xi-\alpha\eta)\right]+\frac{1}{H}M_y+\frac{\tau_{sy}}{\rho_{oH}}-\tau_*V \qquad 4.4$$

where,

ξ= Free surface elevation relative to the geoid

U,V= depth averaged horizontal velocity

H=h+ξ= Total water column

h= bathymetric depth relative to geoid

f= coriolis parameter

P_s= atmospheric pressure at free surface

g= acceleration due to gravity

η= Newtonian equilibrium tide potential

α= effective earth elasticity factor

ρ_o= density of water

τ_{sx}, τ_{sy}= free surface applied stress

E_{h_2} = horizontal eddy diffusion coefficient

$$\tau_* = C_f \frac{\sqrt{(U^2 + V^2)}}{H}$$

C_f= bottom friction coefficient

The ADCIRC-2DDI model can be forced with elevation boundary forcing, variable spatial or temporal free surface stress and atmospheric pressure forcing. ADCIRC can be run in parallel on a multiprocessor with a suitable platform (MPI). This feature reduces the computational burden imposed by simulating at high resolution domain on single CPU. In a parallel run, ADCIRC partitions the grid and other input files to assign them

to independent CPUs. After processing these files, ADCIRC reassembles the output generated by each CPU to give the final result. Thus through parallel run it saves the CPU time as well as computational requirement for simulating a large domain size.

4.2 Model Domain

In this study, the east coast computation domain of Westerink et al. (2008) is used as the model domain. The grid includes the Western North Atlantic Ocean, the Caribbean Sea, and the Gulf of Mexico. The offshore boundary is defined at east coast which extends from Glace Bay to the Corocora Island in eastern Venezuela along the 60^oW meridian. Other boundaries are defined by the eastern coastlines of North, Central and South America. The approximate size of grid in Coastal areas is 0.006^o while in offshore it is 1.15^o. The bathymetry in Gulf of Mexico region is in accordance with detailed database used by Westerink et al. (1992). The key parameters of the grid are as follows

- Number of nodes 1,344,247
- Number of elements 2,628,785
- Area 8.352 X 10^6 km^2
- Maximum depth 7858.09 m
- Grid size in deep ocean 1.15^o
- Grid size in coastal areas 0.006^o

The model domain used for simulations is shown in Figure 6.

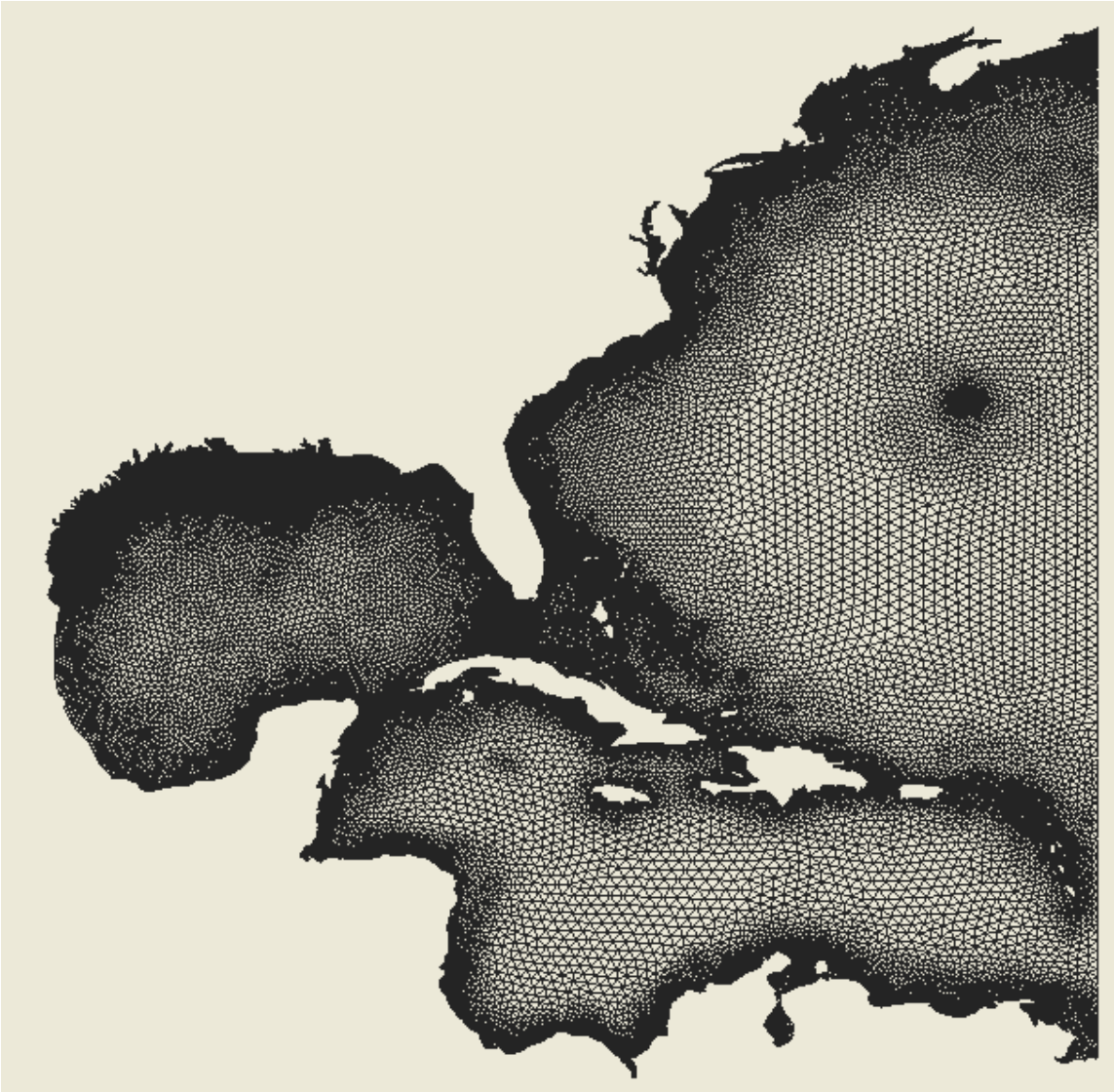

Figure 6 Computational domain

4.3 Wind Field Model

For predicting storm surge ADCIRC uses wind and pressure fields as inputs at every time step. Thus accuracy of results provided by ADCIRC depends upon how accurately wind and pressure field are fed into it. Therefore, the choice of wind model becomes very important to predict storm surge accurately. Development of various wind models

has been discussed in Section 2.3. In this study, the Planetary Boundary Layer (PBL) model of Thompson and Cardone (1996) is used to generate wind and pressure fields.

The PBL model is based upon vertically averaged, horizontal equation of motion in moving coordinate system (Chow, 1971; Cardone et al., 1992). The wind and pressure fields in PBL model are defined as a function of storm parameters like intensity, size, forward speed and Holland B parameter (B, Holland (1998)). In the PBL model Pressure field is defined as an exponential law given by

$$P_c = P_{eye} + \Delta P e^{-(\frac{R_p}{r})^B} \tag{4.5}$$

Where

P_{eye} is the pressure at eye of storm.

ΔP is difference in far away pressure and P_{eye}.

r is the distance from the eye of storm.

R_p is the pressure scale radius for PBL model.

B is a constant in the general range of 0.5-2.5

In PBL model it is assumed that the wind field pattern changes slowly and hurricane wind filed can be described by discrete number of snapshots representing the various phases of wind field and transformation of these phases. PBL computes the wind velocities and pressure at the grid points as described in Figure 7 at specified time steps

based upon storm parameters specified. For this study, inputs for wind speed and pressure were given after every fifteen minutes. The nested grid is obtained by using seven grids with linearly increasing grid spacing (1.25km, 2.5km, 5km, 10km, 20km, 40km, and 80km), with most dense grid near center of hurricane (Figure **7**). The high resolution grid at the center of hurricane helps in predicting the variation in wind and pressure field at high resolution in this region as compare to the outer region where variation in wind and pressure field is comparatively less.

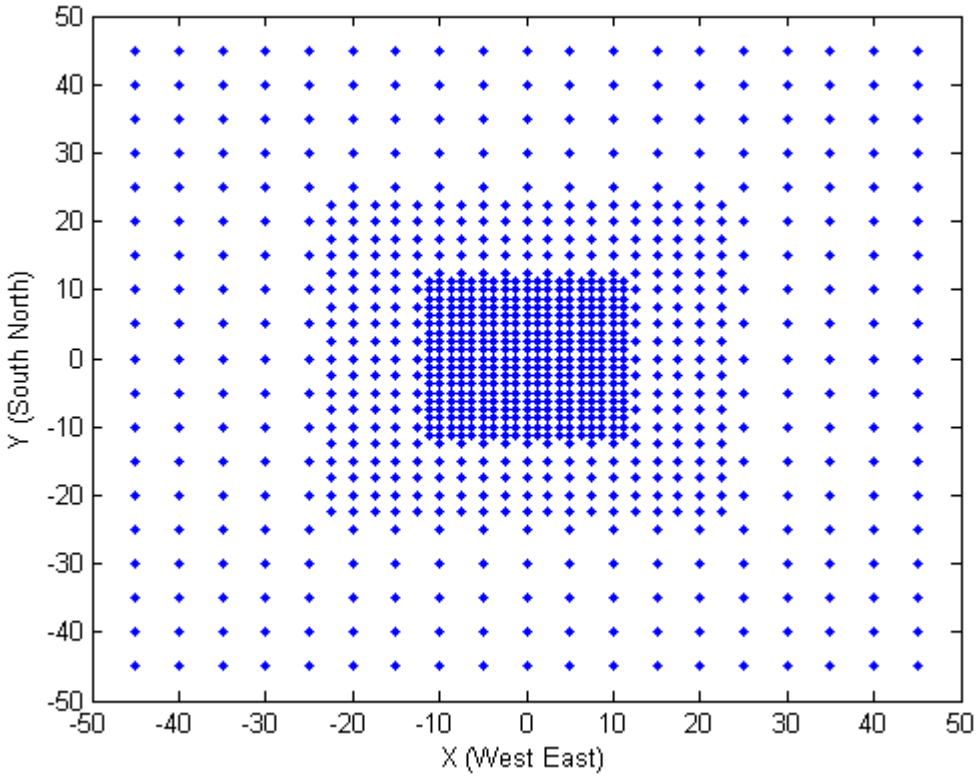

Figure 7 PBL grid nests

Iterative procedure to compute the wind and pressure field is used at each grid point starting with initial guess of gradient of wind field components from hurricane pressure field. Figure 8 shows the contour map and wind velocity for a storm on track near Matagorda Bay.

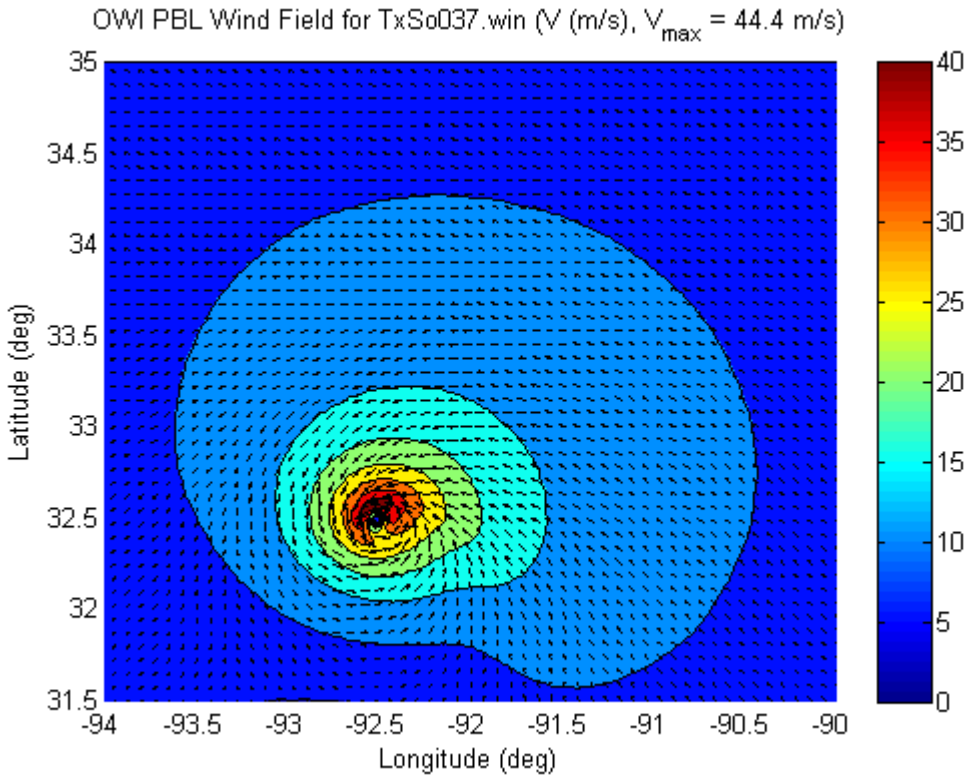

Figure 8 PBL wind field contour profile

4.4 Storms Selection

For this study, total of 106 simulations were made on 9 tracks as shown in Figure 9. Along with variation in track, size and intensity of storms were varied from 11 km to 66 km and 900mb to 960mb respectively. The storm size and intensity for these simulations were specified based upon data set of Irish and Resio (2009).

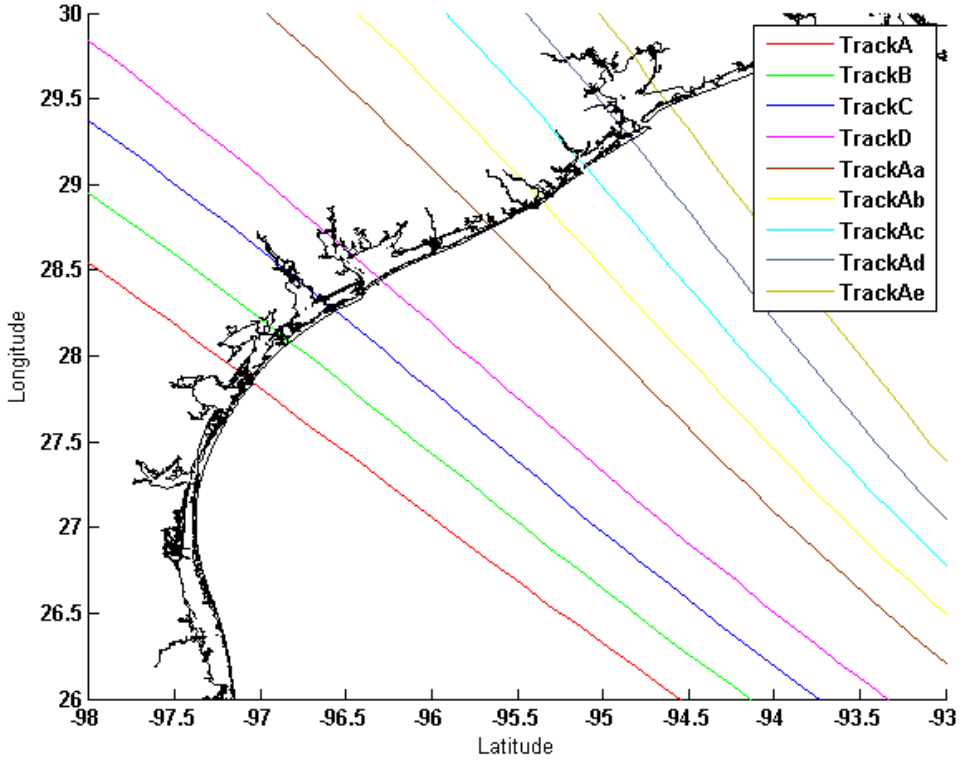

Figure 9 Tacks

Response due to forward speed (5.7 m/s) of hurricane and track angle (17^{o} or less) is assumed less important as compared to the variation in factors like intensity and size of storm, thus forward speed and track angle are kept constant (Irish and Resio 2009). The Holland B parameter was kept to be constant (1.27) until the hurricane is 50 km away from the land fall and after that it was decreased to 0.9.

CHAPTER V

METHODOLOGY

5.1 SLOSH Database Comparison with Open Coast SRFs

SLOSH (Sea Lake and Overland Surge from Hurricanes) is the model used by NOAA for predicting the surge level in case of hurricanes. Its database includes the results of several hypothetical storms for many different basins. The database provides the MEOW (Maximum Envelope of water), where MEOW represents the maximum level of water reached at a location for several storms of same category along with forward speed and direction, but for tracks parallel to each other. The category of hurricane is based upon the Saffir-Simpsons Scale (Table 1)

For the purpose of comparison of the results of SLOSH (Taylor,A and Berger, H 2008) and the SRFs (open coast), two locations have been selected at an open coast area near Matagorda Bay as shown in the figure 10 below. At these locations, SLOSH results have been extracted and plotted along with the surge levels calculated by SRFs.

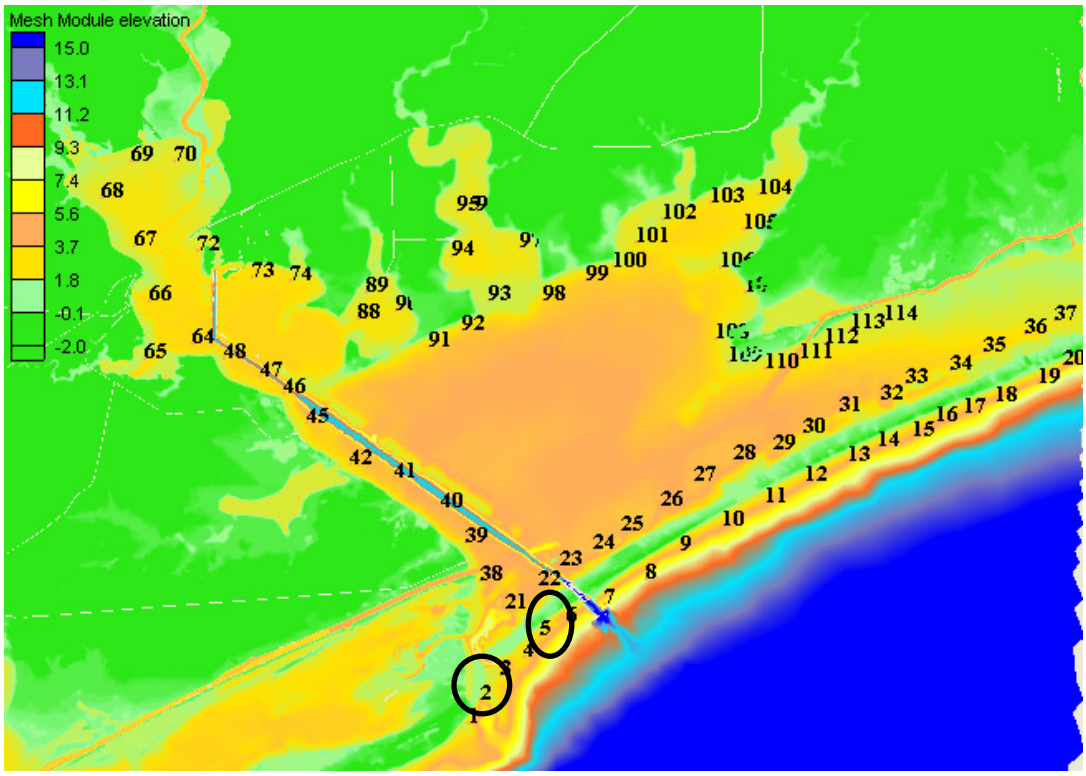

Figure 10 Stations location for SLOSH and SRF comparison

The SLOSH gives the range of surge levels at any station based upon Saffir Simpson category of hurricane and speed of the storm, whereas the surge values from the SRFs depend upon the intensity, size and location of the storm with respect to the station location. Figure 11 through Figure 12 show the results for station 2, and 5. As seen from the plots for both the stations, the SLOSH database gives higher surge values as compared to the SRF by 0.61 to 0.76 m. The reason for this seems to be wave setup which is not included in the SRF term. However, what is most important in comparison is that the SLOSH gives a constant value for each category of the storm, whereas SRF shows that we get a range of values depending upon the landfall location, size and

intensity of the storm. The SRF results show that with the change in landfall location (XXo) with respect to the station location surge value for a particular storm changes.

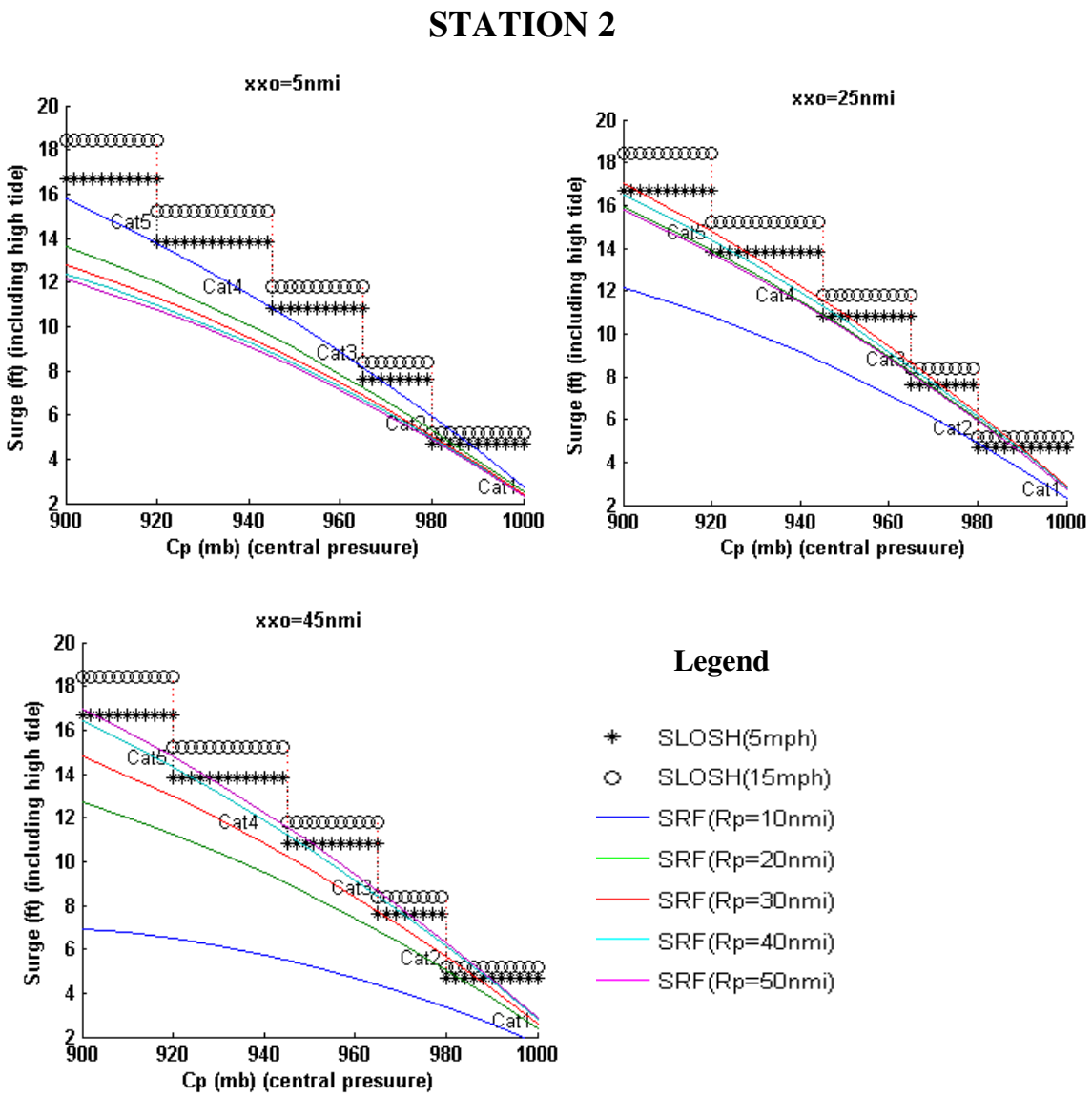

Figure 11 SLOSH and SRF comparison, station 2

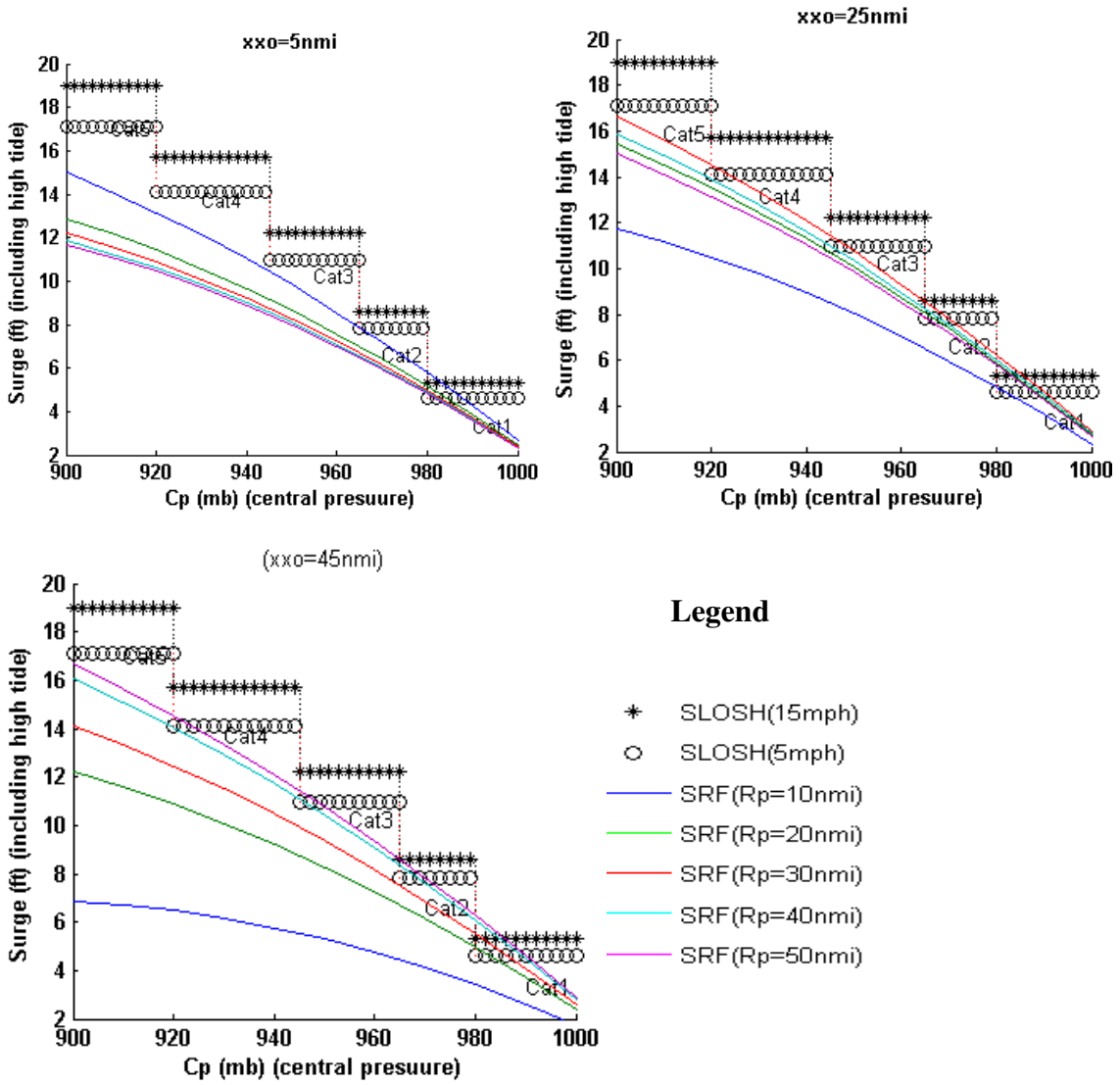

Figure 12 SLOSH and SRF comparison, station 5

5.2 Application of Open Coast SRFs Inside Matagorda Bay

SRFs for open coast, as described in section 2.6 use a linear distance for a station and land fall location. This methodology has worked well for open coast, but inside bay it is not possible to define these linear distances at all locations due to irregular shape of the bay. To check the effectiveness of the methodology inside the bay, inlet location of

Matagorda Bay has been selected to define the linear distances. For all locations inside the bay non-dimensional distances used are that of the inlet station and this non dimensional distance is plotted at each station with the corresponding non-dimensional surge values and other important assumption made is that the lambda value used at all stations inside the bay is obtained from open coast. With these two assumptions the non-dimensional distance and non-dimensional surge values are plotted and the results are shown in the figure 13 below. SRFs give the same shape inside the bay as for the open coast, but simulations are much more scattered inside the bay as compared to the open coast. The R-square value for station at open coast is in range of 0.9 to 0.97, while for stations inside the bay R-square values are in range of 0.55 to .68. Thus we can say that the SRF methodology for open coast does not work well inside the bay.

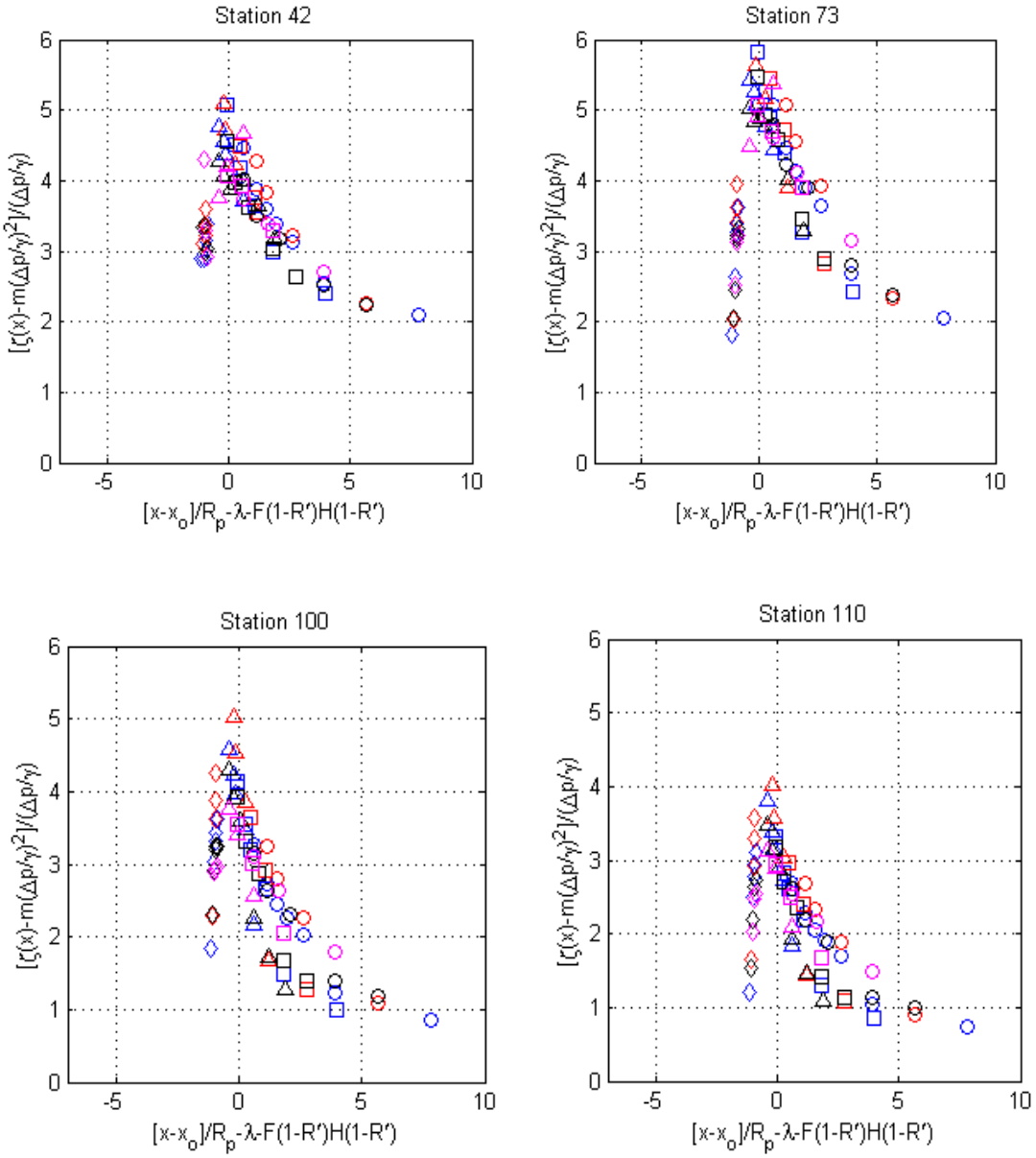

Figure 13 SRF inside the bay with open coast methodology

5.3 Effect of Inlet Opening

As a storm approaches a bay, it pushes the water with it. Water enters into the bay through an inlet opening and sometime by overtopping of a barrier island. Thus the amount of water entering into the bay, and in turn the storm surge inside the bay, is dependent on the inlet opening.

This section deals with the effect of inlet opening on the storm surge inside Matagorda Bay. To study the effect of inlet opening on surge inside the bay, one of the Matagorda Bay openings was blocked as shown in Figure 14.

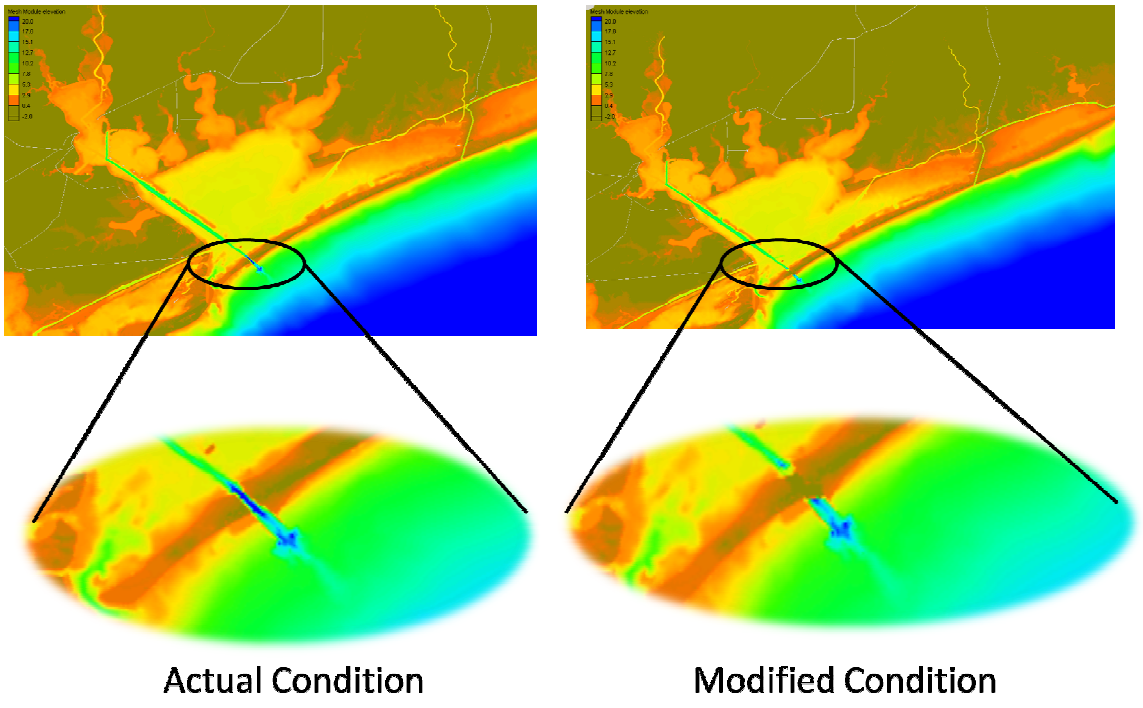

Figure 14 Matagorda Bay, showing actual and modified inlet condition

With the modified grid configuration, storm of size (Rp) 11 km and central pressure 960 mb was simulated on three tracks(A,B,C) as shown in Figure 9.

The simulation results with the inlet opening blocked was compared with the results for inlet open conditions. Figure 15 and Figure 16 Time series for station show time series of the simulation with two conditions for open coast stations 7, 12 for the three tracks.

Time series for two inlet conditions, overlap each other at both the stations. Thus for open coast locations, time series and peak surge values are unaffected by two proposed inlet conditions. Also, the inlet location does not make any difference to the peak surge at open coast. To investigate the effect of inlet opening on peak surge inside the bay, time series for stations inside the bay area are plotted and results are shown below from Figure 17 to Figure 21.

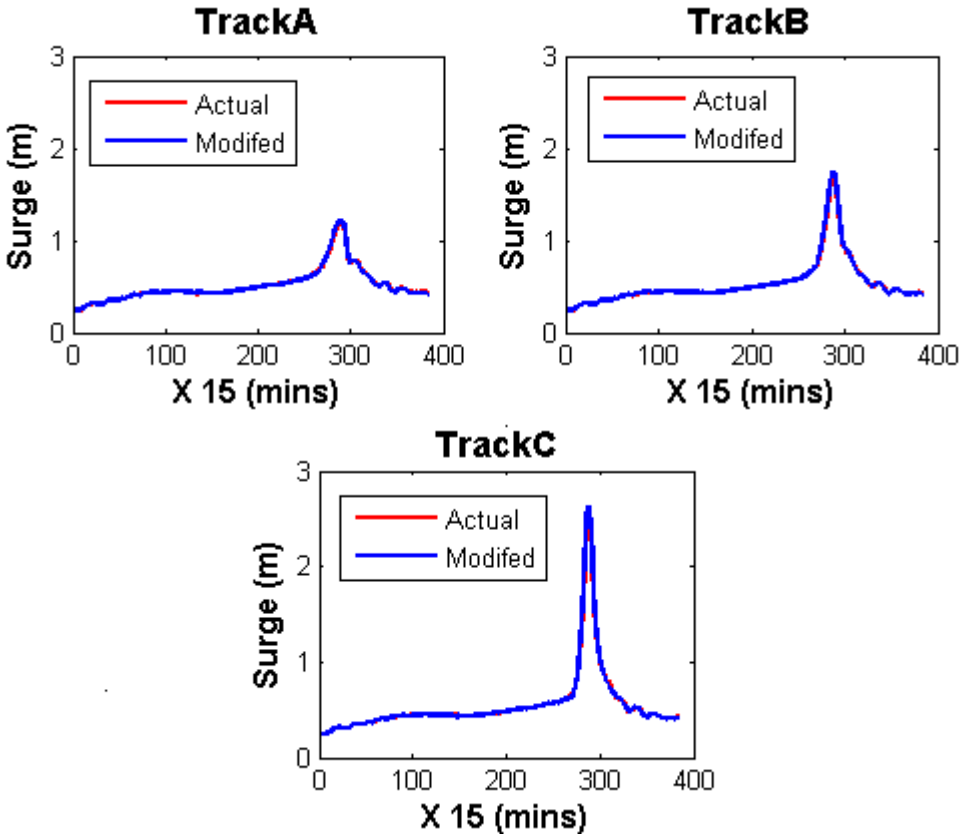

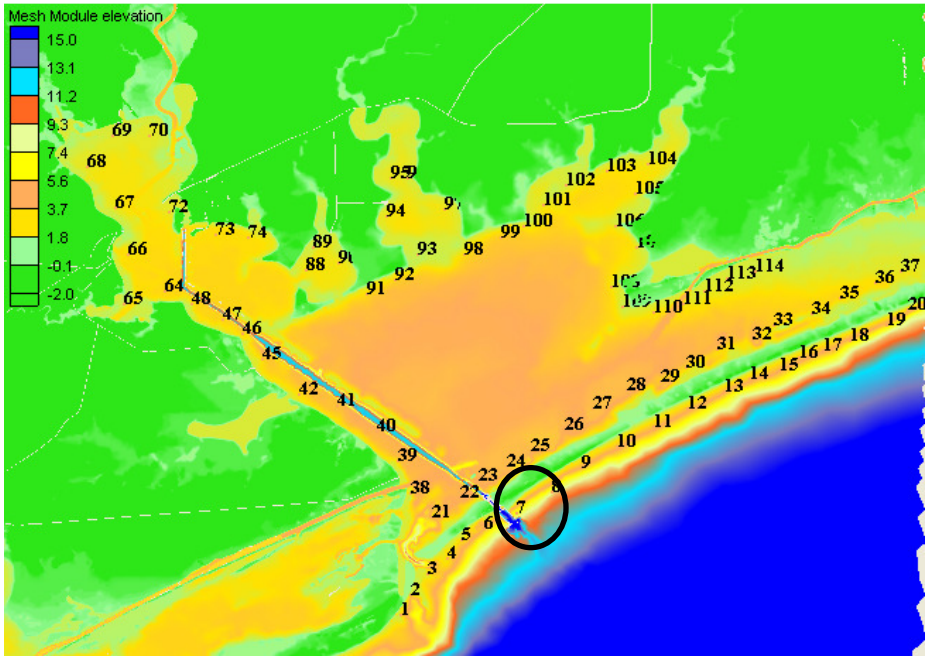

Figure 15 Time series for station 7

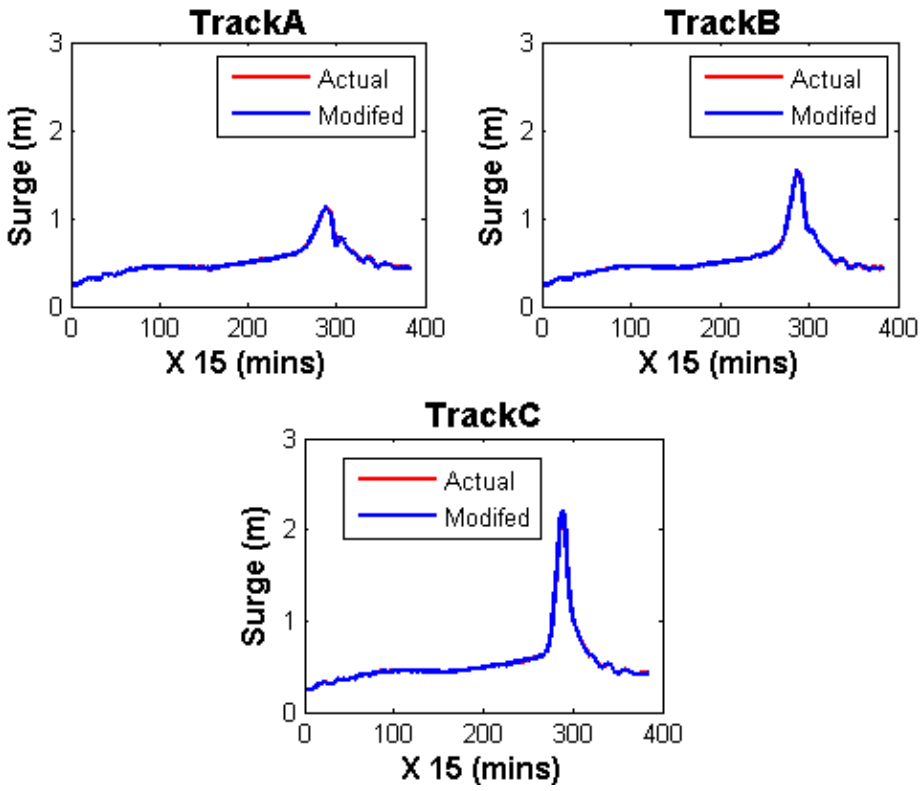

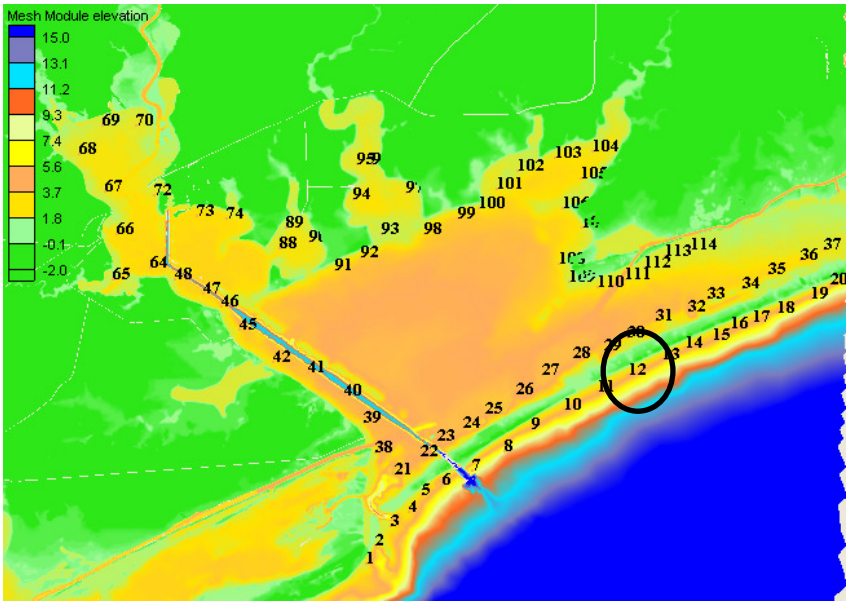

Figure 16 Time series for station 12

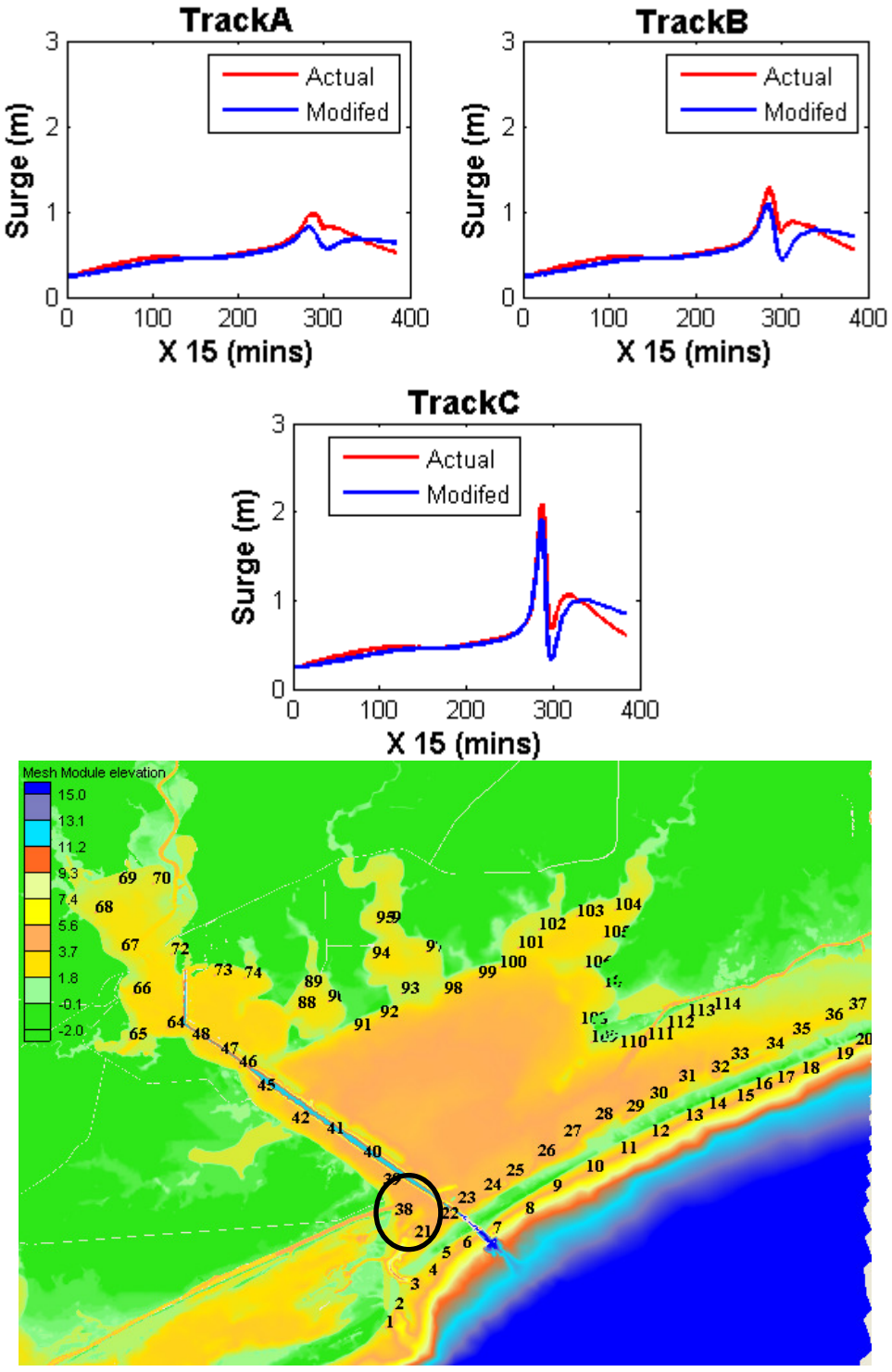

Figure 17 Time series station 38

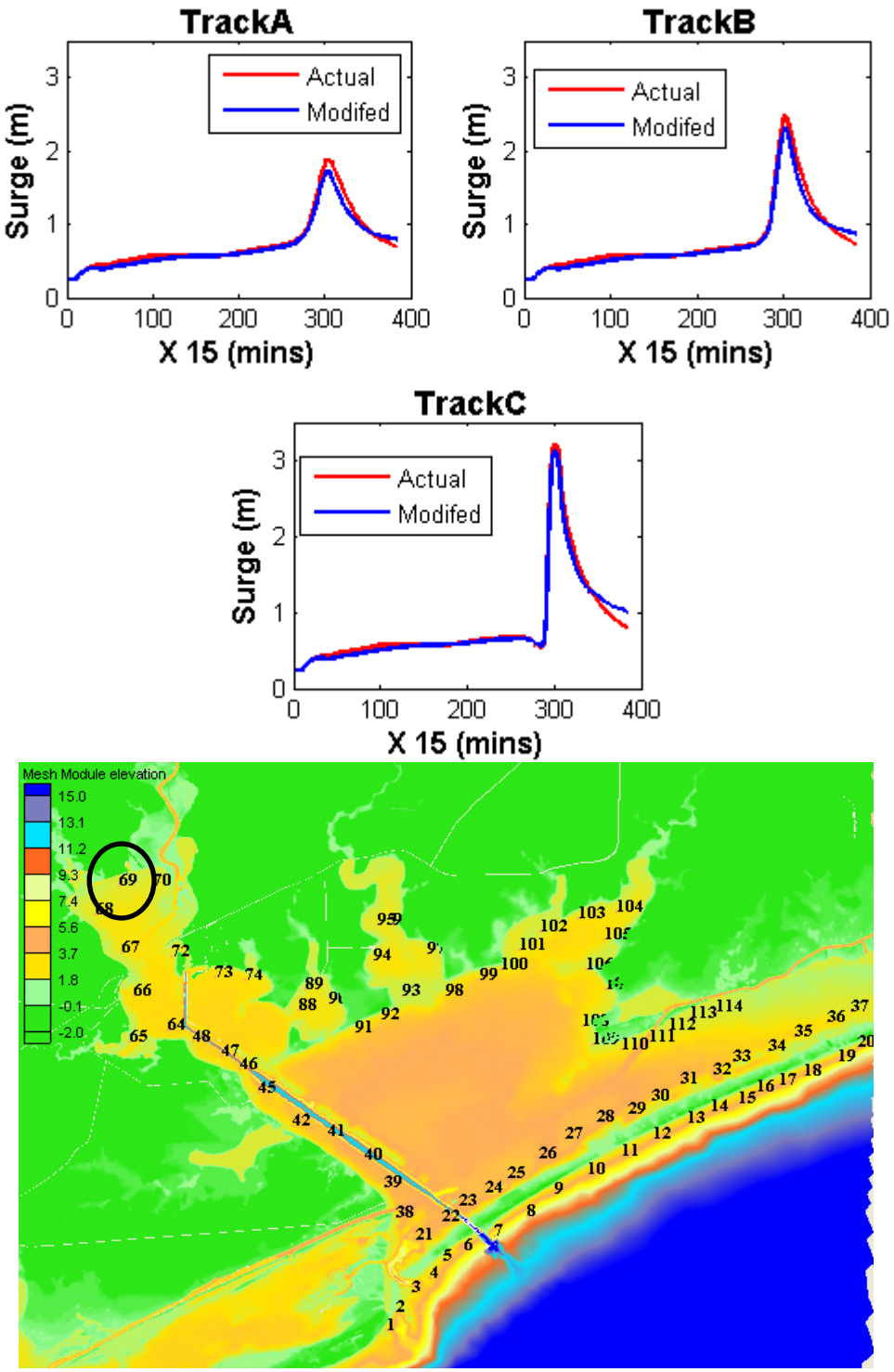

Figure 18 Time series for station 69

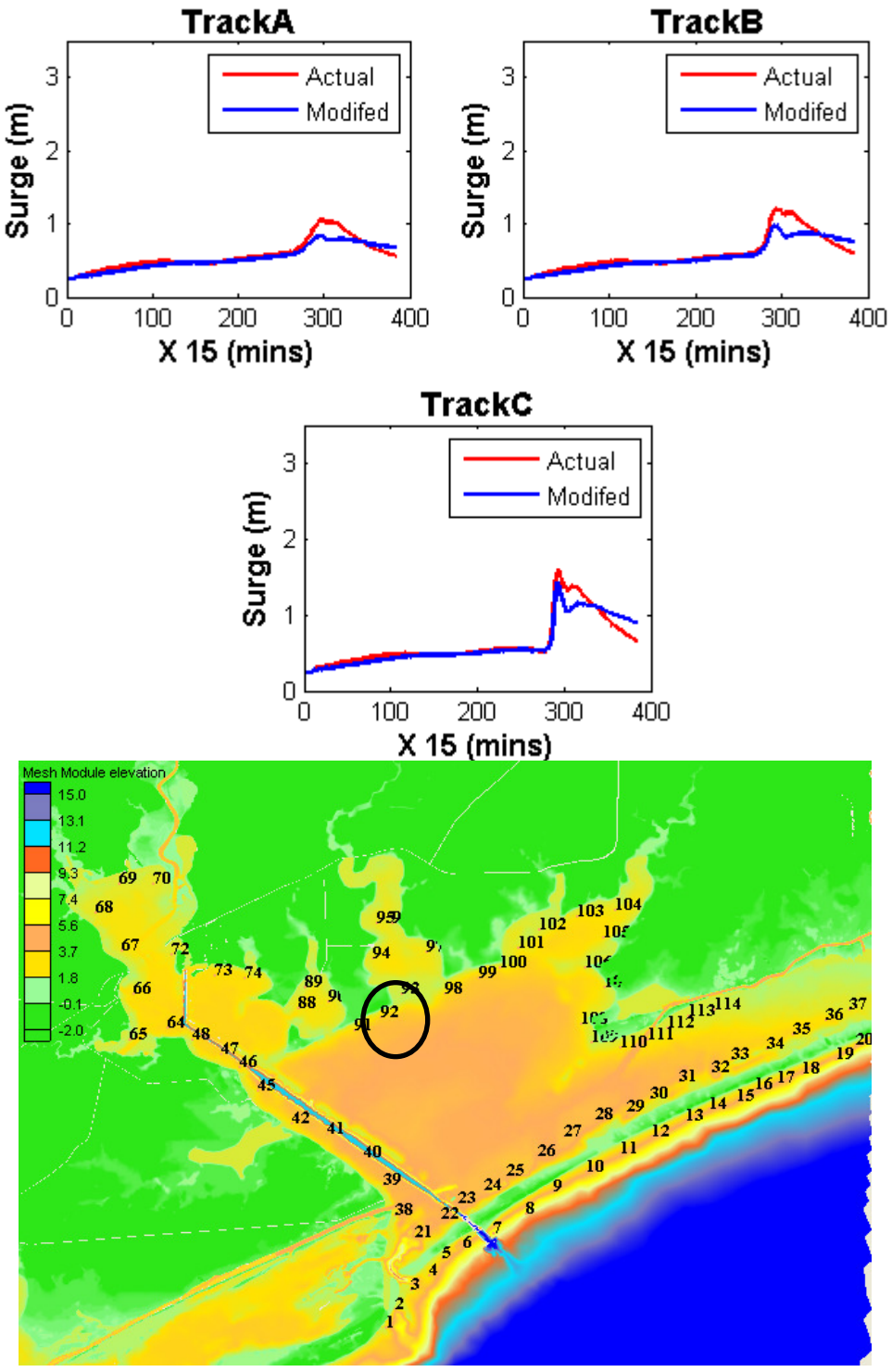

Figure 19 Time series for station 92

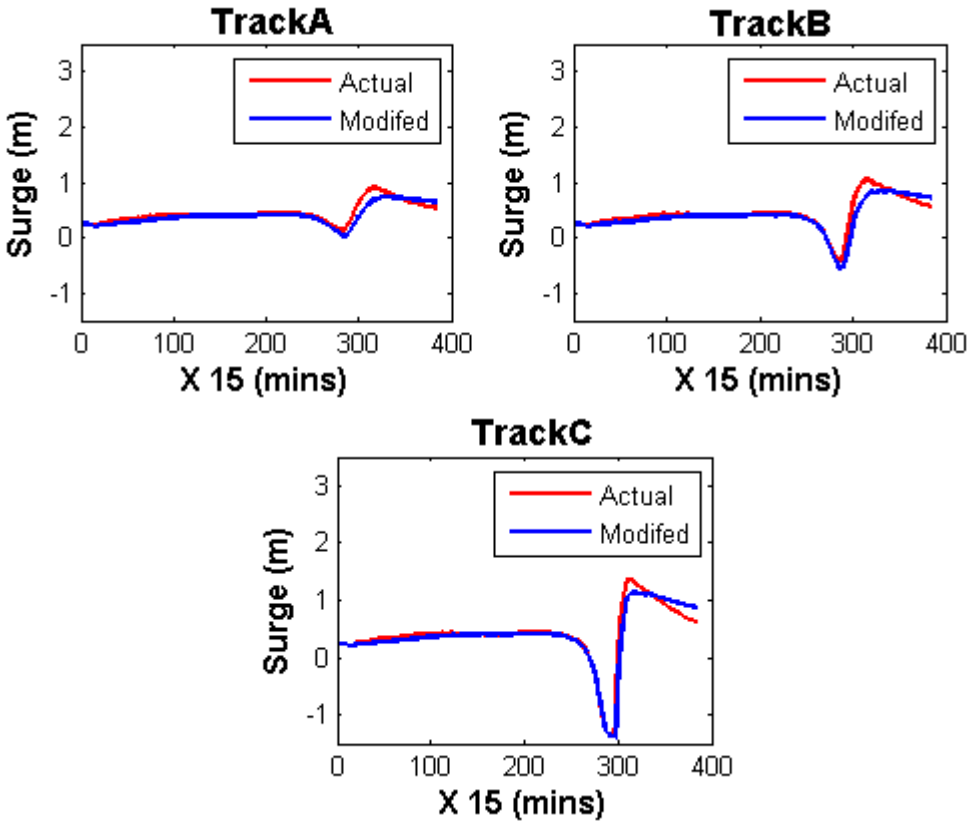

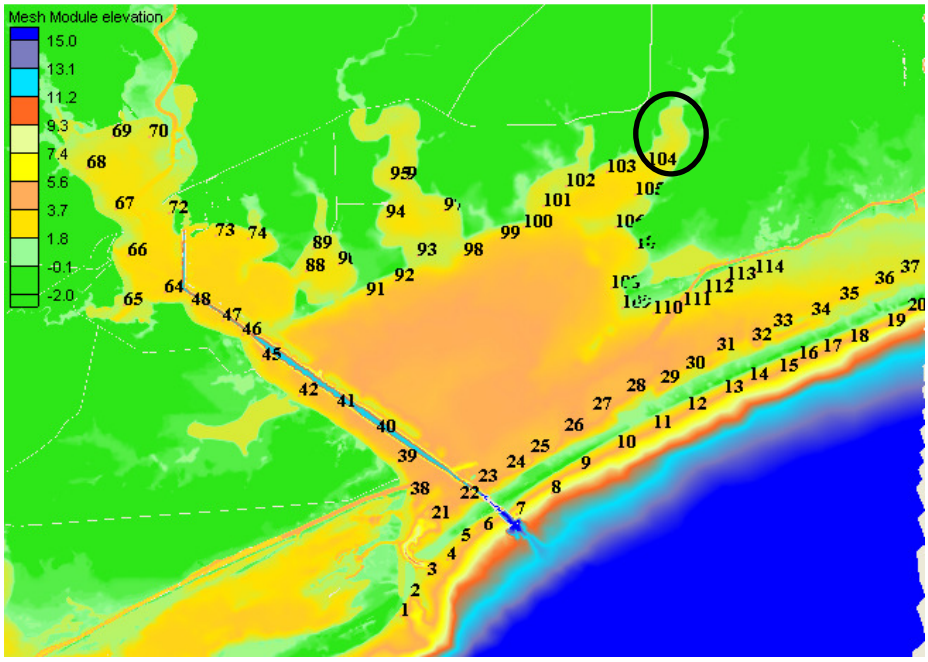

Figure 20 Time series for station 104

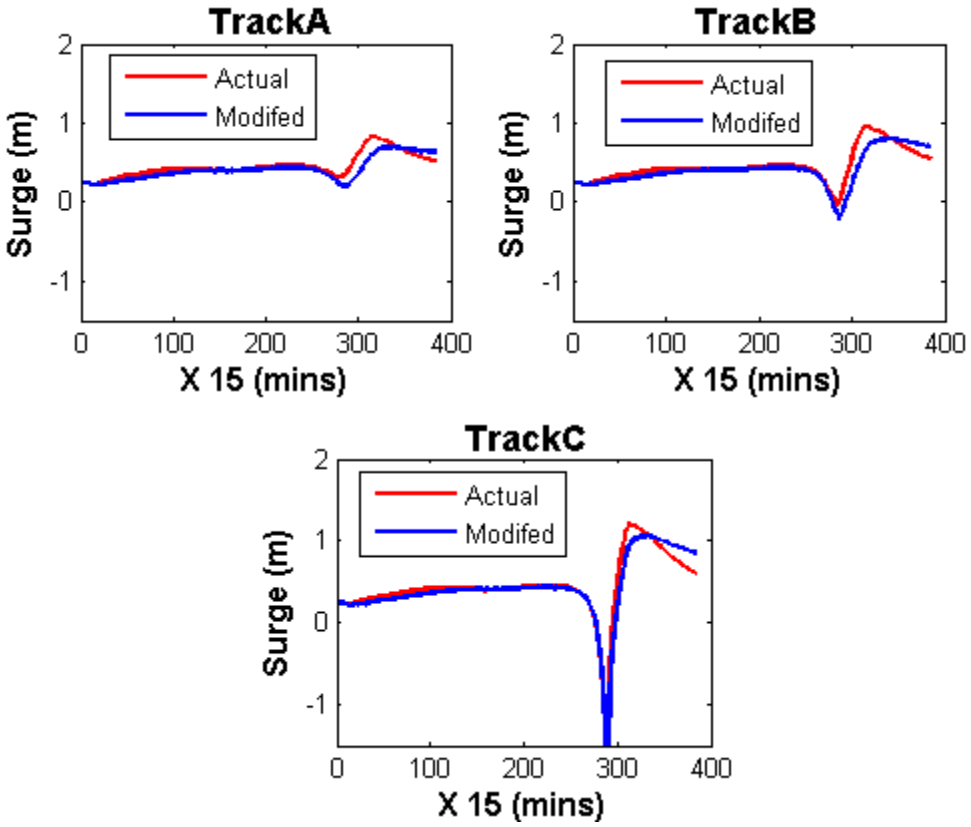

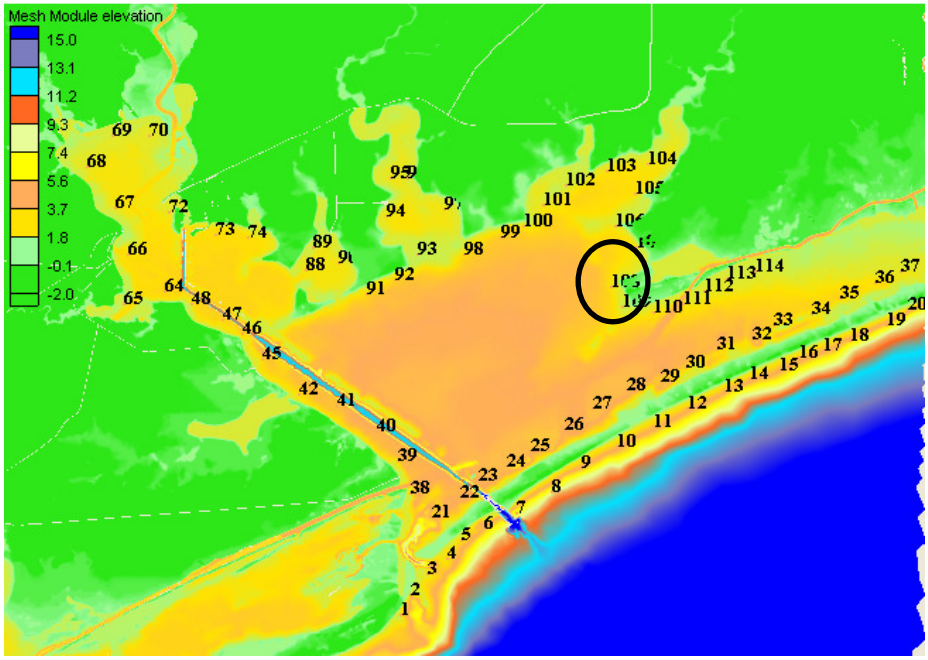

Figure 21 Time series for station 108

As is clear from Figure 7 to Figure 1, the peak surge value inside the bay for the blocked inlet case is less than that of the open inlet case. This is because with inlet closed there is relatively less amount of water entering inside the bay and thus the peak surge value inside the bay decreases.

Table 2 Peak surge ratios for inlet blocked and open conditions

	Track A	**Track B**	**Track C**
Station 7	1.03	1.04	1.05
Station 12	1.00	1.00	1.00
Station 38	0.84	0.85	0.91
Station 69	0.91	0.94	0.97
Station 92	0.79	0.80	0.89
Station 104	0.82	0.79	0.82
Station 108	0.84	0.84	0.84
Average (Station 38 to 108)	0.84	0.84	0.89

Table 2 gives the ratio of peak surge for inlet closed condition versus inlet open condition. For station 7 and station 12, which are open coast stations, the ratio is about 1.00. But for stations 38 to 108, which are the station inside the bay, there is a decrease in the peak surge value as indicated by a ratio less than 1.00.

Further decrease in peak surge value lies between the 11 to 16%, which is same as the percentage of area blocked by closing the inlet (15%). The percentage decrease in peak surge value is similar throughout the bay. So based upon these observations we can conclude that, although inlet opening affect volume of water entering the bay, the percentage decrease in peak surge is similar throughout the bay. Thus the location of opening does not affect the surge distribution inside the bay. Although, change in an area of inlet opening, will affect the SRFs.

5.4 Importance of Center of Gravity

As a storm passes by a bay, there is a set up at one end and a set down at the other end of the bay. Figure 22 shows set-up and set- down in 2-dimensions.

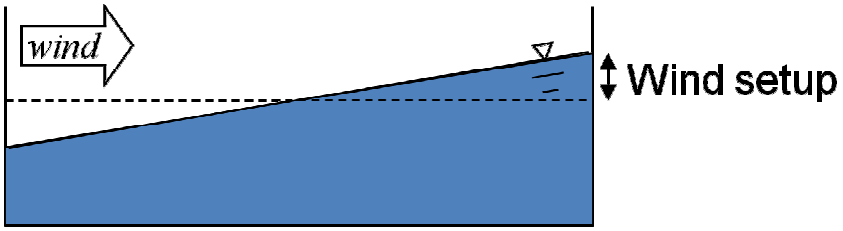

Figure 22 Set-up and set-down in bay (from Irish personal communication 2009)

Thus, Bay responds to an external forcing as a system. We investigated the effect of the center of gravity of the bay on peak storm surge distribution. Considering the volume of

water inside the bay at calm state, the center of gravity of the volume of water is calculated. From the center of gravity of the bay, minimum distance of a storm as is passes by a bay is calculated. This distance is normalized by size of storm to give the non-dimensional distance. The non-dimensional surge as defined in section 2.6 is plotted against this non dimensional distance and the results are shown below.

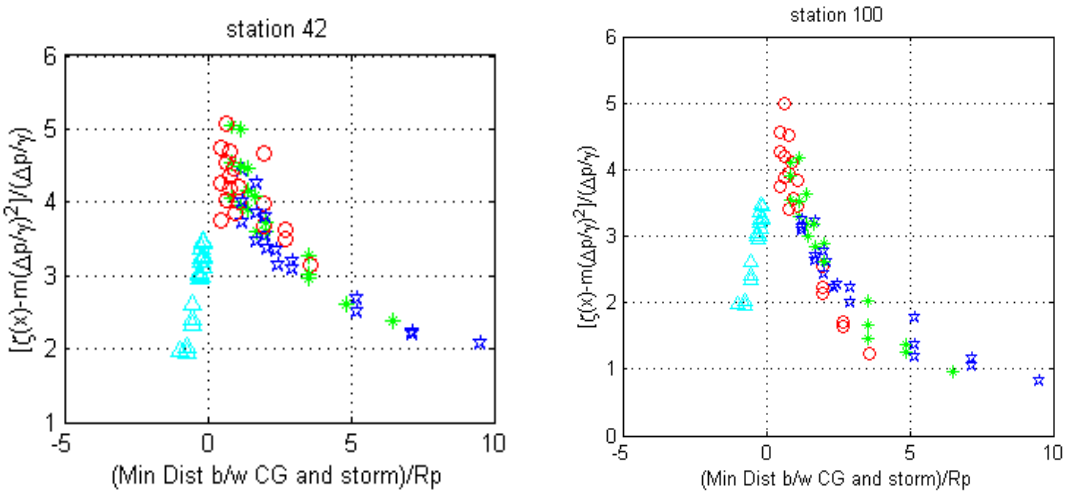

Figure 23 Importance of center of gravity

As shown in Figure 23, the surge values do correlate to the size and minimum distance of storm from the center of gravity of bay. However there is a significant scatter in SRFs particularly for stations located on the west side of the bay, which corresponds to the channel location inside the bay.

5.5 Effect of Channel

As mentioned previously, Matagorda Bay has a deep channel on the west side of bay. To study the effect of channel on the peak surge distribution inside bay, simulations under two conditions were generated. First, using the actual condition i.e. with channel and

second with the channel blocked. For both the cases simulation with storm size (R_p=15Km) and intensity (p=930mb) were used. Peak surge values were extracted from the time series of the two simulations. The contour map of the peak surge obtained is shown in Figure 24 and Figure 25.

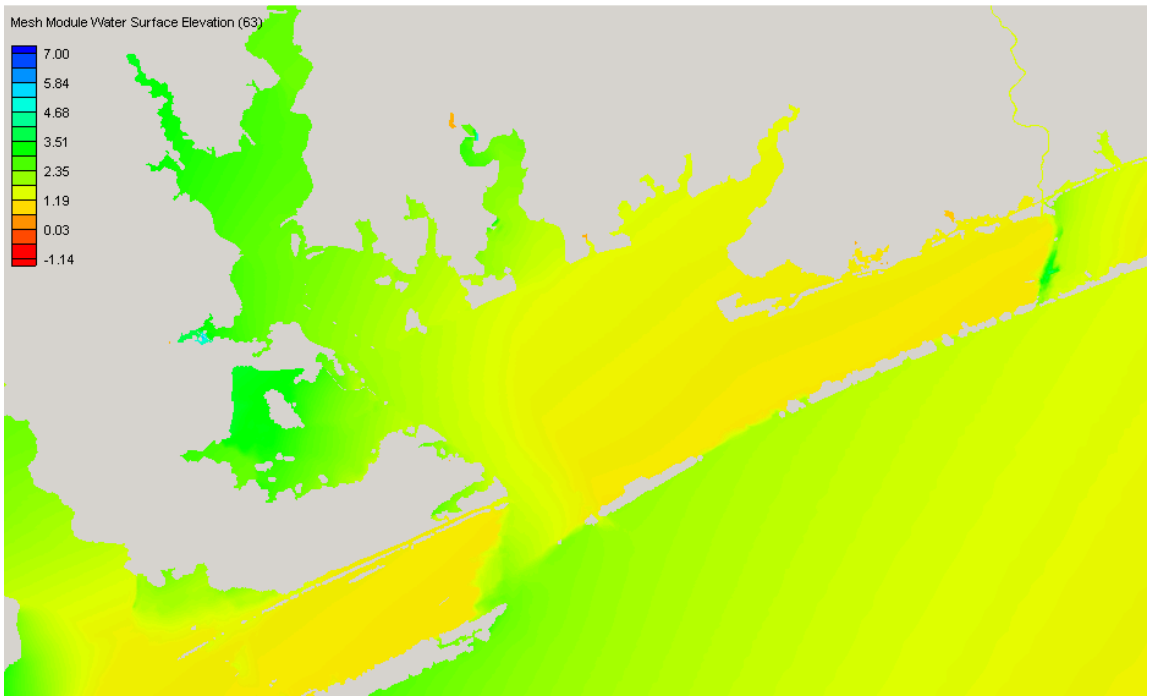

Figure 24 Peak surge in Matagorda Bay with channel

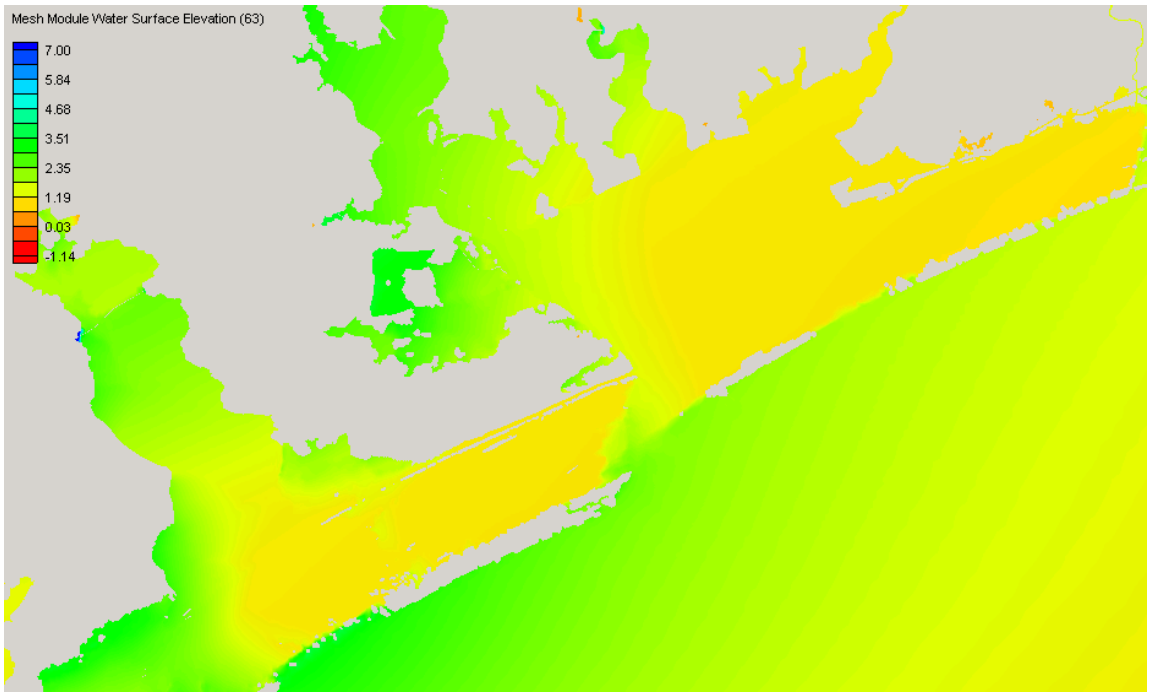

Figure 25 Peak surge in Matagorda Bay without channel

For both cases, peak surge values were same for all the 114 station(s) considered in this study. The contour map of peak surge inside the bay with and without channel shows similar region of peak values. Thus we can say that the existence of a channel does not affect the peak surge levels inside the bay.

5.6 Timing of Peak Surge

Storms on different tracks might cause peak surge values at a station at different times. This might affect a surge response inside the bay. To study this effect, we selected stations at various locations inside Matagorda Bay and water elevation time series were compared for different tracks storms at these stations.

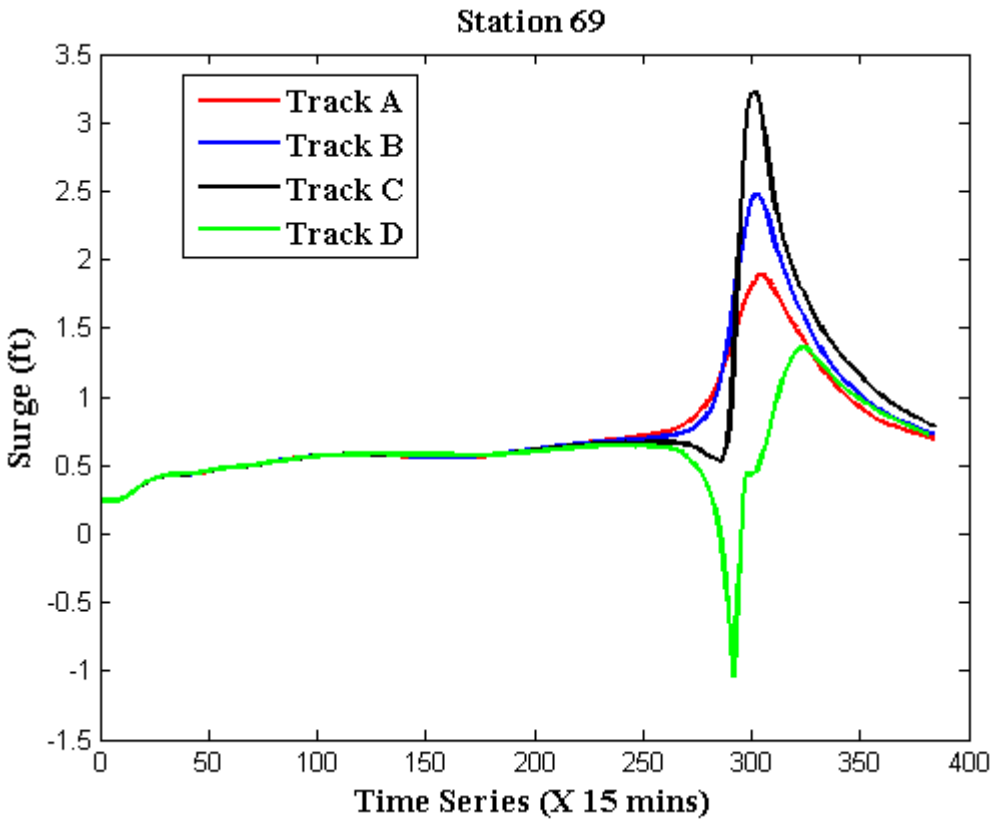

Figure 26 Time series for station 69, Matagorda Bay

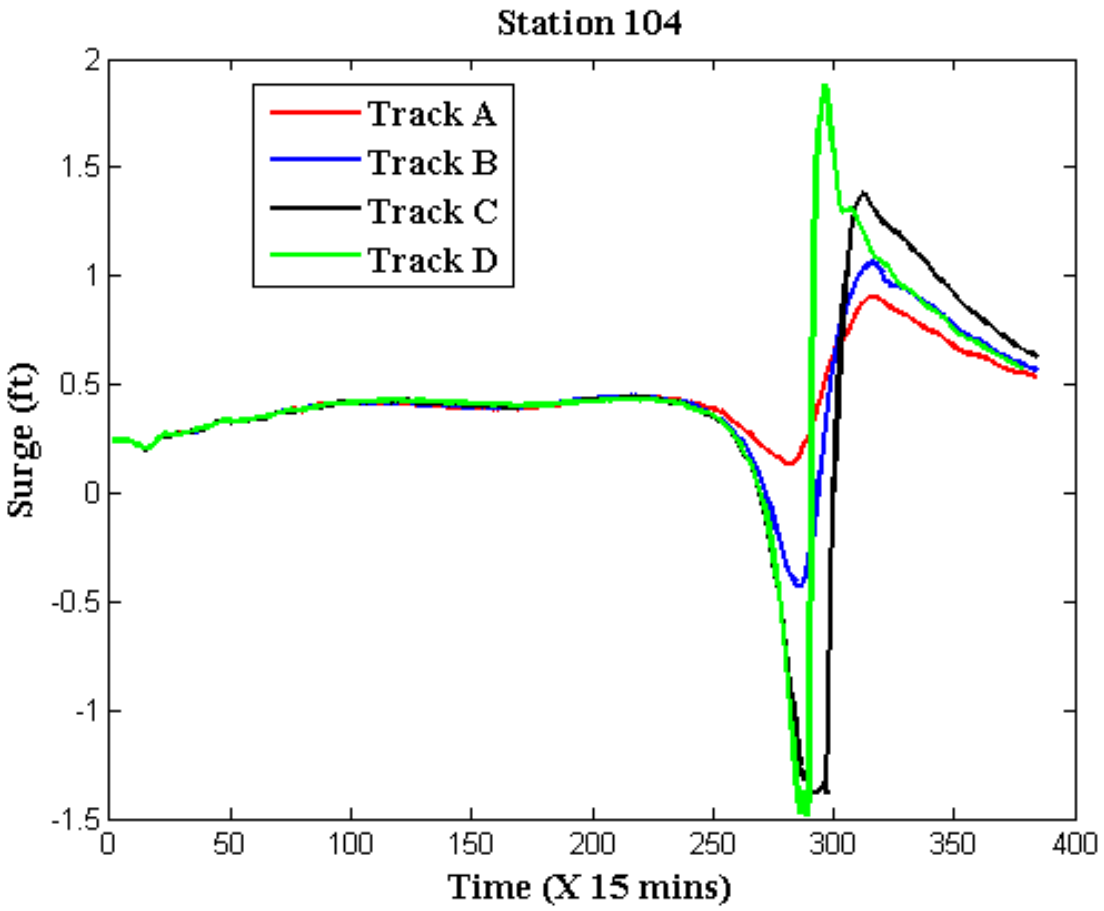

Figure 27 Time series for station 104, Matagorda Bay

Figure 26 and Figure 27 show time series for the storm (R_p=15Km and intensity=960mb) on track A, B, C and D at station 69 and station 104 in Matagorda Bay. For both stations peak surge values for Track A, B, and C (Figure , all on west side of center of gravity of bay) occurs at the same time, while that of Track D (on east side of center of gravity) is shifted slightly in time but does not appear to be significantly

different from trend. Thus, it can be assumed that to the first order, timing of peak surge does not affect the surge response inside the bay.

CHAPTER VI

SRFS METHODOLOGY AND APPLICATION

6.1 Introduction

In this chapter, SRFs inside Matagorda Bay are discussed. The SRFs are based upon the parameters discussed in Chapter V. The approach developed for SRFs in Matagorda Bay is validated by applying this formulation for SRFs in Galveston and Corpus Christi Bays. As shown in the previous Chapter, the Center of Gravity and the non-dimensional surge for open coast are important factors for peak surge distribution inside a bay while the timing of peak surge, inlet width and channel location inside a bay, to the first order, does not affect peak surge distribution inside a bay. In the following section, a methodology for SRFs in Matagorda Bay is defined based upon four tracks (A, B, C, D) as shown in Figure 28.

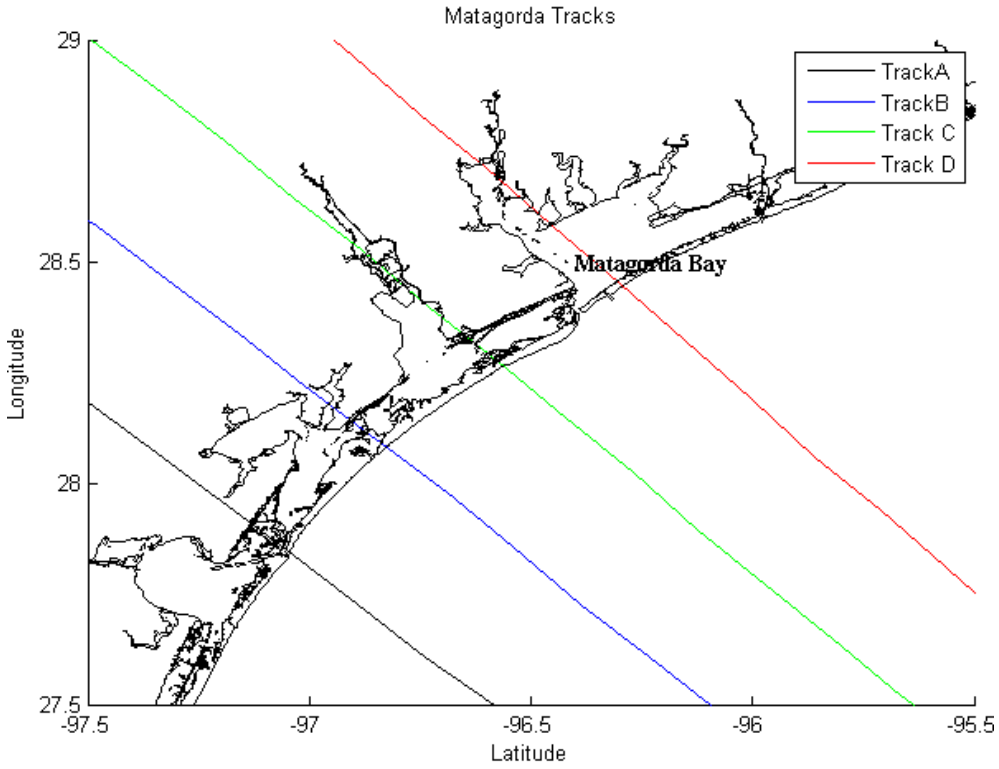

Figure 28 Matagorda Bay Tracks

6.2 SRFs for Matagorda Bay

Features of Matagorda Bay have been discussed in Chapter III. Based upon the factors described in the previous chapter and analysis at 128 stations (Figure 3) in Matagorda Bay using 76 storms on tracks A, B, C, D (Figure 28), the following non-dimensional quantities for SRFs inside Matagorda Bay is proposed.

Non-dimensional surge(ξ), which is given as

$$\xi' = \frac{\gamma\xi}{\Delta p} + m_\chi \Delta p + F(\Delta p, R_p, \xi, S_b) \tag{6.1}$$

The first two terms on the right hand side of equation are the same as that defined for the open coast SRFs. While $\mathrm{F}(\Delta p, \mathrm{R_p}, \xi, S_b)$ is a function of intensity, storm size, surge at the station due to the storm and size of bayS_b. It is defined as

$$\mathrm{F}(\Delta p, \mathrm{R_p}, \xi, S_b) = \begin{cases} \xi c R_p & for\ \frac{\Delta p}{\gamma} < 0.9m\ \&\ R_p > S_b \\ 0 & \text{Otherwise} \end{cases} \quad (6.2)$$

where,

S_b is characteristic size of a bay.

c is a constant determined to be 0.03/m^2 for Matagorda Bay.

Thus, the main difference in the non-dimensional surge for inside the bay and the open coast is that, that for inside a bay, for storms which are larger in size than that of characteristic size of bay and have intensity such that Δp is greater than 0.9, there is an extra term $\xi c R_p$ added to non-dimensional surge for open coast.

Non-dimensional distance(X'), defined as

$$X' = \frac{X_c}{R_p} + \frac{S_b}{X_c} - \boldsymbol{\lambda} + F(\Delta p, R_p, S_b) \quad (6.3)$$

where

X_c is the minimum distance between the Center of Gravity of a bay and the eye of storm as storm passes by the bay.

F (Δp, R_p, S_b) is a function based upon the size of storm, size of bay and intensity of storm and is defined as

$$\text{F}(\Delta p, R_p, S_b) = \begin{cases} \dfrac{(\Delta p - 82.5)}{(0.1 \times S_b \times \gamma)} & \text{for, } R_p < S_b \\ \dfrac{(\Delta p - 82.5)}{(0.1 \times S_b \times \gamma)} & \text{for } \Delta p > 82.5\text{mb \& } R_p > S_b; \\ \dfrac{(82.5 - \Delta p)}{(0.1 \times S_b \times \gamma)} & \text{for } \Delta p < 82.5\text{mb \& } R_p > S_b; \end{cases} \qquad (6.4)$$

Plots between the non-dimensional surge and the non-dimensional distance at stations inside Matagorda Bay are shown in Figure 29 through Figure 32.

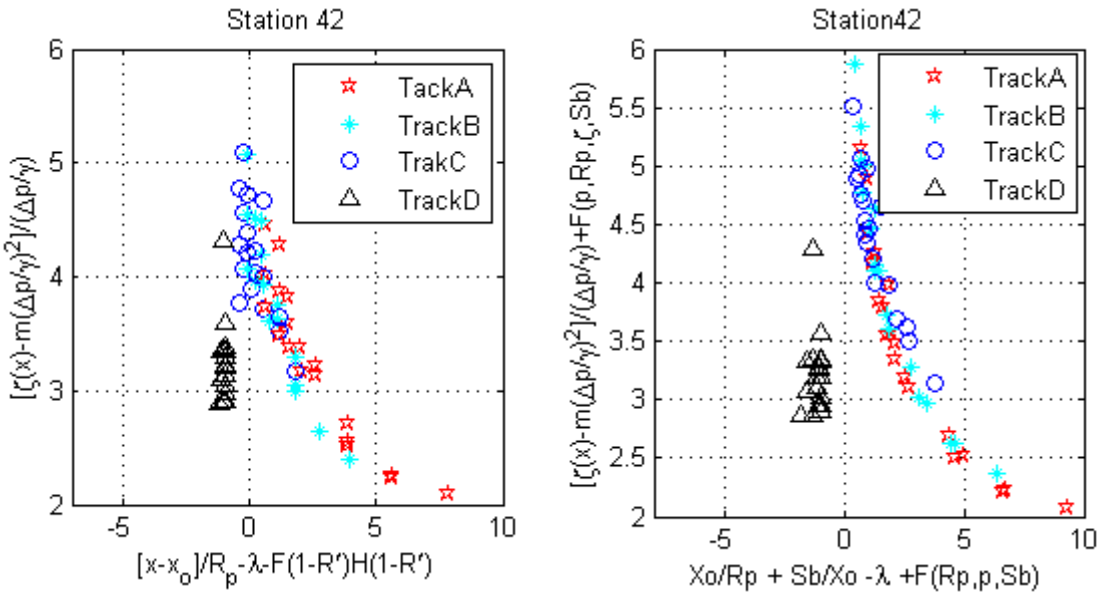

Figure 29 Open coast methodology (left plot), Inside bay methodology (right plot) Matagorda station 42

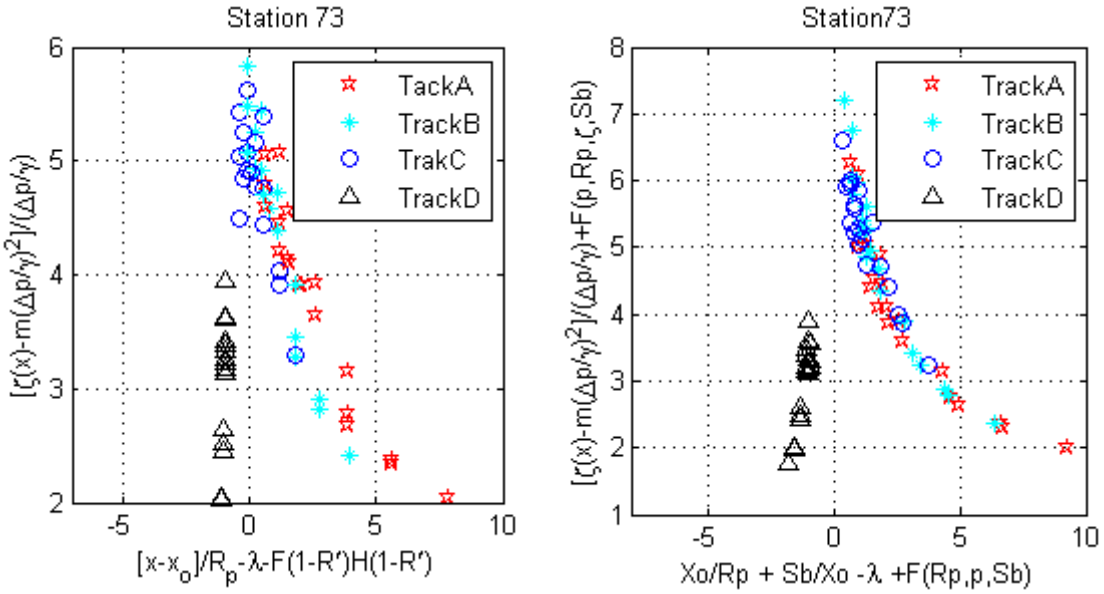

Figure 30 Open coast methodology (left plot), Inside bay methodology (right plot)

Matagorda station 73

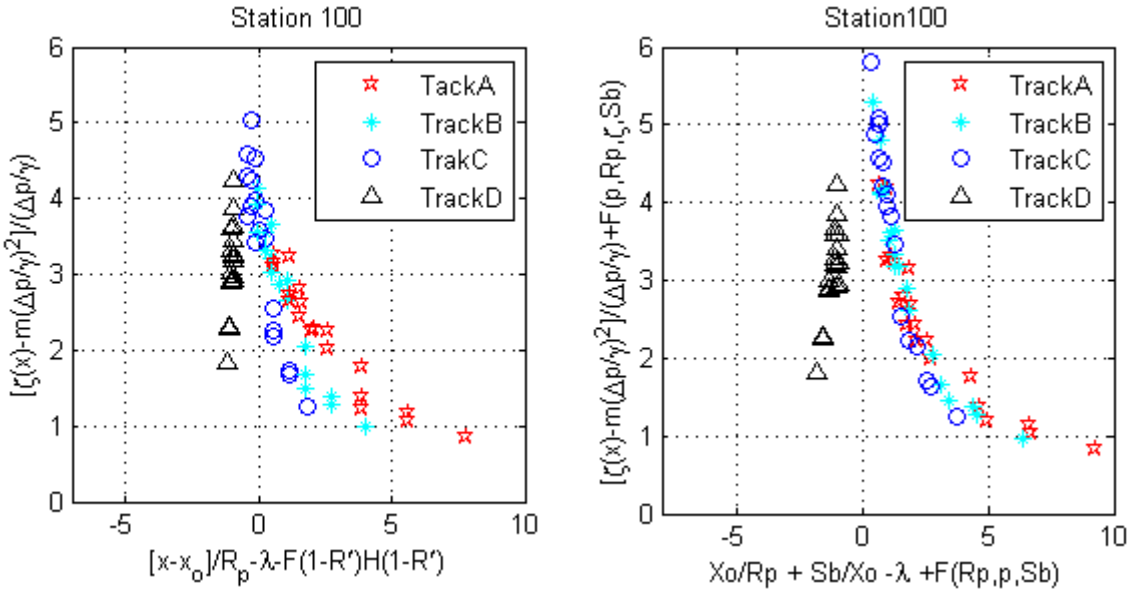

Figure 31 Open coast methodology (left plot), Inside bay methodology (right plot)

Matagorda station 100

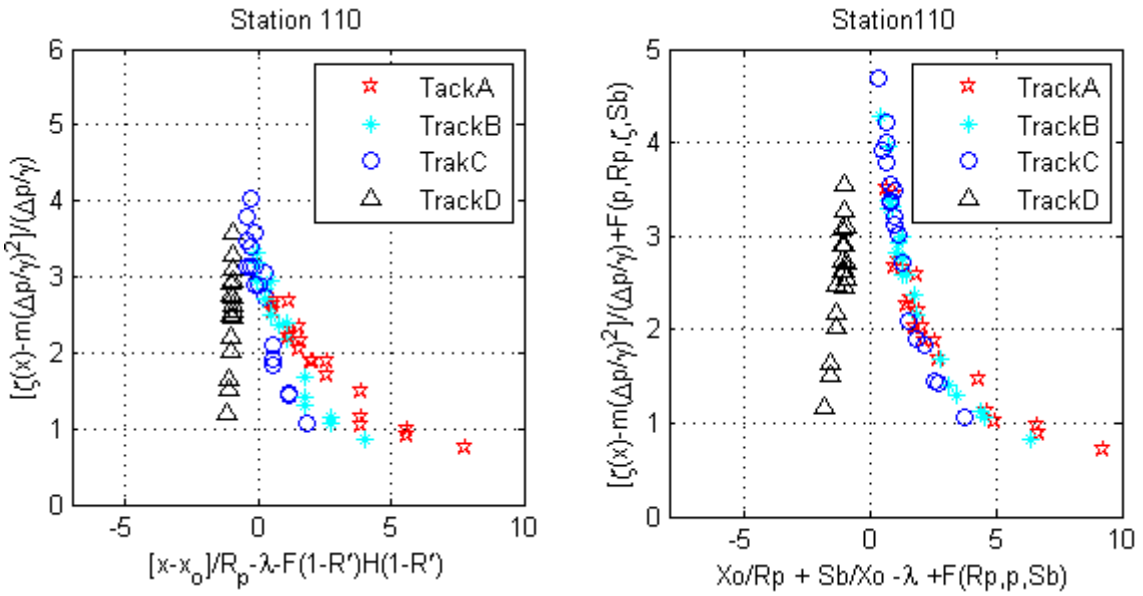

Figure 32 Open coast methodology (left plot), Inside bay methodology (right plot) Matagorda station 110

For Figure through Figure 32, left-hand side shows the non dimensional relationship obtained for bay locations based upon the open coast methodology while the right-hand side shows the non-dimensional relationship for bay stations based upon the new methodology developed for Matagorda Bay. With the open coast methodology we get scatter in the non-dimensional plots which can be attributed to factors like relative size of storm to the size of bay, intensity of the storm and relative location of the storm with respect to center of gravity of the bay. In contrast, with new methodology developed for Matagorda Bay scatter in non-dimensional plots reduced considerably. Thus, with the new methodology SRFs can be predicted more accurately. The non-dimensional surge (ξ') and non dimensional distance (x') at a station are curve fitted using the function of the form:

$$\xi' = a_1 \times \exp\left(-\left(\frac{x'-b_1}{c_1}\right)^2\right) + a_2 \times \exp\left(-\left(\frac{x'-b_2}{c_2}\right)^2\right) + a_3 \times \exp\left(-\left(\frac{x'-b_3}{c_3}\right)^2\right) + a_4 \times \exp\left(-\left(\frac{x'-b_4}{c_4}\right)^2\right) \quad (6.5)$$

The coefficients $(a_1, b_1, c_1, a_2, b_2, c_2, a_3, b_3, c_3, a_4, b_4, c_4)$ at station is determined using linear regression analysis. The number of Gaussian term used at a station varies from station to station. Figure 33 through Figure 40 show the Curve fit to the non-dimensional surge and non-dimensional distance data and comparison between the simulated and SRF predicted surge at station locations 42, 73, 100, and 110.

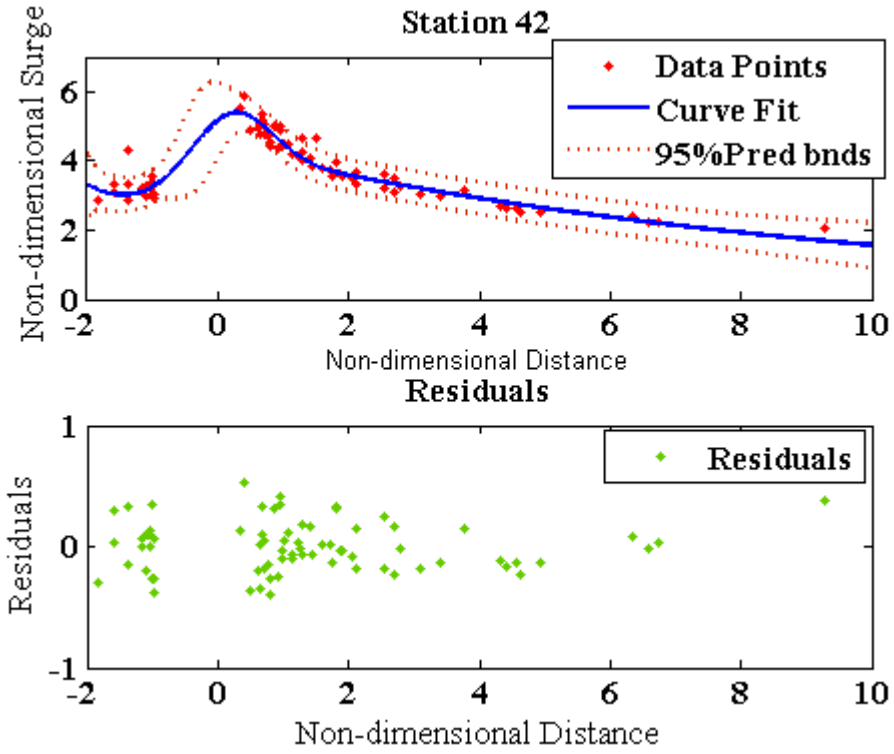

Figure 33 SRF for station 42, R-square = 0.93

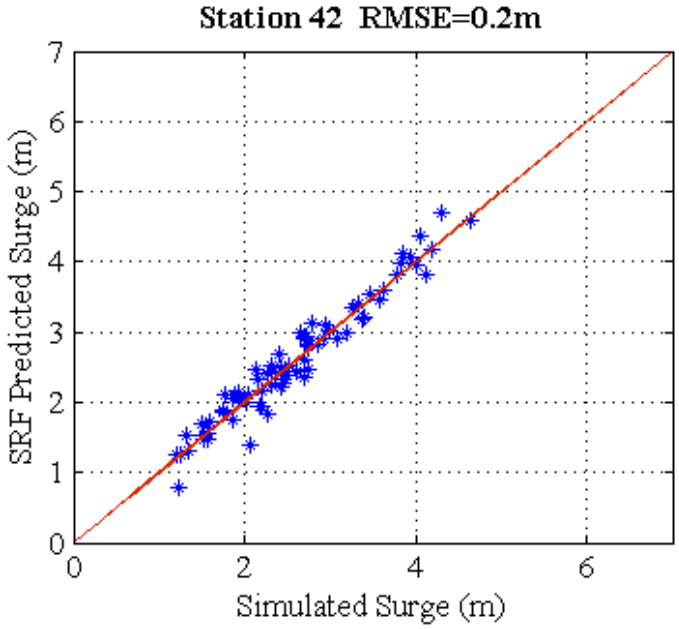

Figure 34 Simulated vs SRF predicted

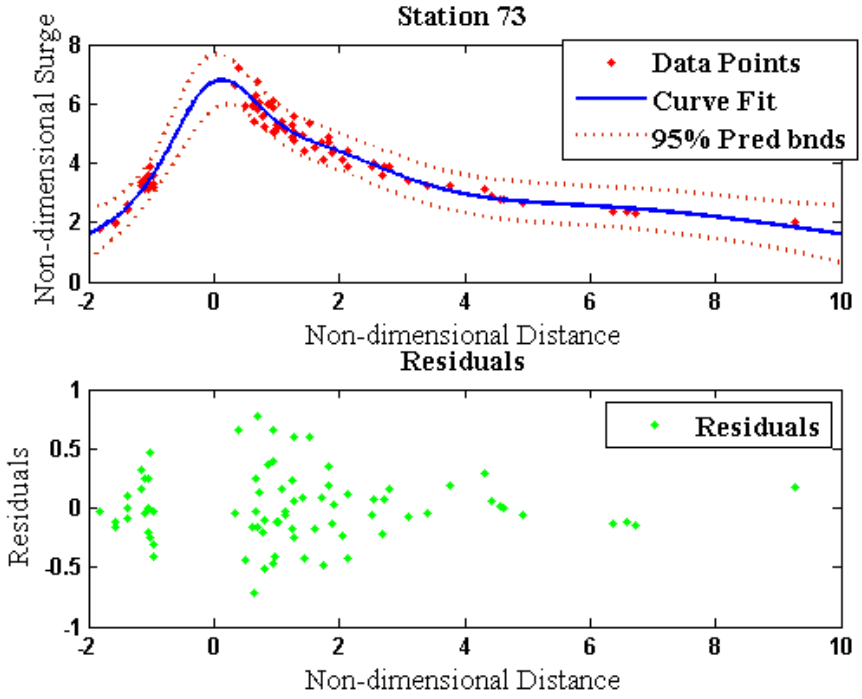

Figure 35 SRF for station 73, R-square = 0.95

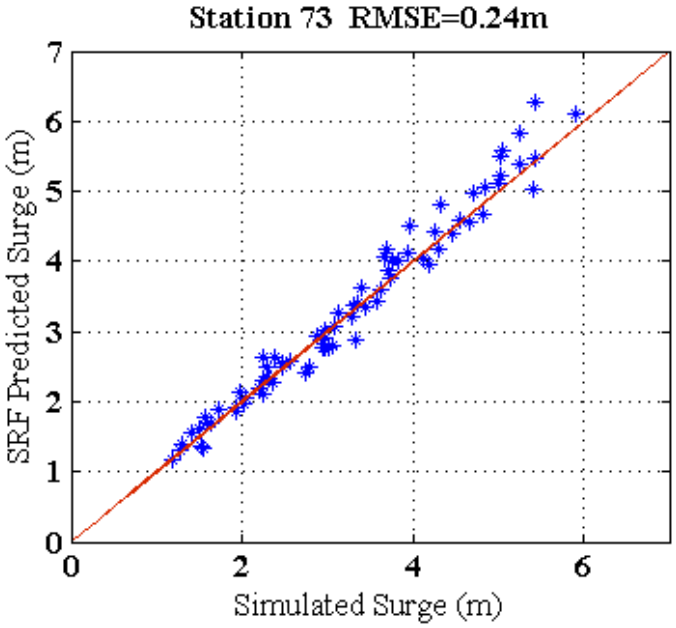

Figure 36 Simulated vs SRF predicted

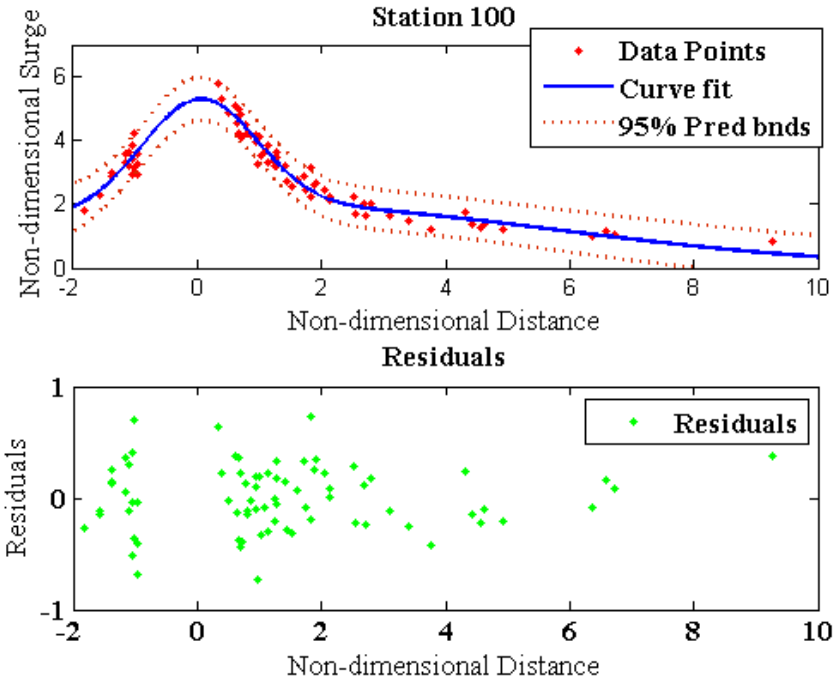

Figure 37 SRF for station 100, R-square 0.93

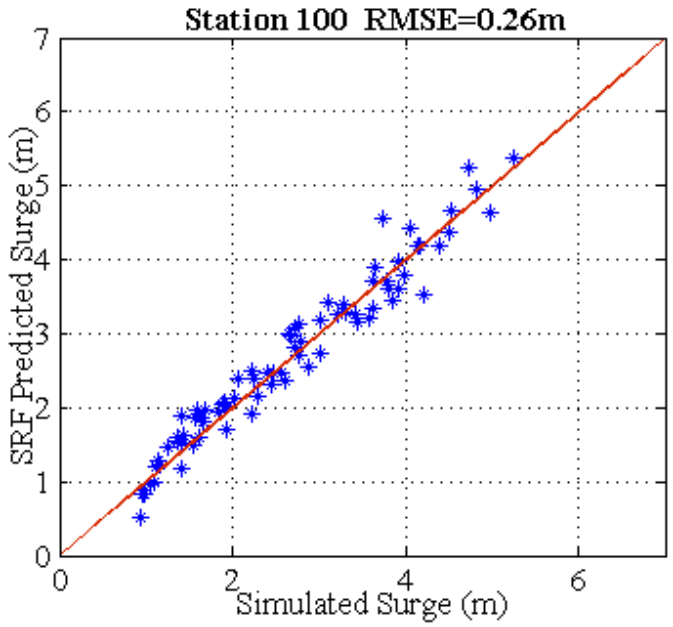

Figure 38 Simulated vs SRF predicted

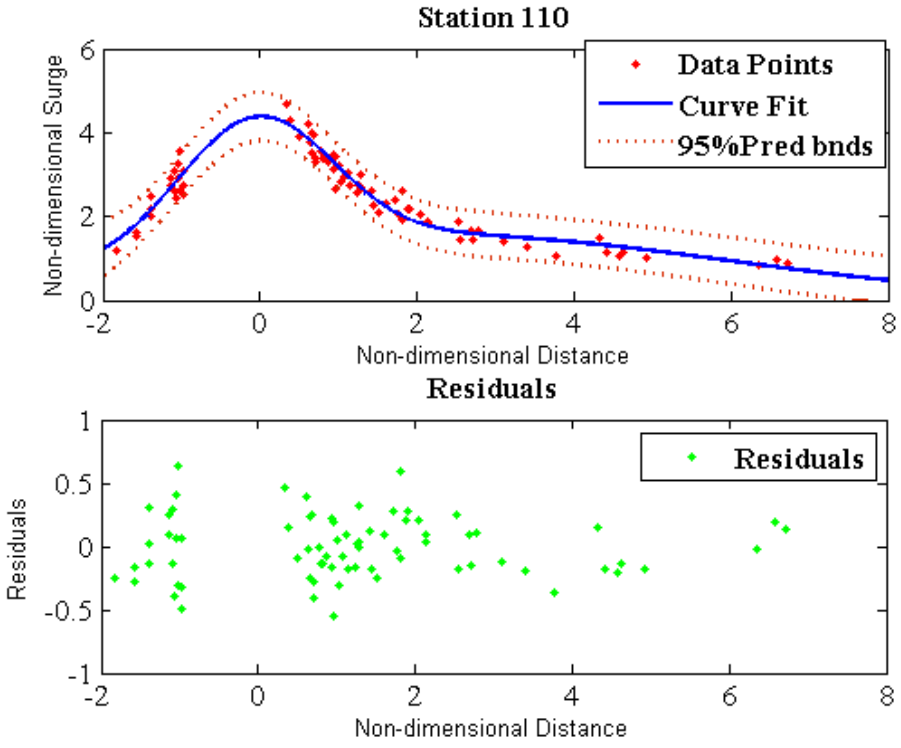

Figure 39 SRF for station 110, R-square 0.93

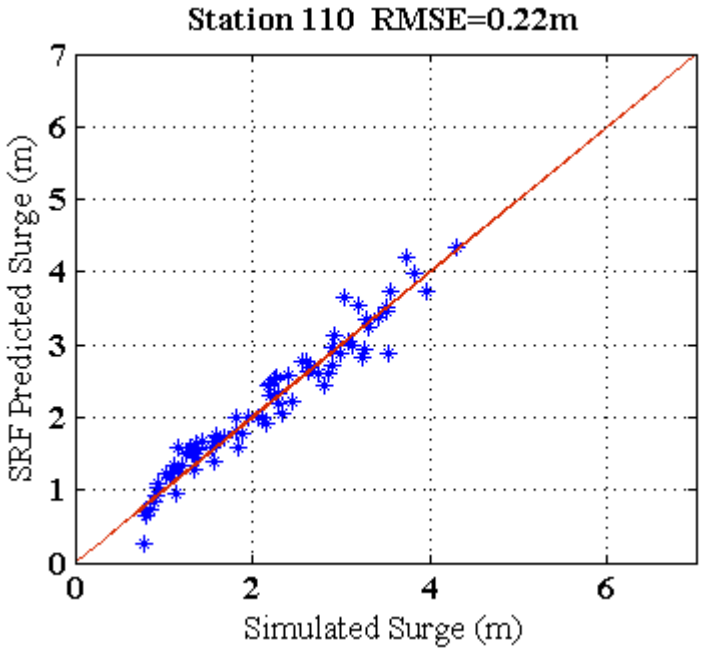

Figure 40 Simulated vs SRF predicted

These plots show the 95% prediction bounds for the Curve fit. As is clear from the figures most of the simulation results lie within 95% confidence interval. Figure 33 through Figure 40 also shows the residual (non-dimensional predicted surge – non-dimensional simulated surge) plots for the fit. As is clear from the residual plots there is random scatter about the zero line, thus there is no bias in predicted SRFs. With the open coast methodology, R-square values for SRF is approximately 0.67 as compared to 0.91 using the new methodology. R-square value for the Curve fit at Matagorda stations lies in 0.91 to 0.97. The plots also show the comparison between simulated surge and the surge predicted by SRF. Root Mean Square Error (RMSE) for Matagorda Bay is between 0.2 to 0.28 m as compared to RMSE of 0.52 to 0.64 m with open coast methodology. The plots also show that in region where non-dimensional distance is zero,

we do not have simulations results. Thus to define SRF in this region we need to have more simulations.

6.3 Application to Galveston

Features of Galveston Bay have been discussed in Chapter III. Based upon the SRF methodology developed for Matagorda Bay, SRFs for 159 stations inside Galveston Bay are developed using 5 tracks (Aa, Ab, Ac, Ad, Ae) shown in Figure 41 with total of 30 storm simulations on them with R_p value varying from 5 to 35 km and the intensity of storm varying from the 900mb to 960mb.

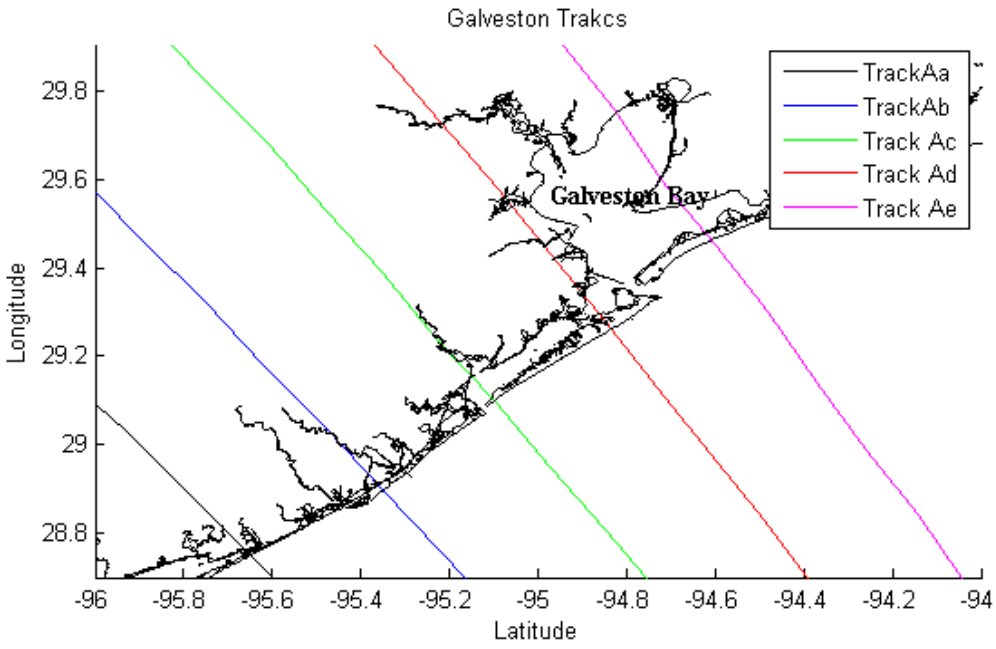

Figure 41 Galveston Bay Tracks

The parameters which changes for Galveston bay compared to Matagorda Bay for applying the SRF methodology inside Galveston bay are

- Center of gravity of bay
- Size of bay (20Km)
- Lambda value =0.99 (based upon the Song 2009)
- Constant c ($0.05/m^2$)

Figure 42 through Figure 47 show the non-dimensional relationship developed for Galveston Bay using 30 storms on five tracks (Aa, Ab, Ac, Ad, Ae).

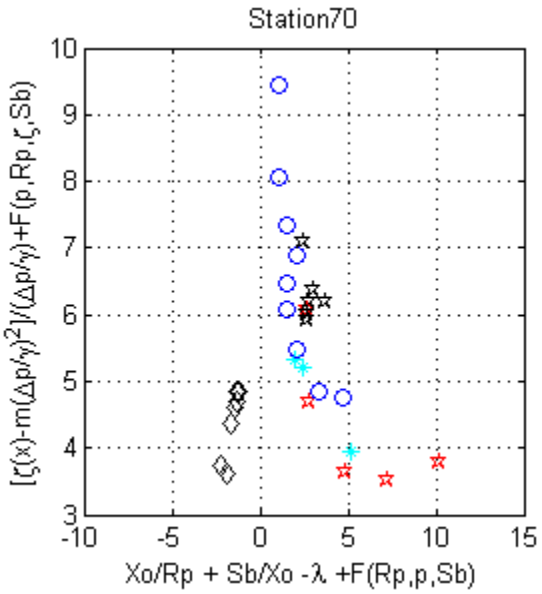

Figure 42 Non-dimensional Plot Galveston station 70

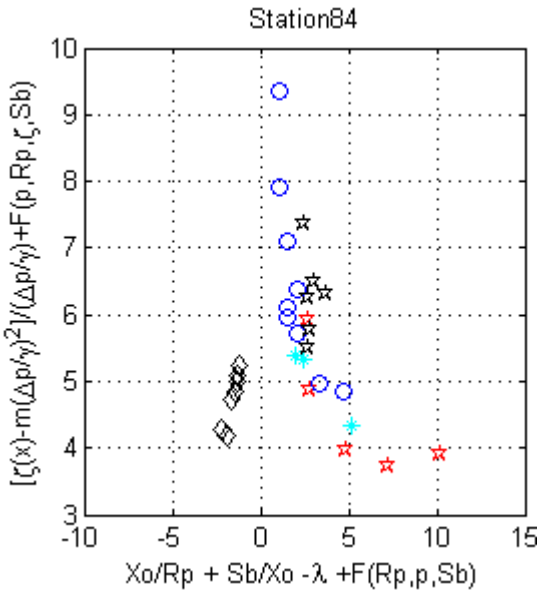

Figure 43 Non-dimensional plot Galveston station 84

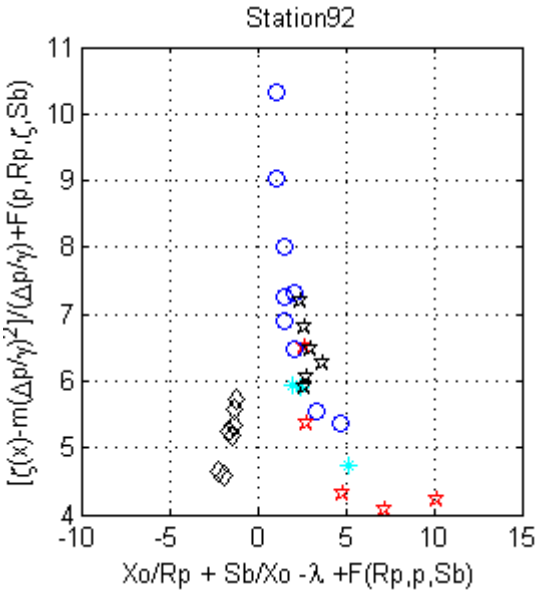

Figure 44 Non-dimensional Plot Galveston station 92

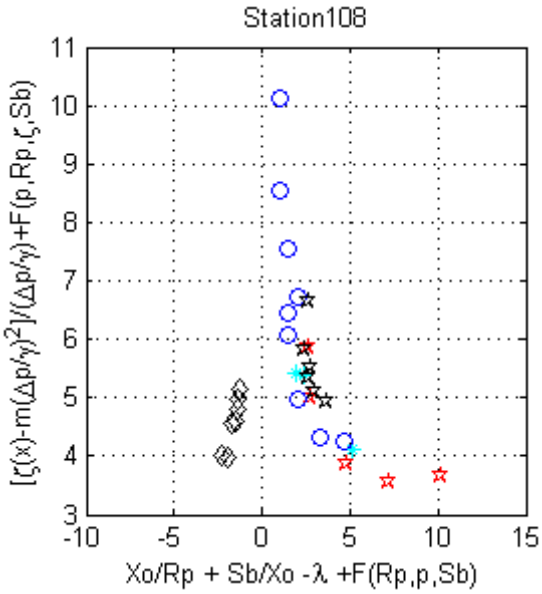

Figure 45 Non-dimensional Plot Galveston station 108

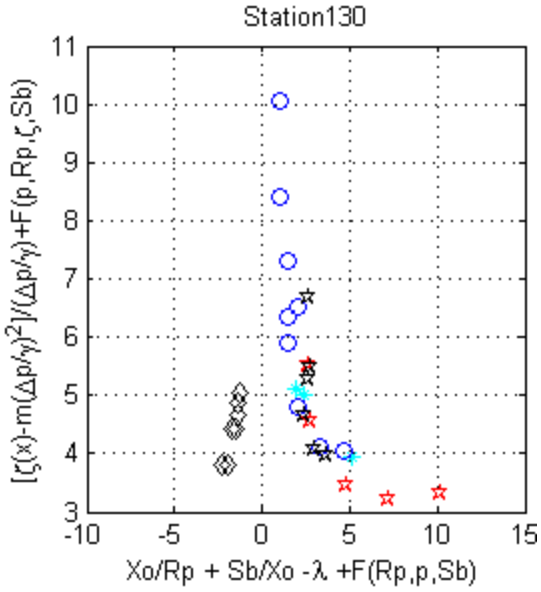

Figure 46 Non-dimensional Plot Galveston station 130

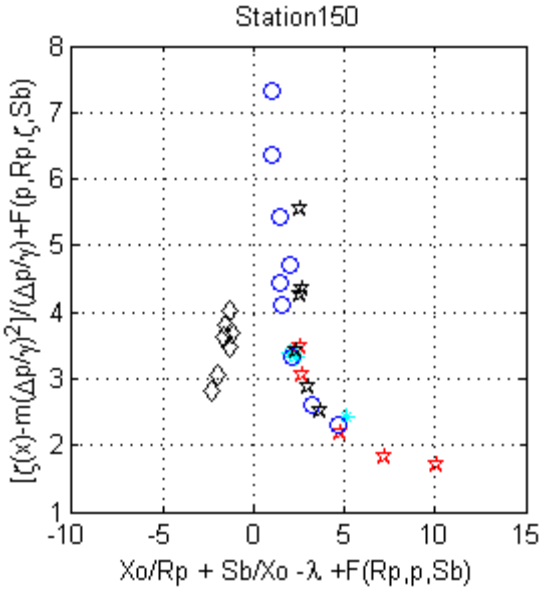

Figure 47 Non-dimensional Plot Galveston station 150

As is clear from Figure 42 through Figure 47, the methodology developed for the Matagorda Bay works well for the Galveston region. Figure 48 and Figure 50 show the curve fit to the data at locations 92 and 108 in Galveston Bay based upon the Curve fit.

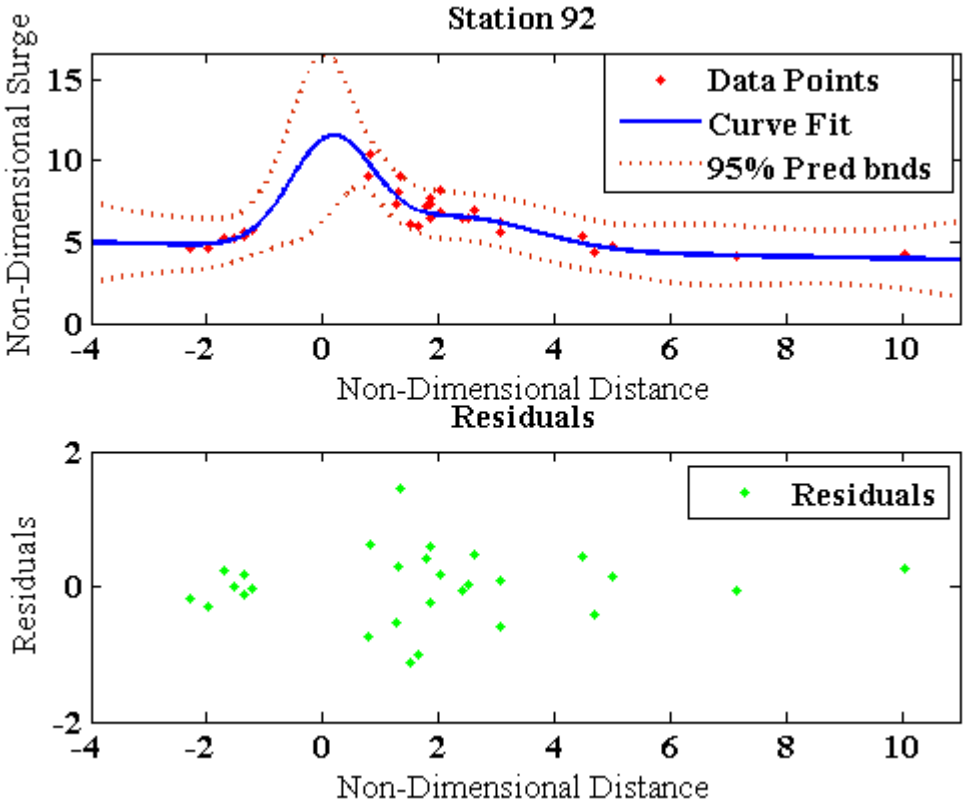

Figure 48 SRF for station 92, R-square 0.82

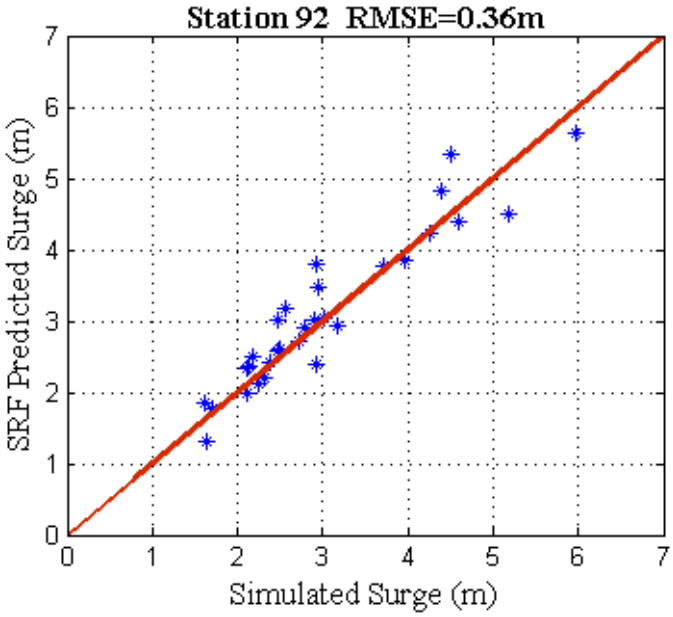

Figure 49 Simulated vs SRF predicted

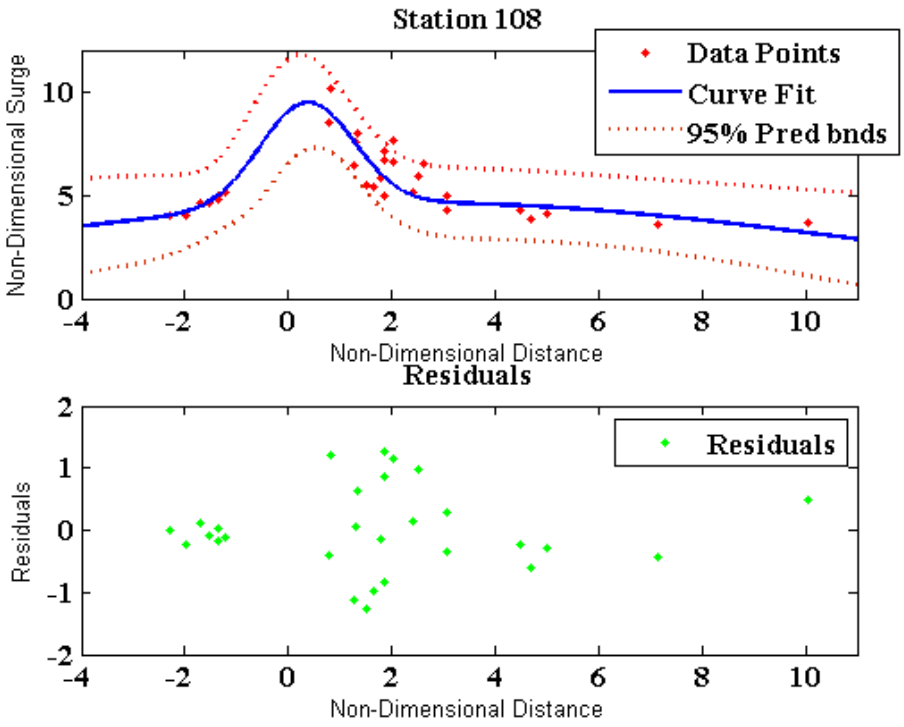

Figure 50 SRF for station 108, R-square 0.82

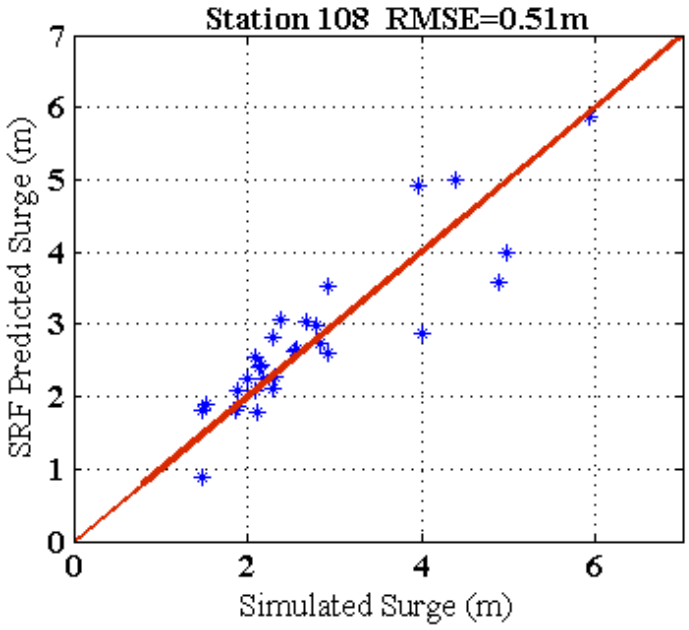

Figure 51 Simulated vs SRF predicted

The plots show the predicted SRFs, 95% prediction bound for SRFs and the comparison between the SRF predicted surge and the simulated surge. Except one simulation at station 108 all of the simulations results are within the 95% prediction bound. Residuals plots shows scatter around zero which shows that the fit is unbiased. R-square values for Curve fit at Galveston bay lies in 0.81 to 0.88. The R-square value for Galveston is lower than that of Matagorda Bay, thus the fit in this region is not as good as Matagorda Bay. The Figure 49 and Figure 51 show comparison between simulated storm surge values and the SRF predicted surge. RMSE for Galveston Bay is between 0.30m to 0.57m. RMSE at Galveston is higher than that of Matagorda Bay; this can be attributed to the bigger size of bay and the variation in the continental shelf width which has not been taken into account. Also we need to have more data in region where non-dimensional distance approaches zero to define SRFs more accurately.

6.4 Preliminary Application to Corpus Christi

A contour map and the key features for Corpus Christi are discussed in chapter III. Here we will apply the methodology developed for Matagorda Bay to Corpus Christi Bay. The key parameters which change for Corpus Christi bay are

- Center of gravity of bay
- Size of Bay (10Km)
- Lambda value=0.74 (based upon the Song 2009)
- Constant c ($0.01/m^2$)

Tracks considered for Corpus Christi bay are tracks A and track B, which are same as that for Matagorda Bay. Figure 52 shows the position of the tracks A and B with respect to the Corpus Christi Bay.

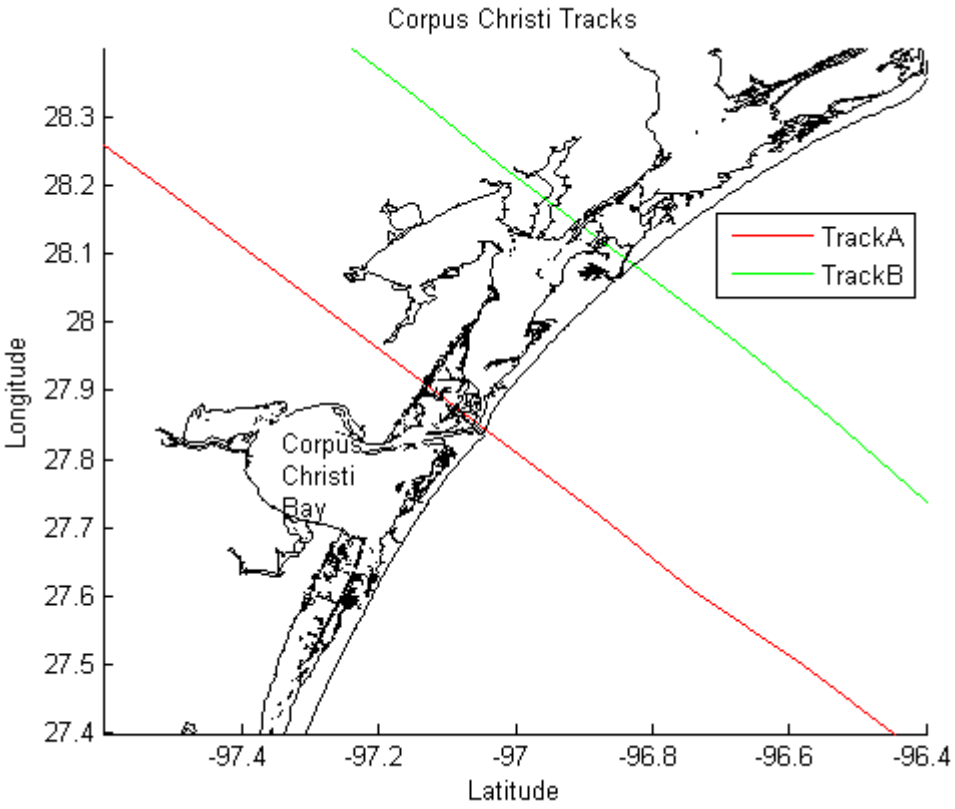

Figure 52 Corpus Christi Bay Tracks

Figure 53 through Figure 56 shows non dimensional plots at station 56, 67, 84, 95 for Corpus Christi. The methodology works well in Corpus Christi for Tracks A and B as simulations collapse on to a single function.

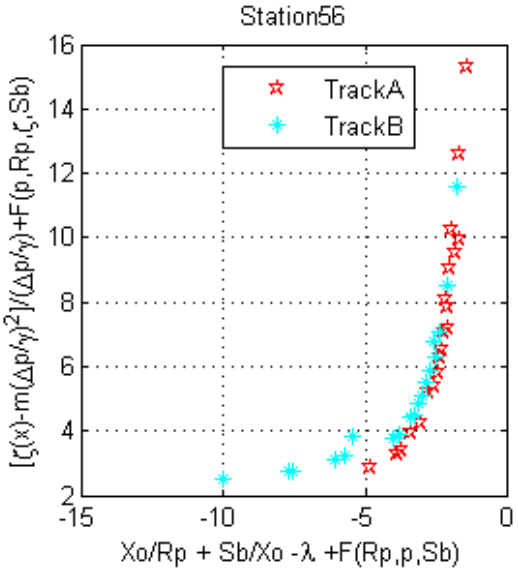

Figure 53 Non-dimensional Plot Corpus Christi station 56

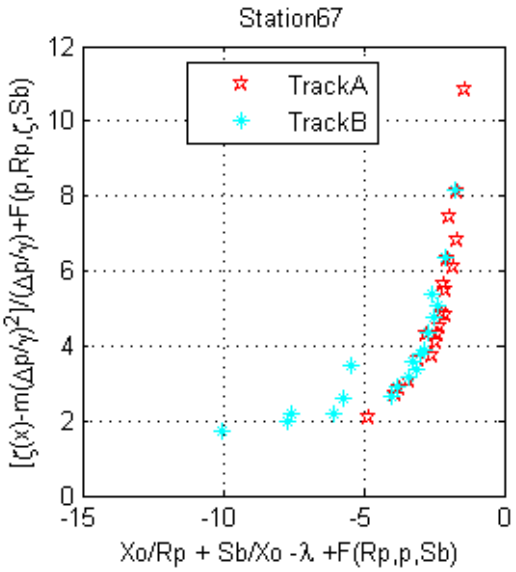

Figure 54 Non-dimensional Plot Corpus Christi station 67

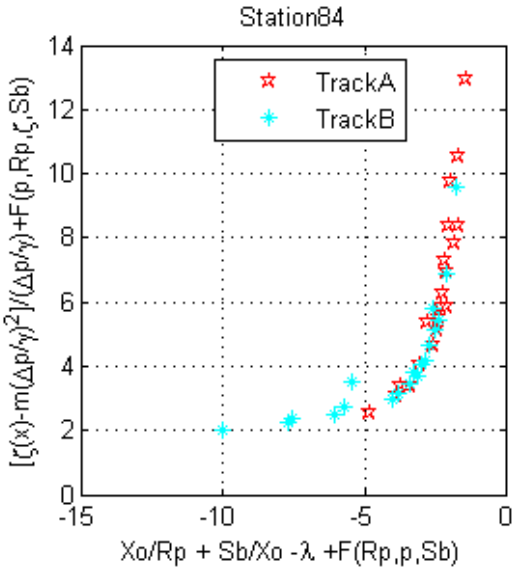

Figure 55 Non-dimensional Plot Corpus Christi station 84

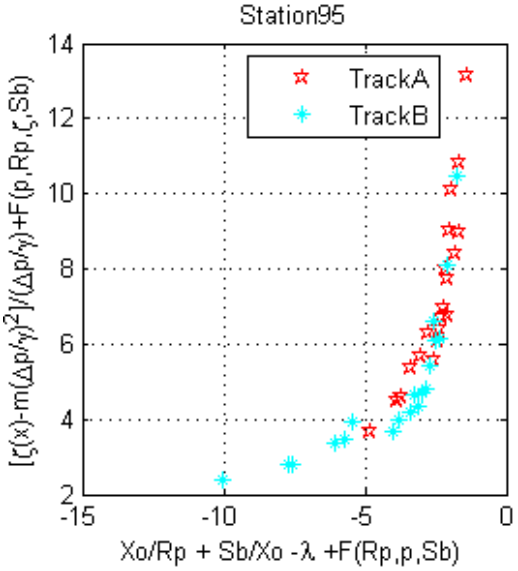

Figure 56 Non-dimensional Plot Corpus Christi station 95

The SRFs for Corpus Christi show promising results, but to generate the SRFs for positive non-dimensional distance, more simulation on tracks towards the west side of Corpus Christi needs to be added. Figure 57 to Figure 60 shows the curve fit to non dimensional data and comparison between the SRF predicted surge and the simulated surge for selected Corpus Christi Bay location.

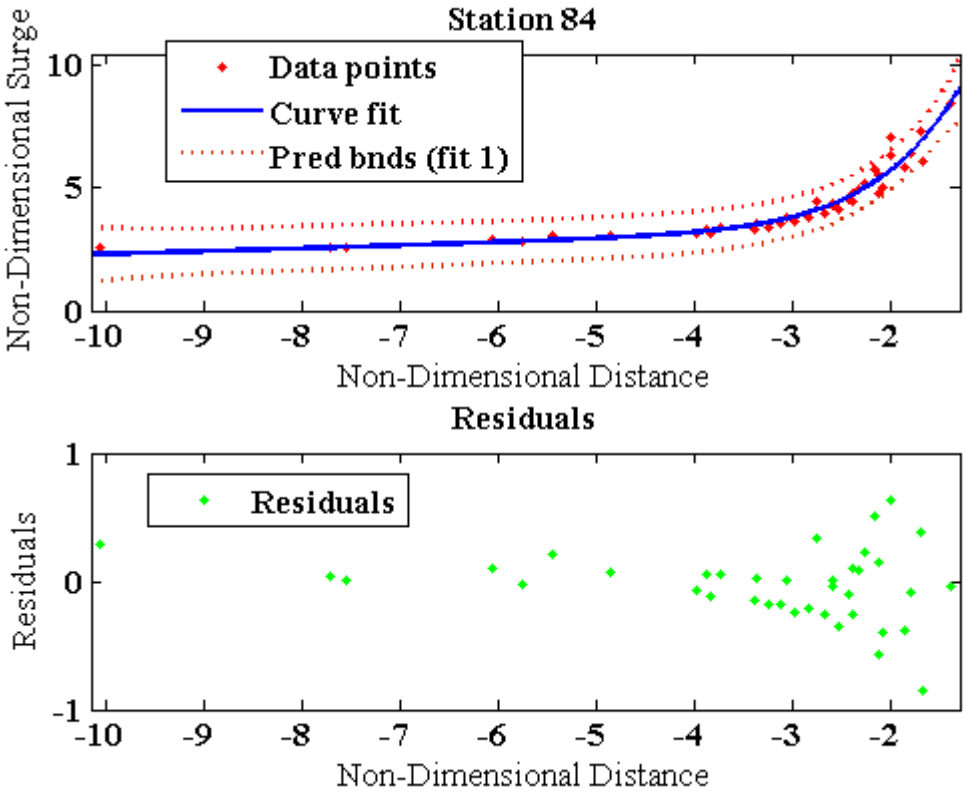

Figure 57 SRF for station 84, R-square 0.94

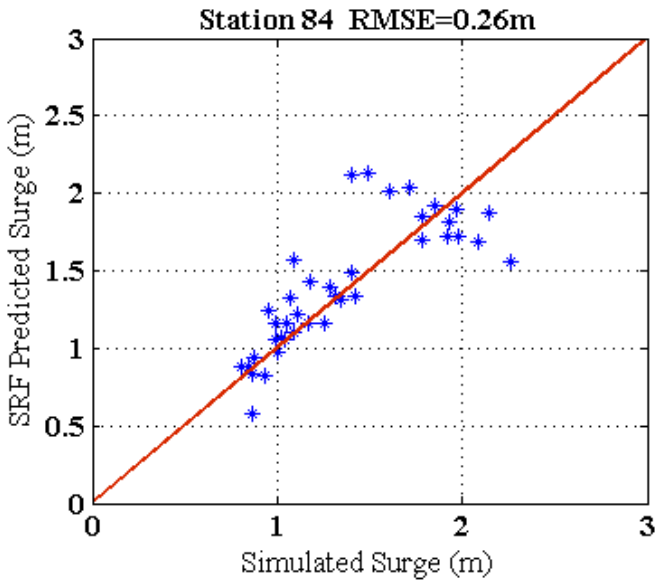

Figure 58 Simulated vs SRF predicted

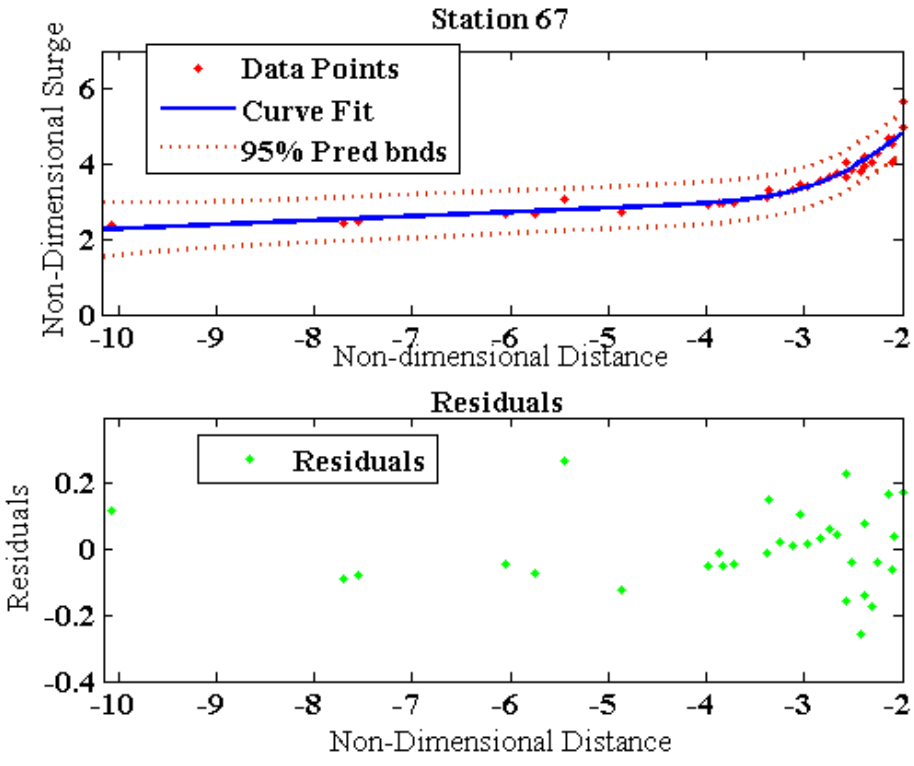

Figure 59 SRF for station 67, R-square 0.95

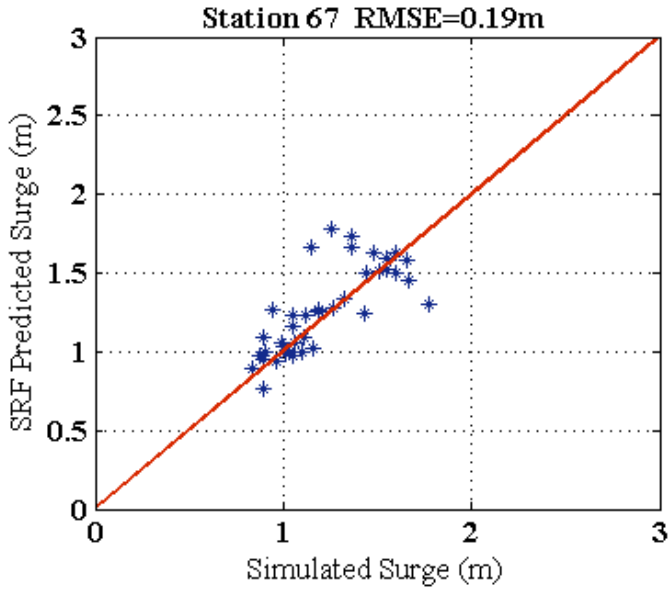

Figure 60 Simulated vs SRF predicted

SRFs predicted for Corpus Christi work well for track A and B as all simulation lies in 95% prediction bound. The residual plots have a scatter around the zero, which shows for unbiased fit. R-square value for Curve fit at Corpus Christi Bay stations lies in range of 0.92 to 0.97, which is comparable to that of Matagorda Bay. Figure 58 and Figure 60 show the comparison between simulated and SRF predicted surge values at station 84 and 67 inside Corpus Christi Bay. The values lies close to the bisection line (y=x), expect for region where non-dimensional value approaches zero. This can be attributed to fact that we did not consider any track on right hand side of zero in non-dimensional plot. Thus fit in this region is not accurate. Thus more simulations on tracks to the south side of Corpus Christi are required to predict SRFs completely. The RMSE between SRFs predicted and simulated surge values for Corpus Christi stations lie in range of 0.17 to 0.32.

CHAPTER VII

SUMMARY AND DISCUSSION

In this thesis, development of SRFs for bays has been explored. The importance of various relevant parameters for SRFs is determined. As shown in Chapter V, storm surge inside bays is not affected by a location of channel, timing of surge, and inlet width. Also, surge inside the bay is correlated with the center of gravity of bay, characteristic size of bay, intensity of storm, and size of storm. Based upon these parameters non-dimensional distance and surge values are defined, these non-dimensional quantities are used to predict the Surge Response Functions inside Matagorda Bay. The methodology developed for predicting SRFs for Matagorda Bay shown to have worked inside Galveston and Corpus Christi Bay. Although RMSE error for Galveston Bay is higher as compared to Matagorda Bay, but the methodology developed gives the general trend for storm surge values. For Corpus Christi Bay, RMSE is comparable with RMSE of Matagorda bay. It should be noted that for predicting SRFs at Corpus Christi more storms towards south side of Bay should be considered.

Also, for three bays most of simulated results lie in 95% confidence interval. R-square values for Curve fit at Matagorda and Corpus Christi Bay are identical with values between 0.9 to 0.97, while at Galveston Bay R-square values are relatively lower with R-square values between 0.78 - 0.88. Also based upon this we have seen higher RMSE at Galveston Bay compared to Matagorda or Corpus Christi Bay.

Also, for non-dimensional surge inside the bay, the value of constant ‘c’ has been varied for three bays. Corpus Christi has c=0.05, Matagorda Bay c=0.03 and for Galveston c=0.01. This can be attributed to change in continental shelf width as one move from Corpus Christi to Galveston Bay. The values for λ based upon open coast work (song 2009) have worked well for inside bays also.

Comparison of SRFs (open coast, Irish and Resio 2009) with SLOSH Model data base is also presented. While SLOSH model gives one value of surge for a given category of storm, SRF approach gives range of values based upon the landfall location, intensity and size of storm.

Thus SRFs methodology developed for Matagorda Bay has shown promising results in both Galveston and Corpus Christi Bay. Thus, this method can be used to predict the surge levels in the bay with accuracy defined for 3 bays in earlier chapters. The values of ‘c’ proposed here for 3 bays seems to be related to the continental shelf width, but more work needs to be done to find the exact relation between the constant ‘c’ and the shelf width. To define the SRFs in the region where non-dimensional distance approaches zero (Maximum value for SRF), more simulation results are required for all three bays. To further improve SRFs inside bays, parameters like track angle and forward speed of storm should be considered and the response of bay to these changes should be studied.

REFERENCES

Cardone,V.J, Greenwood C.V., Greenwood J.A. (1992) "Unified program for the specification of the hurricane boundary winds over surface of specified roughness" CERC 92-1, U.S Army Engrs, Wtrwy, Experiment Station, Vicksburg, Miss.

Cardone V.J.,Cox A.T., Greenwood J.A., and Thompson E.F 1994, "Upgrade of tropical cyclone surface wind field model." CERC 94-14, U.S Army Engrs, Wtrwy, Experiment Station, Vicksburg, Miss.

Dean, R.G. and Dalrymple, R. A. (2002) Water Wave Mechanics for Engineers and Scientists. *Advanced Series on Ocean Engineering*, Volume 2. World Scientific Publishing Co., Hackensack, NJ.

FEMA "Hurricane Hazards" accessed on 8th July 2009 [http://www.fema.gov/hazard/hurricane/hu_hazard.shtm]

Gray, W. G. (1982). "Some inadequacies of finite element models." *Adv. WaterResources,* 5(September), 171-177.

Greenberg, D. A., Dupont, F., Lyard, F. H., Lynch, D. R., and Werner, F.E. (2007). "Resolution issues in numerical models of oceanic and coastal circulation." *Continental Shelf Research*, 27, 1317-1343.

Irish, J.L., and Resio, D.T. (2009) "A hydrodynamics-based surge scales for hurricanes." *Ocean Eng*., in press.

Irish, J. L., Resio, D. T., and Cialone, M. A. (2008a). "A surge response function approach to coastal hazard assessment—Part 2: Quantification of spatial attributes of response functions." *Nat Hazards,* 10.1007/s11069-009-9381-4.

Irish, J. L., Resio, D. T., and Ratcliff, J. J. (2008b). "The influence of storm size on hurricane surge." *J. Phys. Oceanogr.*, 38(9), 2003-2013.

Luettich, R.A., Westerink, J. J., and Scheffner, N.W. "ADCIRC: An advanced three dimensional circulation model for shelves, coasts, and estuaries: Report 1: Theory and Methodology of ADCIRC-2DDI and ADCIRC-3DL," *Technical Report DRP-92-6*, US Army Corps of Engineers, Washington, DC.

Mark, D.J. and Scheffner N.W.(1993) " Validation of continental scale storm surge model for the coast of Delaware." *Proc. of Estuarine and Coast. Modeling Conference,* ASCE., New York, 249-263.

NOAA. (Unknown) "Hurricane Preparedness" accessed on 6th March 2009.

[http://www.nhc.noaa.gov/HAW2/english/intro.shtml]

Older, M.E. (1981) “A two-dimensional finite-element advection model with variable resolution.” M.Sc. Thesis. Naval Post Graduate School Report ADA107511: Monterey, CA.

Pritchard, D.W. (1971) “The movement and mixing of contaminants in tidal estuaries”. E.A. Pearson, ed. Proceedings of the First International Conference on Waste Disposed in the Marine Environment, Pergamon Press, Oxford, MA 512–525.

Provost, C.L, Le, Bernier.C, and Balyo.E, (1994). “A comparison of two numerical methods for integrating a quasi-geotropic multilayer model of ocean circulations: Finite element and finite difference method” *Computational Physics* 110, 341-359.

Resio, D. T. and Irish, L. J. (2009). "A surge response function approach to coastal hazard assessment. Part 1: Basic concepts." *Nat. Hazards*, 10.1007/s11069-009-9379-y

Song, Y.K (2009) “Extreme hurricane surge estimation for Texas coastal bridges using dimensionless surge response functions.” M.S. Thesis, Texas A&M University College Station.

Taylor, A and Berger, H. (2008) “SLOSH display package” Evaluation Branch, Meteorological Department Lab, NOAA, U.S Dept of Commerce. *SLOSH Display CD* 20th June 2008.

Thompson, E. F., and Cardone, V.J. (1996). "Practical modeling of hurricane surface wind fields." *Journal of Waterway, Port, Coastal, and Ocean Engineering*, July/August 1996, 198-205.

Westerink, J.J., Luettich, R. A., Feyen, J.C., Atkinson, J.H., Dawson, C., Roberts, H.J., Powell, M.D., Dunion, J.P., Kubatko, E.J., and Pourtaheri, H. (2008). "A basin to channel-scale unstructured grid hurricane storm surge model applied to southern Louisiana." *Monthly Weather Review*, 136, March, 833-864.

Westerink J.J., Luettich, R. A., and Scheffner N.W. (1994). "ADCIRC: An advanced three-dimensional circulation model for shelves, coasts, and estuaries: Report 4: Hurricane strom surge modeling using large domains." *Technical Report DRP- 92-6*, US Army Corps of Engineers, Washington, DC.

Westerink, J.J., Luettich, R. A., Baptista, A. M., Scheffner, N.W., and Farrar, P. (1992). "Tide and storm surge predictions using finite element model." *Journal of Hydraulic Engineering*, 118(10), 1373-1390.

Westerink, J. J., Muccino, J. C., and Luettich, R. A. (1991). "Tide and hurricane storm surge computations for the Western North Atlantic and Gulf of Mexico." *Proc. of the Esturine and Coastal Modeling*, Tampa, FL, 538-550.

APPENDIX A

DEVELOPMENT OF PARAMETERIZED SURGE RESPONSE FUNCTIONS FOR COASTAL BAYS

Table A-1 Stations Location inside Matagorda Bay

Station No.	Lon	Lat
1	-96.4019	28.3452
2	-96.3938	28.3601
3	-96.3812	28.3761
4	-96.3663	28.3888
5	-96.3548	28.4025
6	-96.3376	28.4106
7	-96.3135	28.4232
8	-96.2860	28.4393
9	-96.2630	28.4576
10	-96.2366	28.4737
11	-96.2079	28.4886
12	-96.1827	28.5024
13	-96.1540	28.5161
14	-96.1345	28.5253
15	-96.1116	28.5322
16	-96.0966	28.5414
17	-96.0783	28.5471
18	-96.0576	28.5552
19	-96.0301	28.5666
20	-96.0140	28.5781
21	-96.3776	28.4195
22	-96.3559	28.4343
23	-96.3424	28.4479
24	-96.3208	28.4587
25	-96.3018	28.4709
26	-96.2761	28.4871
27	-96.2545	28.5033
28	-96.2288	28.5169
29	-96.2031	28.5236
30	-96.1828	28.5344
31	-96.1598	28.5480
32	-96.1327	28.5561
33	-96.1165	28.5669
34	-96.0867	28.5750
35	-96.0651	28.5872

Table A-1 Continued

Station No.	Lon	Lat
36	-96.0380	28.5994
37	-96.0191	28.6075
38	-96.3938	28.4384
39	-96.4033	28.4627
40	-96.4195	28.4857
41	-96.4506	28.5047
42	-96.4790	28.5142
43	-96.5156	28.4966
44	-96.5385	28.4871
45	-96.5074	28.5412
46	-96.5223	28.5601
47	-96.5372	28.5710
48	-96.5615	28.5831
49	-96.4249	28.4195
50	-96.4209	28.4303
51	-96.4317	28.4560
52	-96.4466	28.4790
53	-96.4682	28.4912
54	-96.4871	28.4939
55	-96.4993	28.4790
56	-96.5467	28.4668
57	-96.5737	28.4830
58	-96.5710	28.5074
59	-96.5385	28.5182
60	-96.5304	28.5439
61	-96.5548	28.5601
62	-96.5710	28.5601
63	-96.5994	28.5628
64	-96.5818	28.5926
65	-96.6129	28.5831
66	-96.6102	28.6210
67	-96.6197	28.6562
68	-96.6414	28.6873
69	-96.6224	28.7117
70	-96.5940	28.7117
71	-96.5751	28.6873

Table A-1 Continued

Station No.	Lon	Lat
72	-96.5791	28.6535
73	-96.5426	28.6359
74	-96.5183	28.6332
75	-96.4993	28.6061
76	-96.6387	28.6481
77	-96.6576	28.6684
78	-96.6806	28.6981
79	-96.6305	28.7319
80	-96.6035	28.7414
81	-96.5548	28.7279
82	-96.5602	28.7089
83	-96.5588	28.6846
84	-96.5588	28.6616
85	-96.5372	28.7130
86	-96.5223	28.6805
87	-96.5061	28.6778
88	-96.4736	28.6088
89	-96.4682	28.6264
90	-96.4493	28.6143
91	-96.4276	28.5899
92	-96.4060	28.6007
93	-96.3884	28.6210
94	-96.4127	28.6494
95	-96.4087	28.6792
96	-96.3965	28.6792
97	-96.3681	28.6548
98	-96.3532	28.6210
99	-96.3248	28.6332
100	-96.3072	28.6427
101	-96.2923	28.6589
102	-96.2748	28.6738
103	-96.2436	28.6846
104	-96.2125	28.6900
105	-96.2220	28.6670
106	-96.2369	28.6427
107	-96.2207	28.6264

Table A-1 Continued

Station No.	Lon	Lat
108	-96.2409	28.5953
109	-96.2315	28.5804
110	-96.2085	28.5764
111	-96.1855	28.5831
112	-96.1692	28.5926
113	-96.1517	28.6021
114	-96.1300	28.6075
115	-96.4263	28.6143
116	-96.4276	28.6454
117	-96.4330	28.6873
118	-96.3708	28.6914
119	-96.3505	28.6643
120	-96.3289	28.6670
121	-96.3059	28.6968
122	-96.2802	28.7076
123	-96.2504	28.7049
124	-96.2247	28.7238
125	-96.1936	28.6657
126	-96.2031	28.6359
127	-96.1625	28.6359
128	-96.1368	28.6359

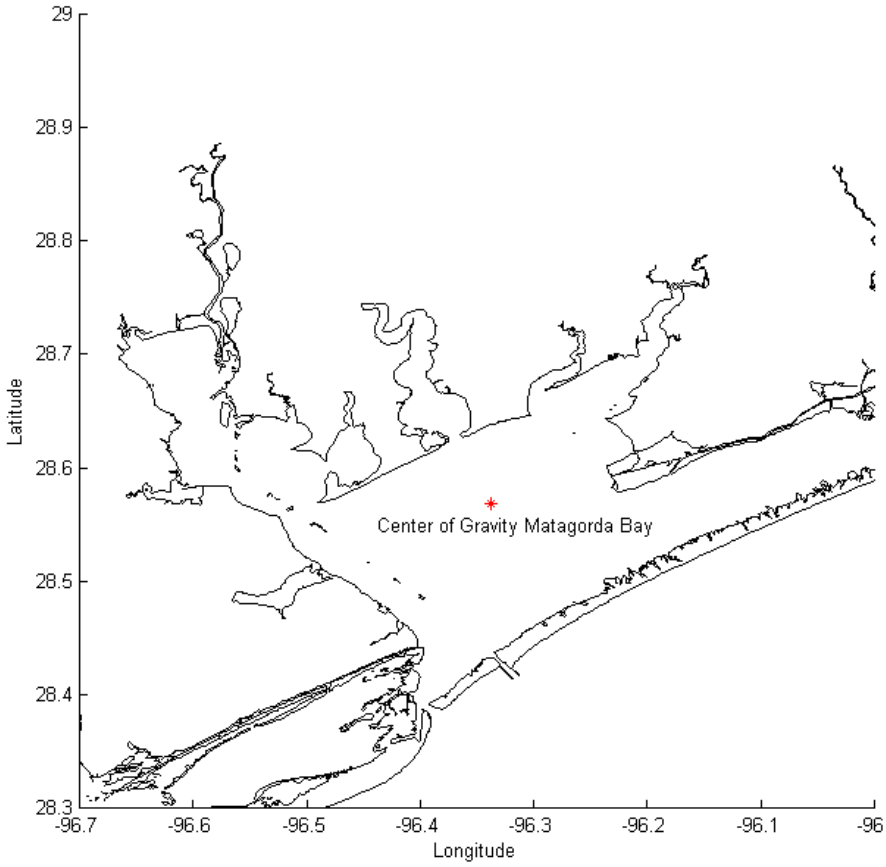

Figure A- 1 Center of gravity, Matagorda Bay

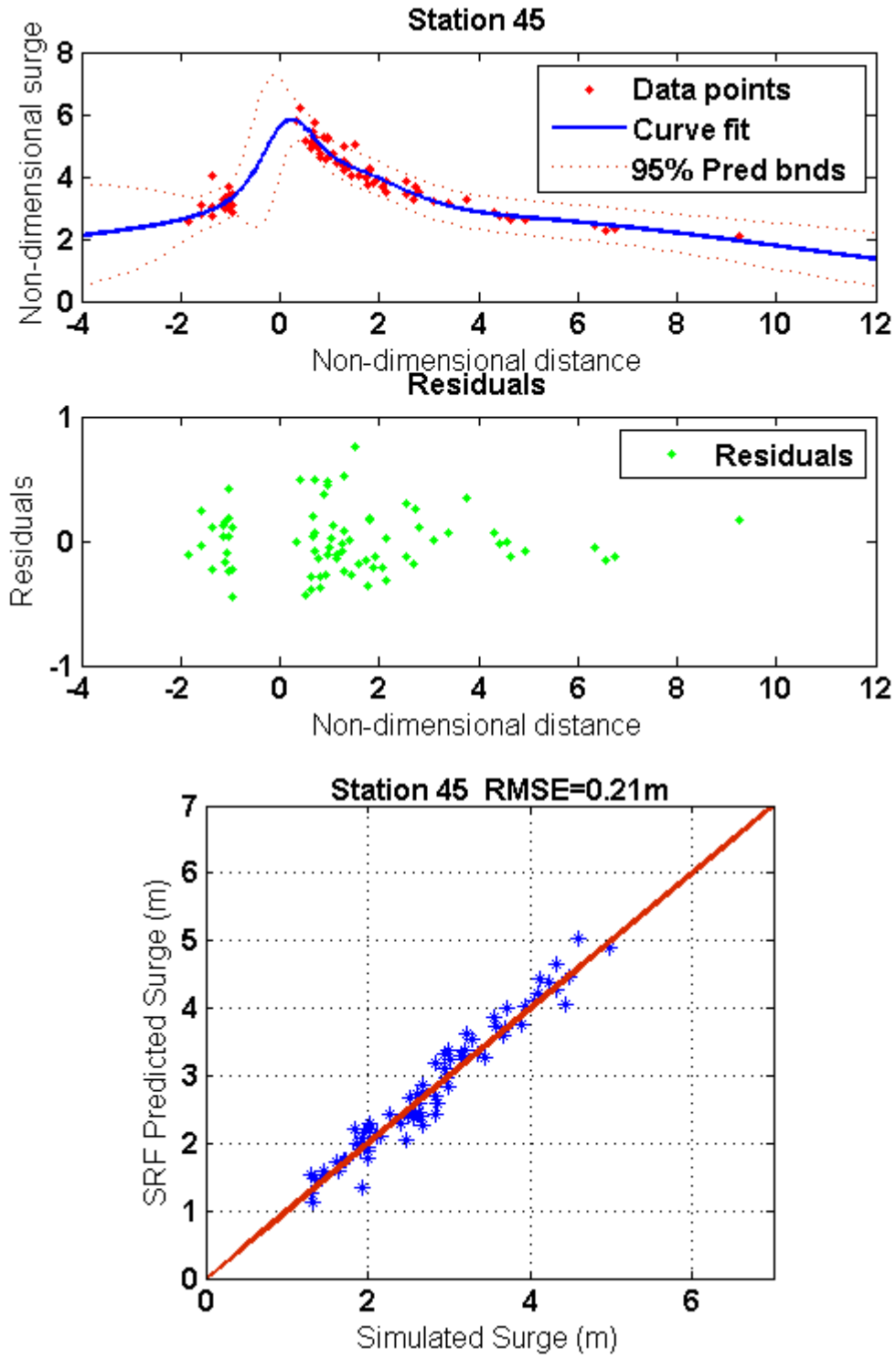

Figure A- 2 SRF at station 45 inside Matagorda Bay

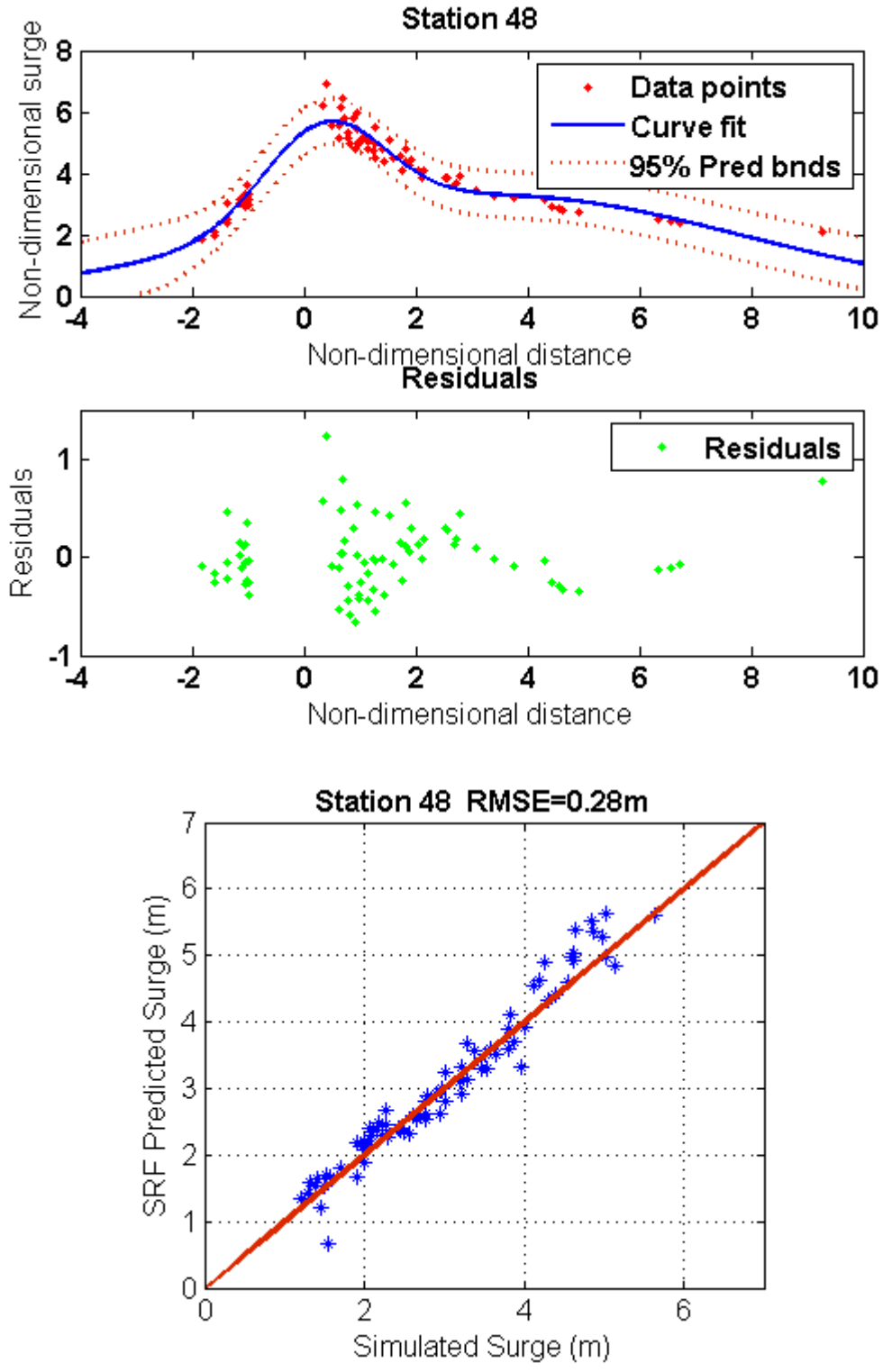

Figure A- 3 SRF at station 48 inside Matagorda Bay

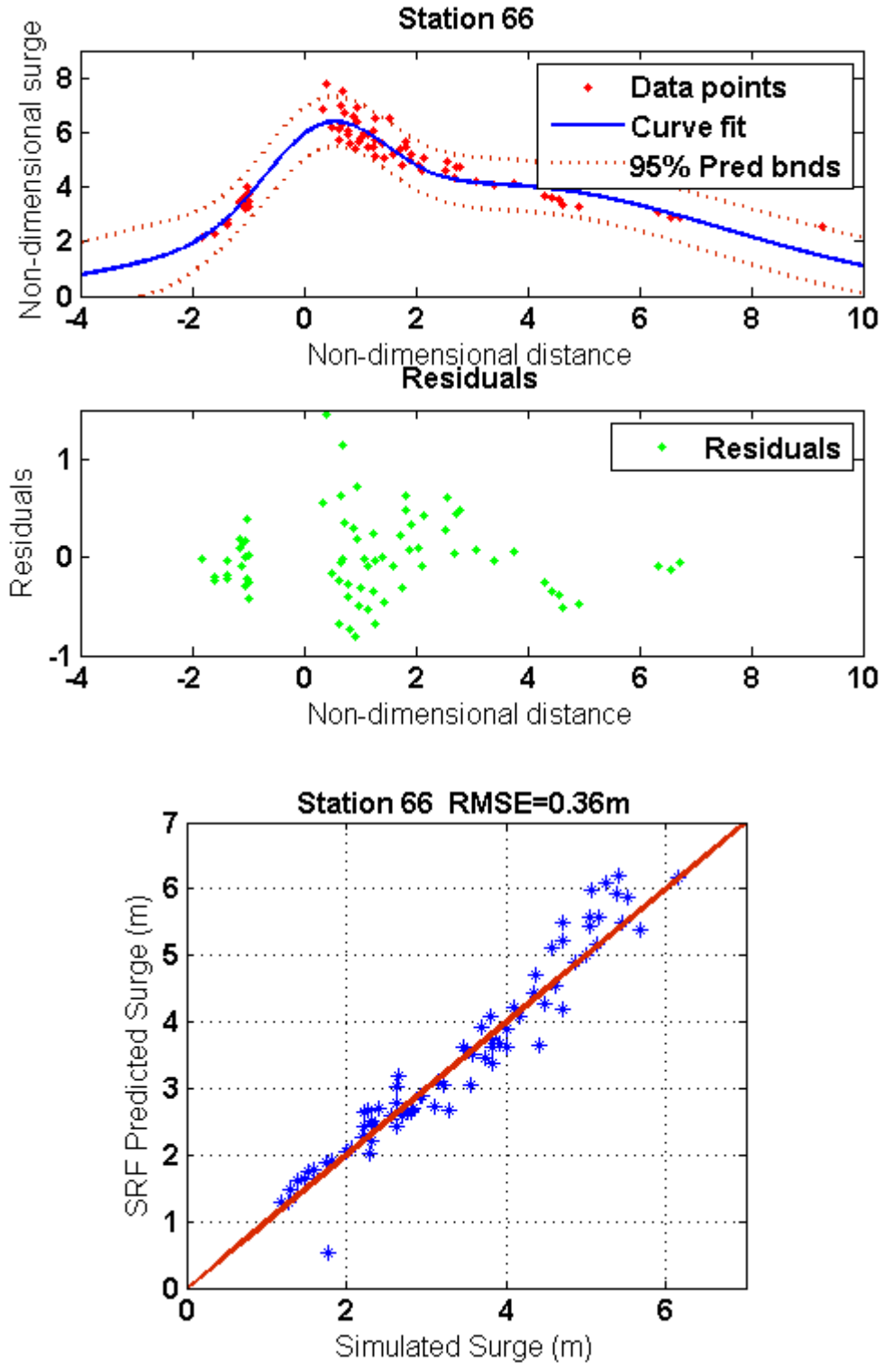

Figure A- 4 SRF at station 66 inside Matagorda Bay

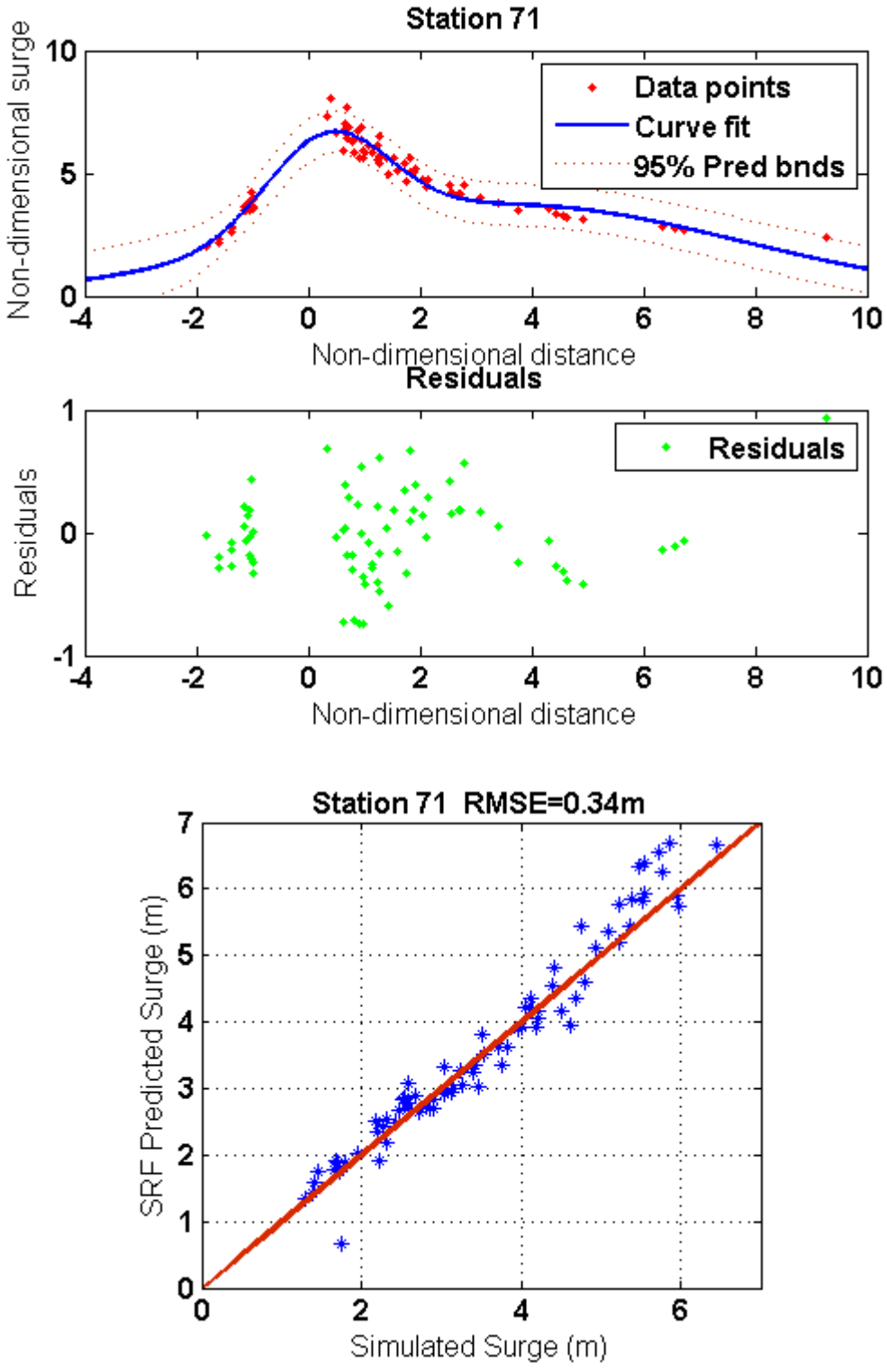

Figure A- 5 SRF at station 71 inside Matagorda Bay

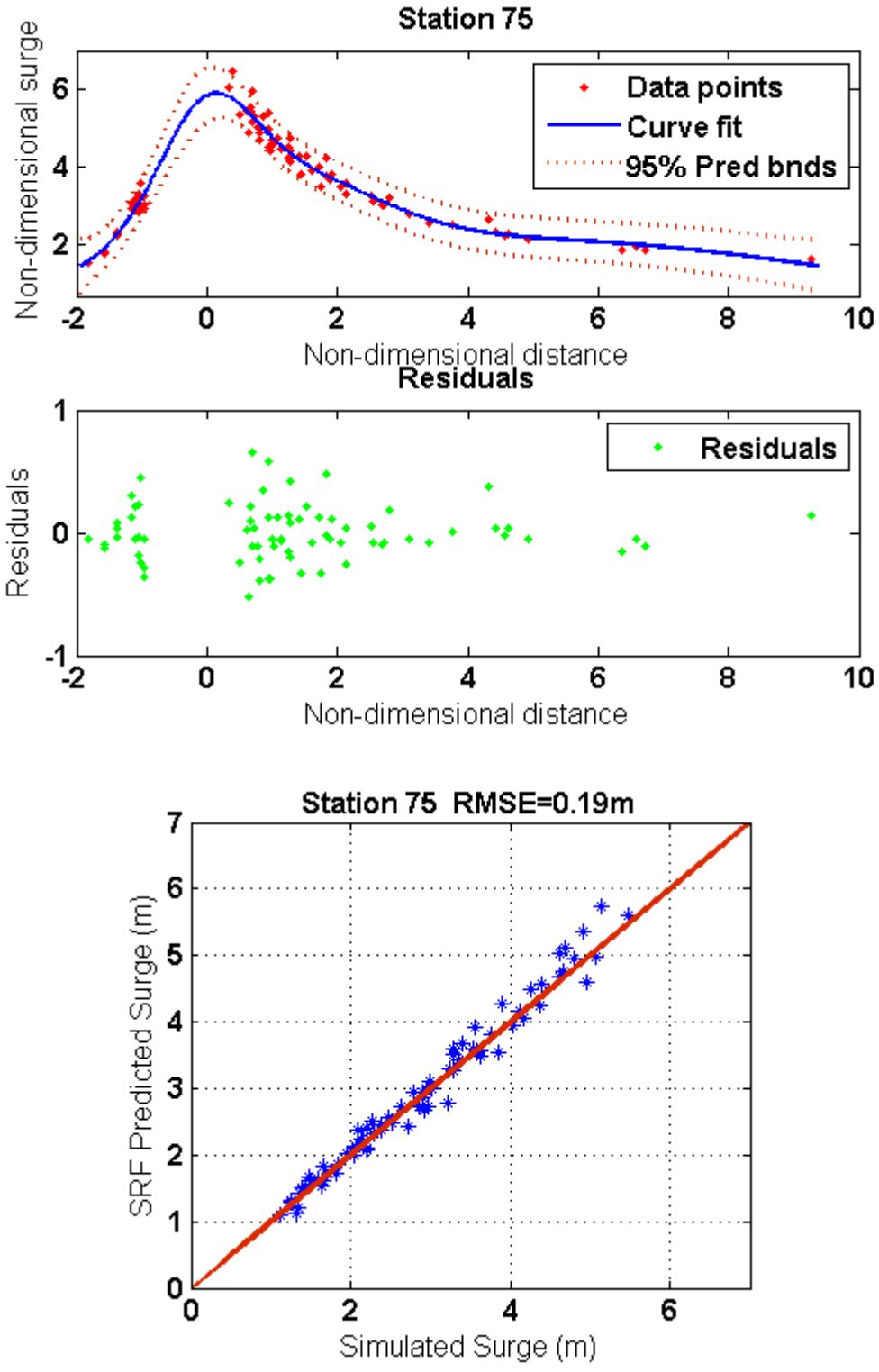

Figure A- 6 SRF at station 75 inside Matagorda Bay

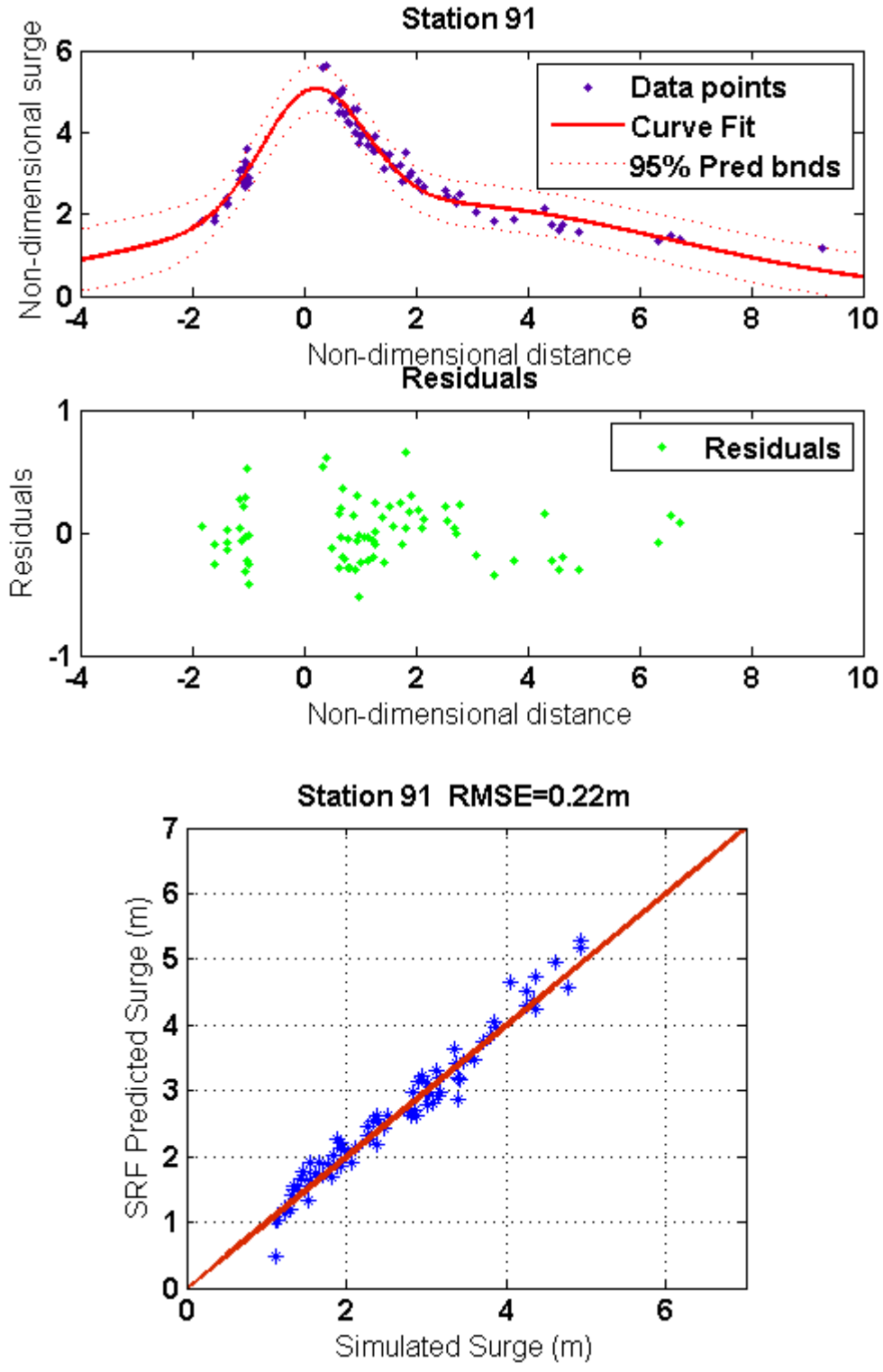

Figure A- 7 SRF at station 91 inside Matagorda Bay

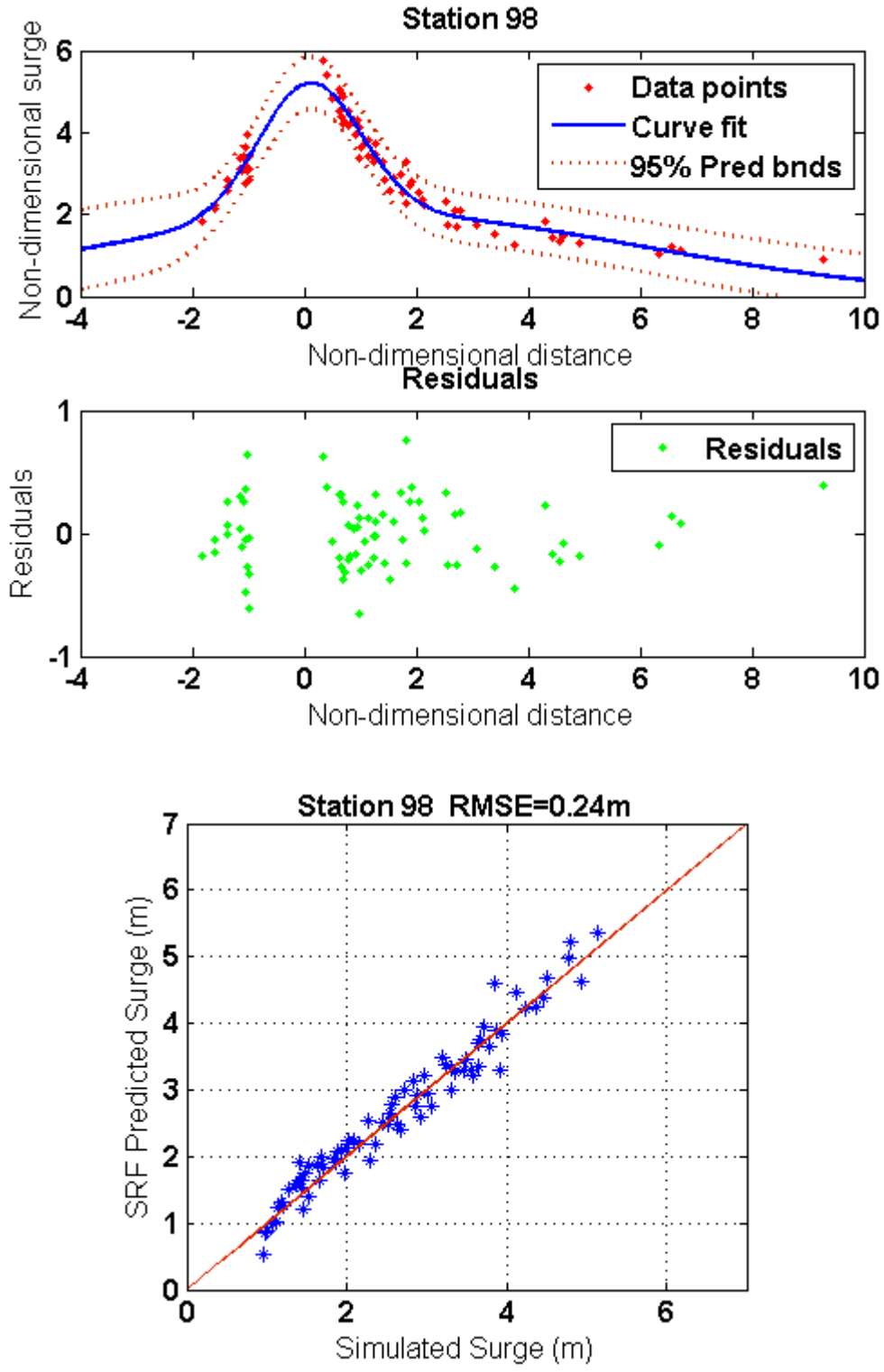

Figure A- 8 SRF at station 98 inside Matagorda Bay

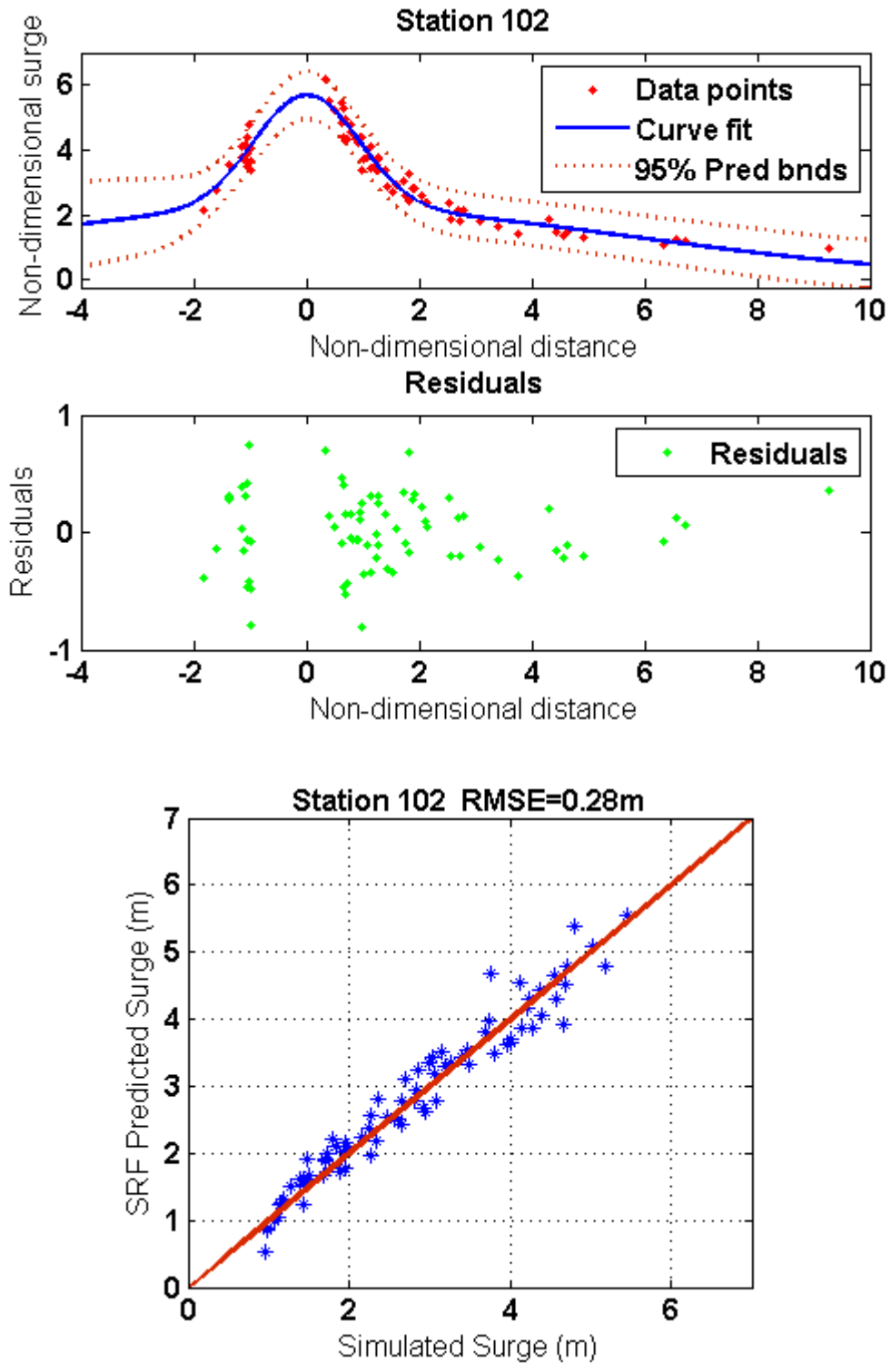

Figure A- 9 SRF at station 102 inside Matagorda Bay

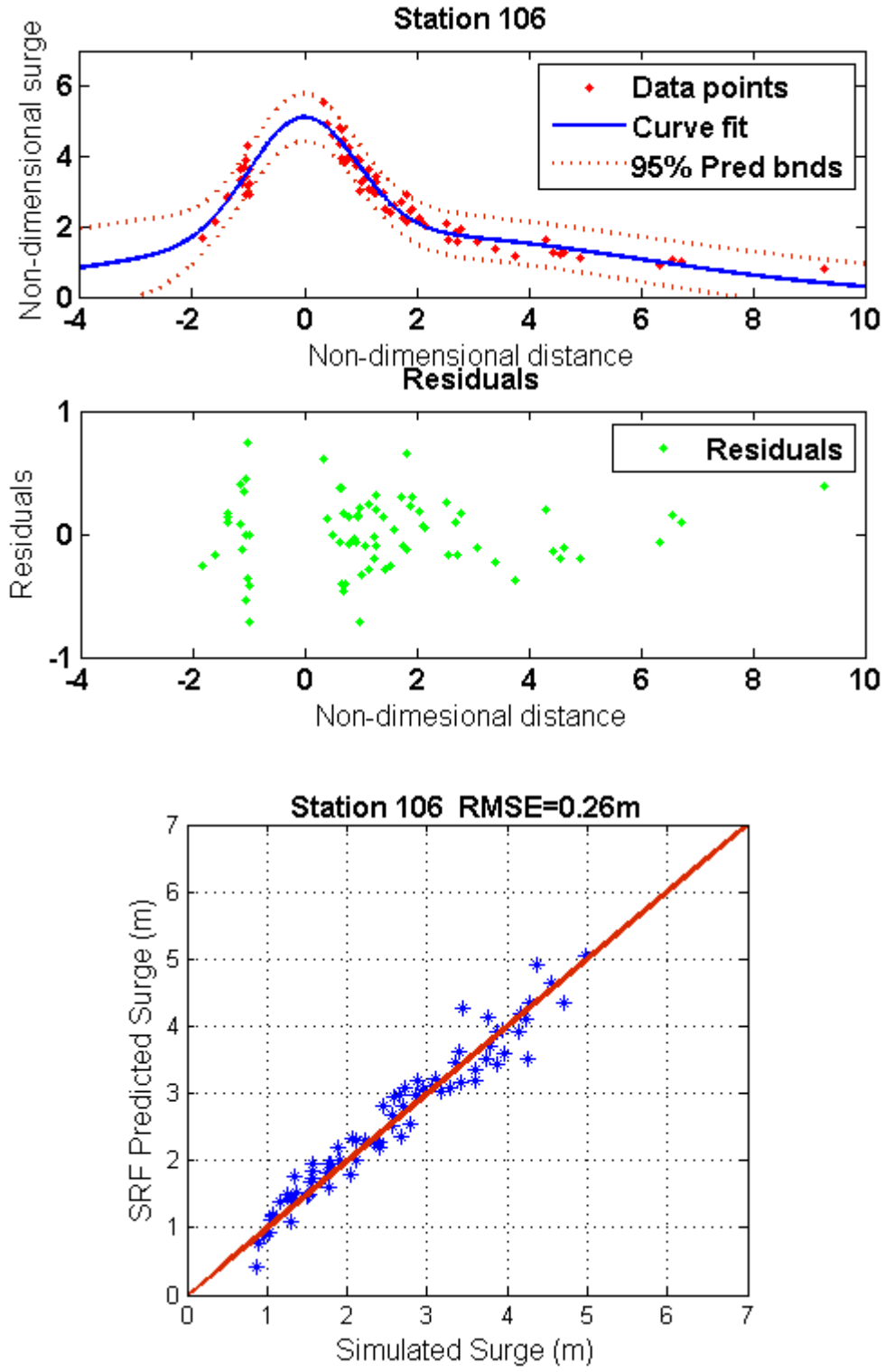

Figure A- 10 SRF at station 106 inside Matagorda Bay

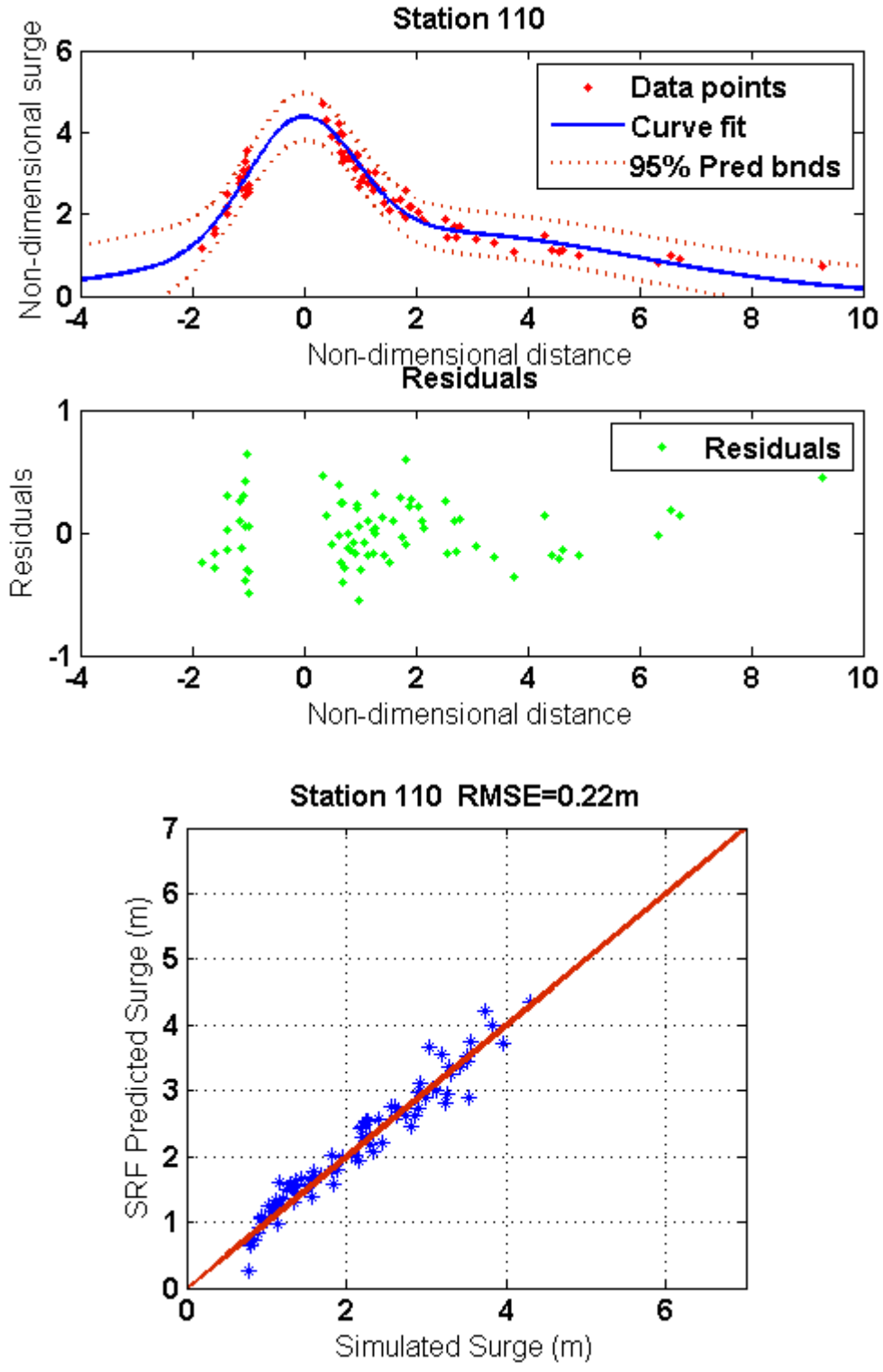

Figure A- 11 SRF at station 110 inside Matagorda Bay

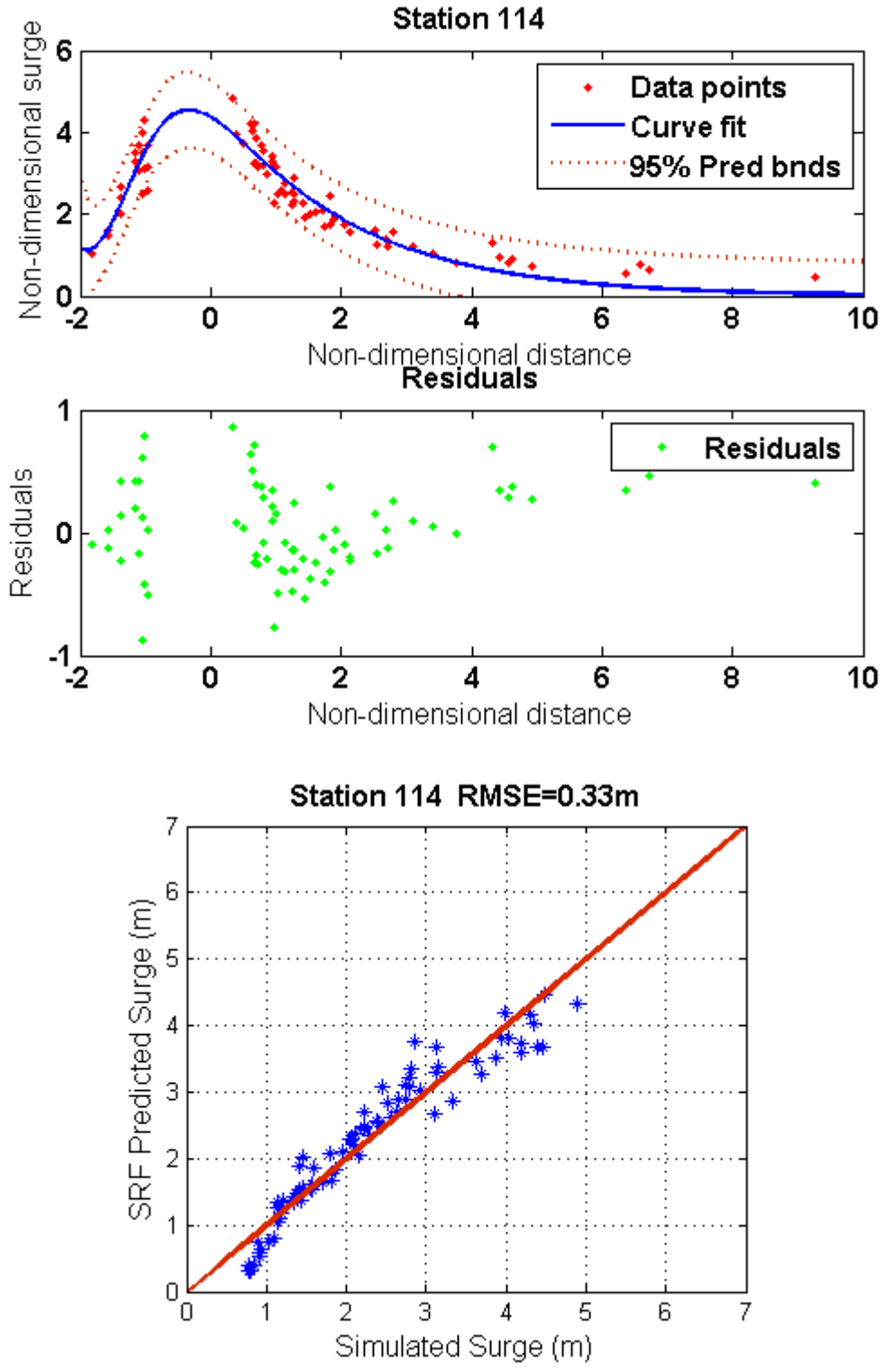

Figure A- 12 SRF at station 114 inside Matagorda Bay

Table A-2 Stations Location inside Galveston Bay

Station No.	Lon	Lat
1	-94.9282	29.2033
2	-94.9173	29.2112
3	-94.9026	29.2200
4	-94.8829	29.2308
5	-94.8672	29.2406
6	-94.8446	29.2485
7	-94.8289	29.2544
8	-94.8112	29.2692
9	-94.7925	29.2829
10	-94.7748	29.2957
11	-94.7640	29.3055
12	-94.7492	29.3164
13	-94.7335	29.3262
14	-94.7148	29.3262
15	-94.7227	29.3645
16	-94.7286	29.3714
17	-94.7197	29.3832
18	-94.7128	29.3940
19	-94.6991	29.4029
20	-94.6922	29.4147
21	-94.6745	29.4255
22	-94.6568	29.4343
23	-94.6430	29.4432
24	-94.6263	29.4520
25	-94.6096	29.4609
26	-94.5919	29.4678
27	-94.5693	29.4756
28	-94.5496	29.4845
29	-94.5339	29.4933
30	-94.5123	29.4973
31	-94.9655	29.2131
32	-94.9400	29.2308
33	-94.9213	29.2436
34	-94.9065	29.2603
35	-94.8859	29.2682
36	-94.8761	29.2751

Table A-2 Continued

Station No.	Lon	Lat
37	-94.8790	29.2908
38	-94.8721	29.2967
39	-94.8495	29.3026
40	-94.8348	29.3085
41	-94.8318	29.3173
42	-94.8289	29.3311
43	-94.8259	29.3478
44	-94.8180	29.3557
45	-94.7787	29.3891
46	-94.7659	29.4029
47	-94.7532	29.4147
48	-94.7355	29.4275
49	-94.7246	29.4432
50	-94.7060	29.4579
51	-94.6922	29.4717
52	-94.6686	29.4786
53	-94.6529	29.4845
54	-94.6430	29.4864
55	-94.6332	29.4855
56	-94.6185	29.4923
57	-94.6057	29.4982
58	-94.6027	29.5159
59	-94.5909	29.5287
60	-94.5683	29.5346
61	-94.5506	29.5346
62	-94.5369	29.5307
63	-94.5142	29.5277
64	-94.8937	29.3095
65	-94.8859	29.3173
66	-94.8888	29.3321
67	-94.8908	29.3439
68	-94.8898	29.3547
69	-94.8839	29.3645
70	-94.8751	29.3714
71	-94.8829	29.3862
72	-94.8819	29.3960
73	-94.8829	29.4088

Table A-2 Continued

Station No.	Lon	Lat
74	-94.8869	29.4304
75	-94.9026	29.4402
76	-94.9164	29.4422
77	-94.9321	29.4284
78	-94.9331	29.4461
79	-94.9301	29.4619
80	-94.9213	29.4766
81	-94.9095	29.4874
82	-94.9154	29.5022
83	-94.9380	29.5051
84	-94.9626	29.5120
85	-94.9901	29.5218
86	-95.0078	29.5327
87	-95.0166	29.5503
88	-95.0117	29.5631
89	-95.0009	29.5759
90	-94.9871	29.5916
91	-94.9783	29.5975
92	-94.9852	29.6103
93	-94.9989	29.6221
94	-95.0088	29.6359
95	-95.0058	29.6546
96	-94.9970	29.6614
97	-94.9862	29.6732
98	-94.9763	29.6841
99	-94.9832	29.6998
100	-94.9803	29.7214
101	-94.9695	29.7195
102	-94.9577	29.7116
103	-94.9409	29.7086
104	-94.9331	29.6978
105	-94.9291	29.6821
106	-94.9183	29.6673
107	-94.8967	29.6654
108	-94.8810	29.6703
109	-94.8613	29.6870
110	-94.8534	29.7096

Table A-2 Continued

Station No.	Lon	Lat
111	-94.8446	29.7293
112	-94.8279	29.7450
113	-94.8259	29.7617
114	-94.8230	29.7784
115	-94.8112	29.7814
116	-94.7994	29.7794
117	-94.7846	29.7814
118	-94.7718	29.7883
119	-94.7551	29.7952
120	-94.7394	29.8001
121	-94.7276	29.7971
122	-94.7217	29.7893
123	-94.7237	29.7775
124	-94.7079	29.7775
125	-94.6932	29.7853
126	-94.6961	29.7666
127	-94.6942	29.7558
128	-94.7001	29.7421
129	-94.6971	29.7234
130	-94.6991	29.7086
131	-94.6991	29.6890
132	-94.7040	29.6723
133	-94.7060	29.6546
134	-94.7069	29.6359
135	-94.7158	29.6241
136	-94.7197	29.6133
137	-94.7305	29.5966
138	-94.7394	29.5887
139	-94.7414	29.5769
140	-94.7591	29.5612
141	-94.7738	29.5562
142	-94.7826	29.5317
143	-94.7699	29.5228
144	-94.7541	29.5199
145	-94.7374	29.5209
146	-94.7227	29.5248
147	-94.7040	29.5317

Table A-2 Continued

Station No.	Lon	Lat
148	-94.6824	29.5366
149	-94.6637	29.5376
150	-94.6421	29.5425
151	-94.6165	29.5494
152	-94.5968	29.5553
153	-94.5742	29.5612
154	-94.5614	29.5749
155	-94.5467	29.5671
156	-94.5359	29.5562
157	-94.5270	29.5435
158	-94.5162	29.5405
159	-94.5034	29.5405

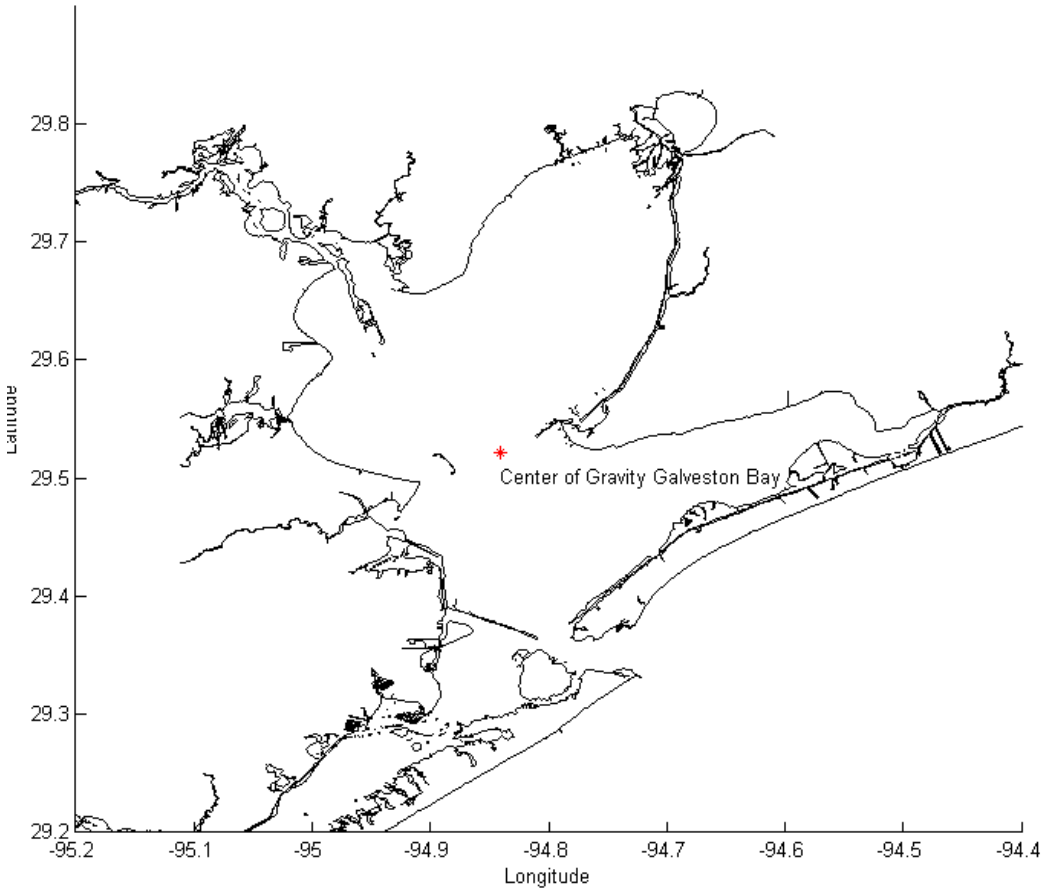

Figure A- 13 Center of gravity, Galveston Bay

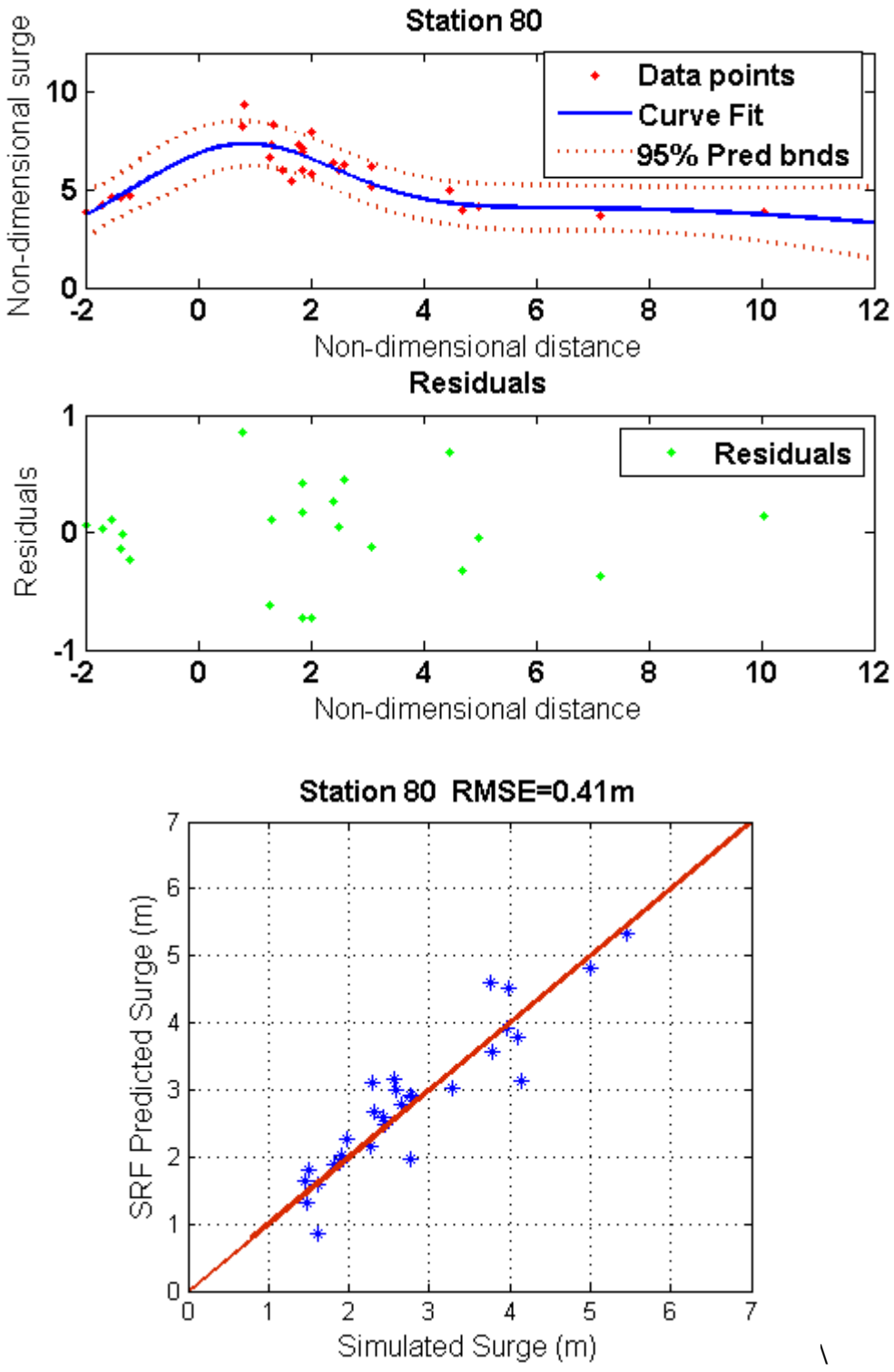

Figure A- 14 SRF at station 80 inside Galveston Bay

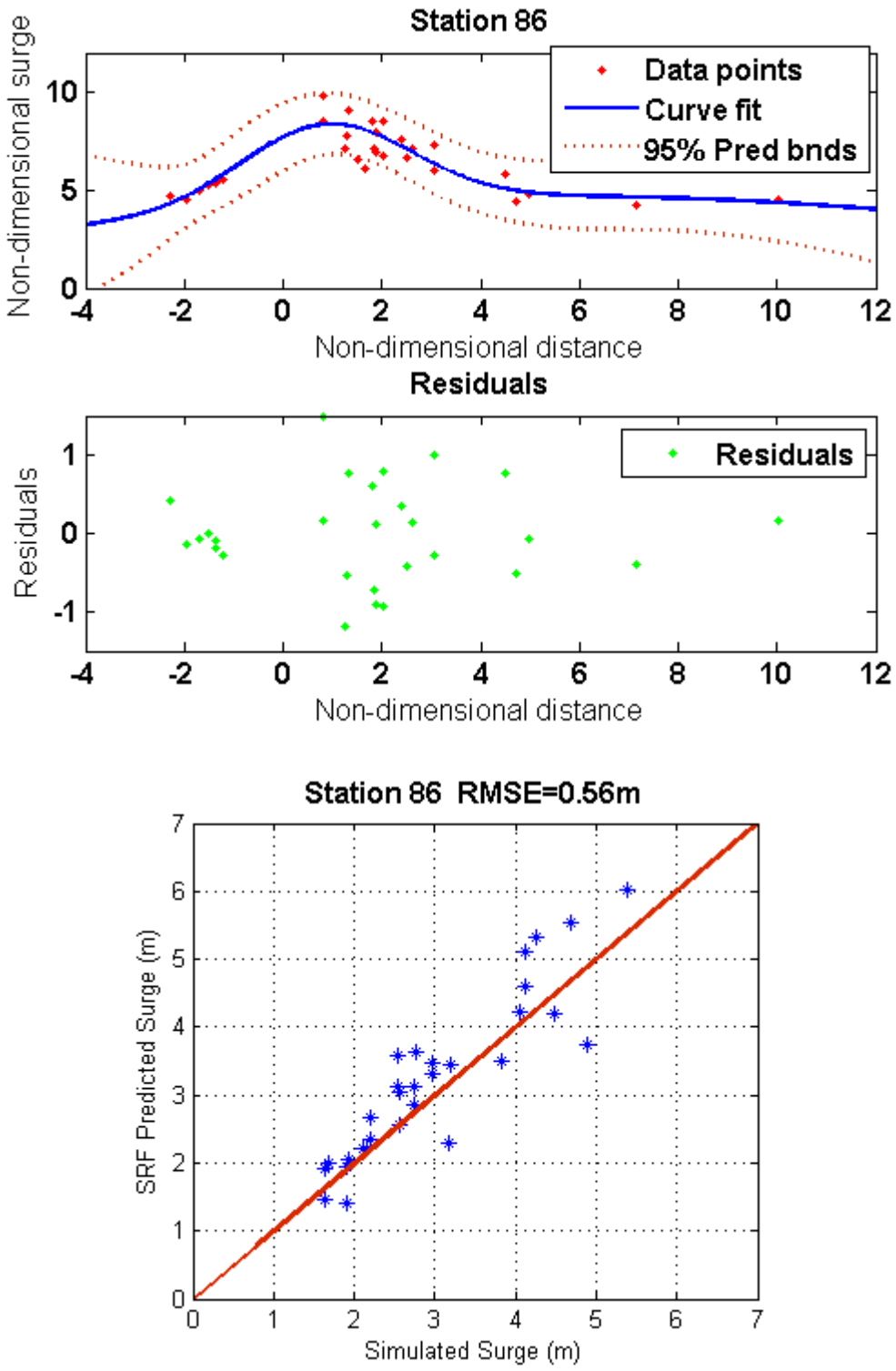

Figure A- 15 SRF at station 86 inside Galveston Bay

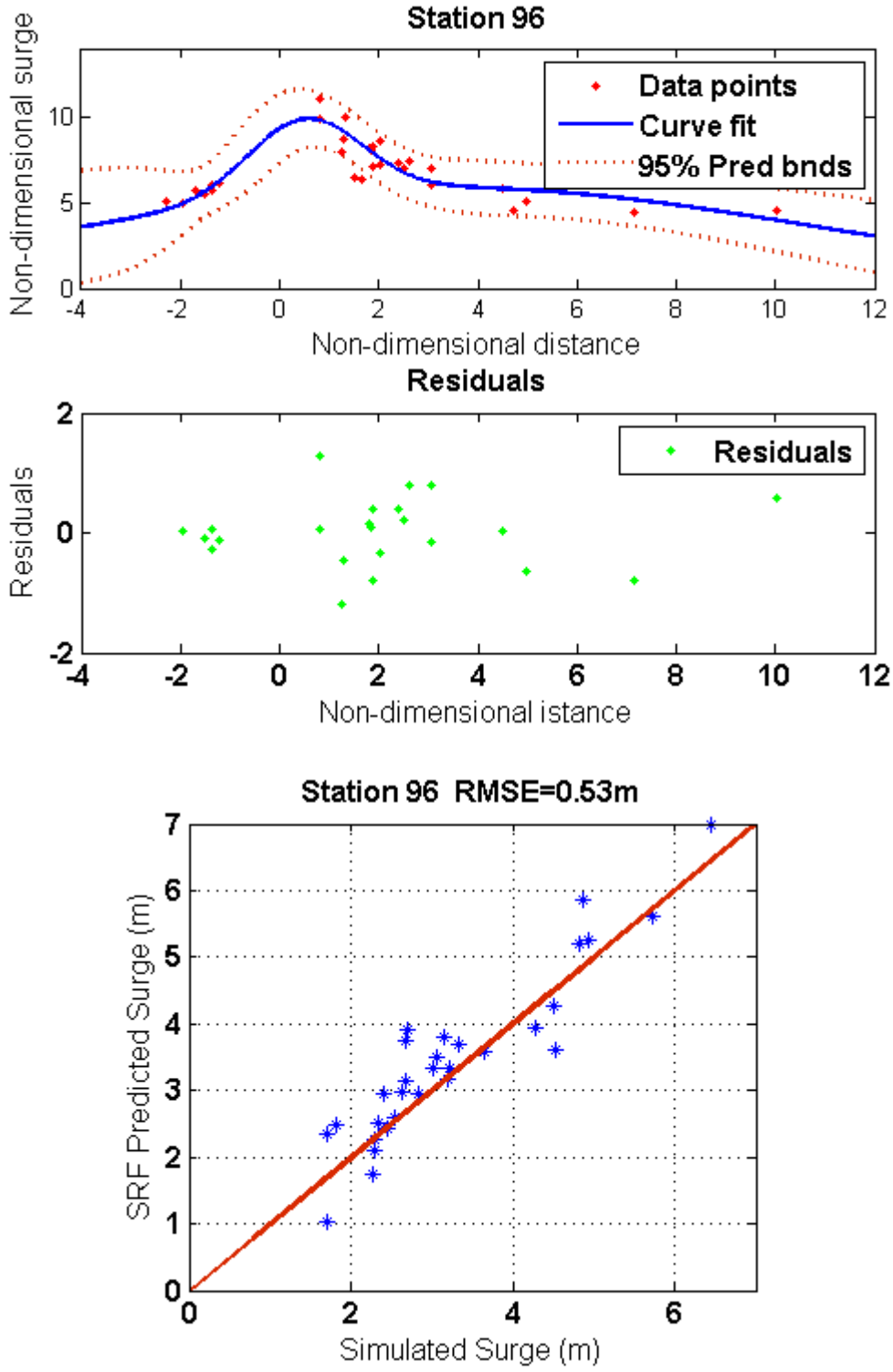

Figure A- 16 SRF at station 96 inside Galveston Bay

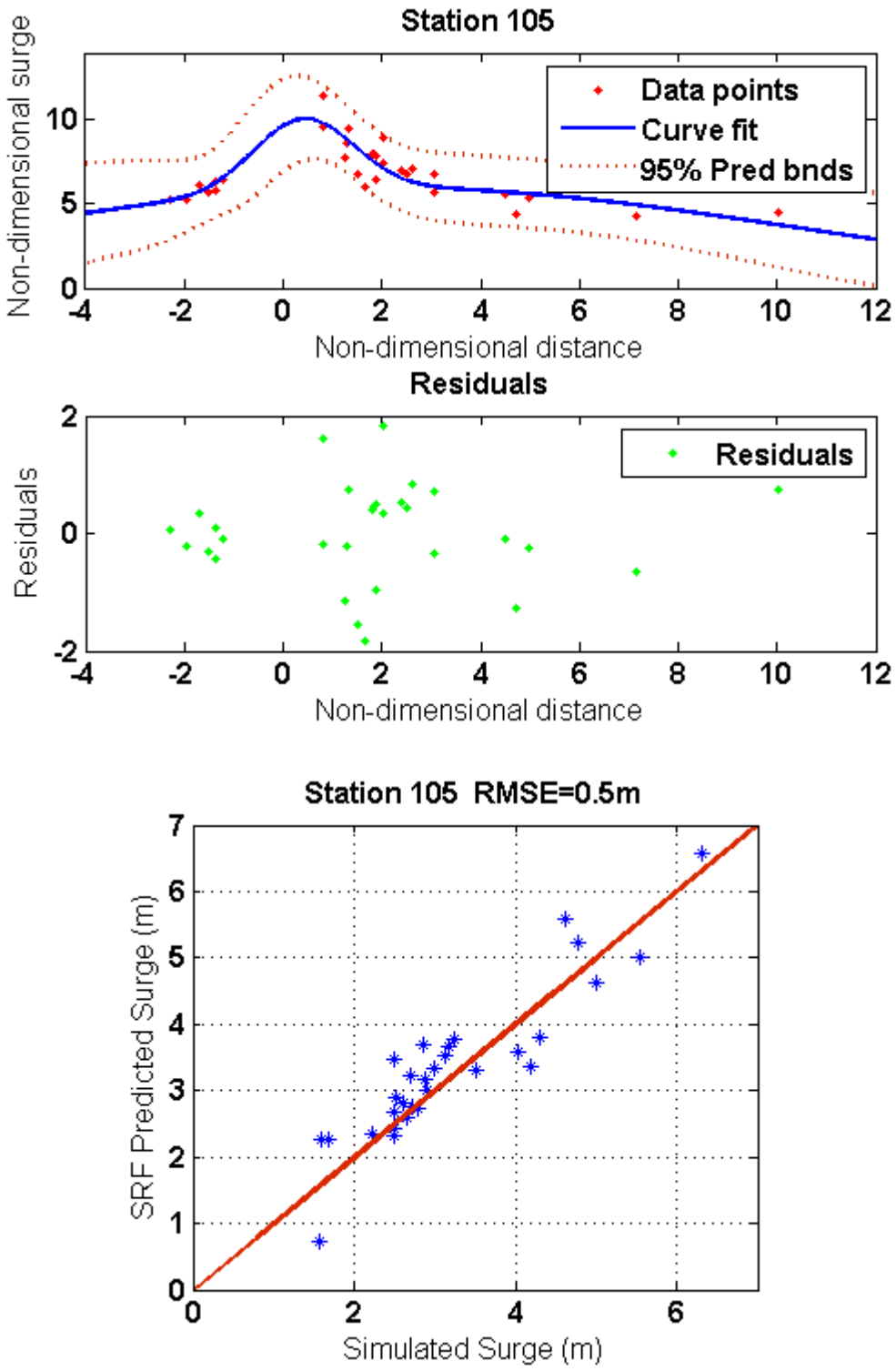

Figure A- 17 SRF at station 105 inside Galveston Bay

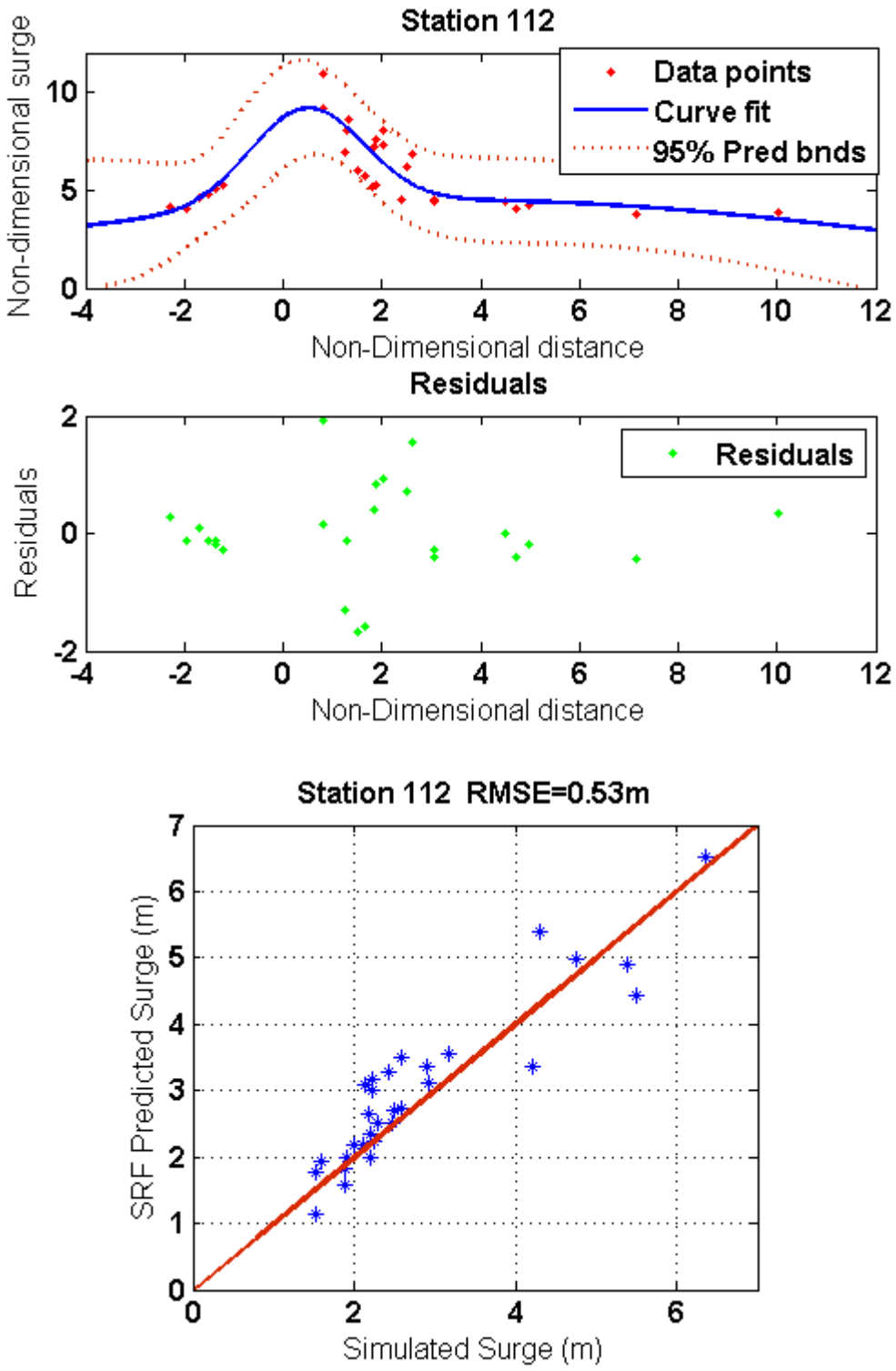

Figure A- 18 SRF at station 112 inside Galveston Bay

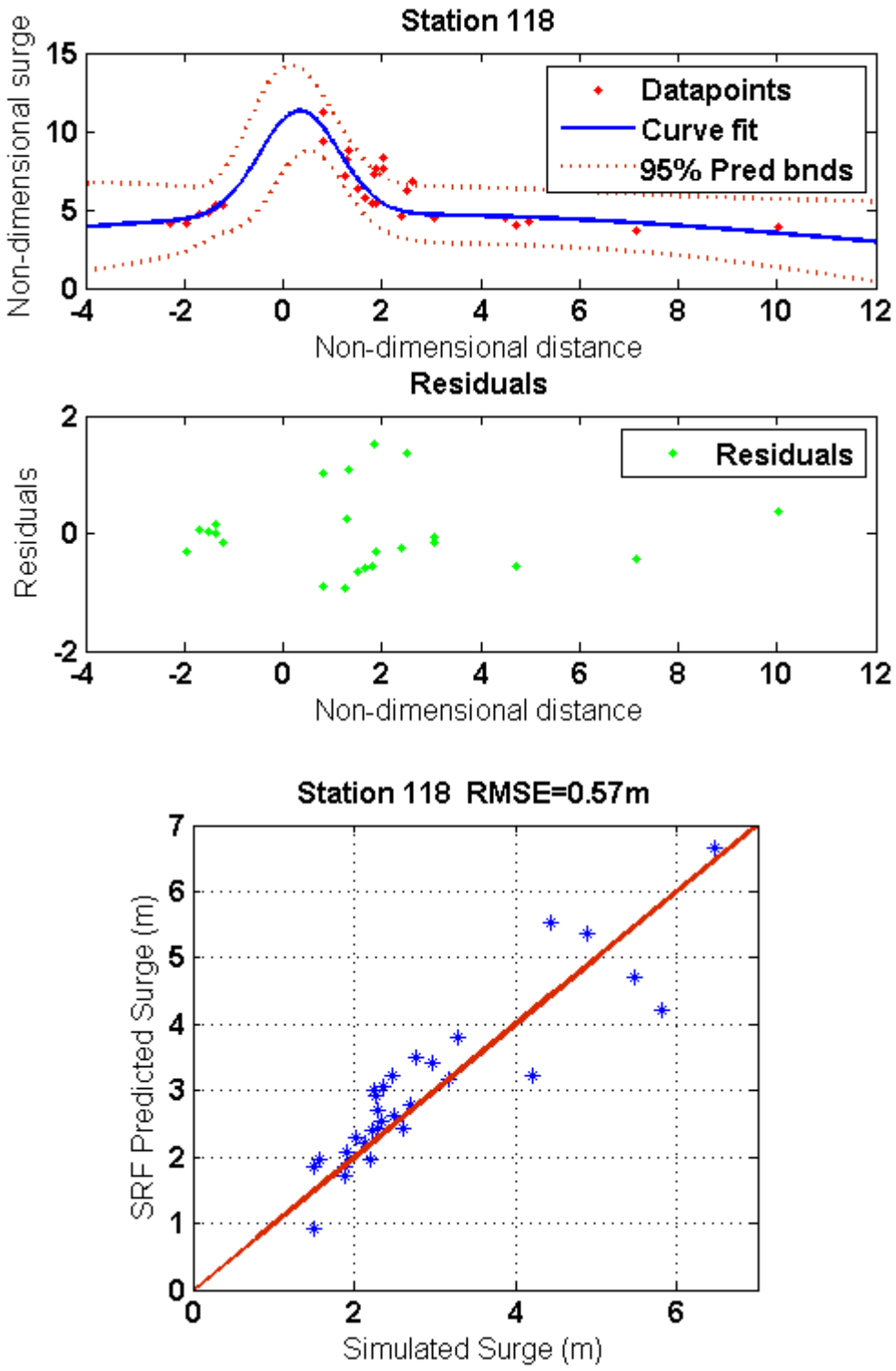

Figure A- 19 SRF at station 118 inside Galveston Bay

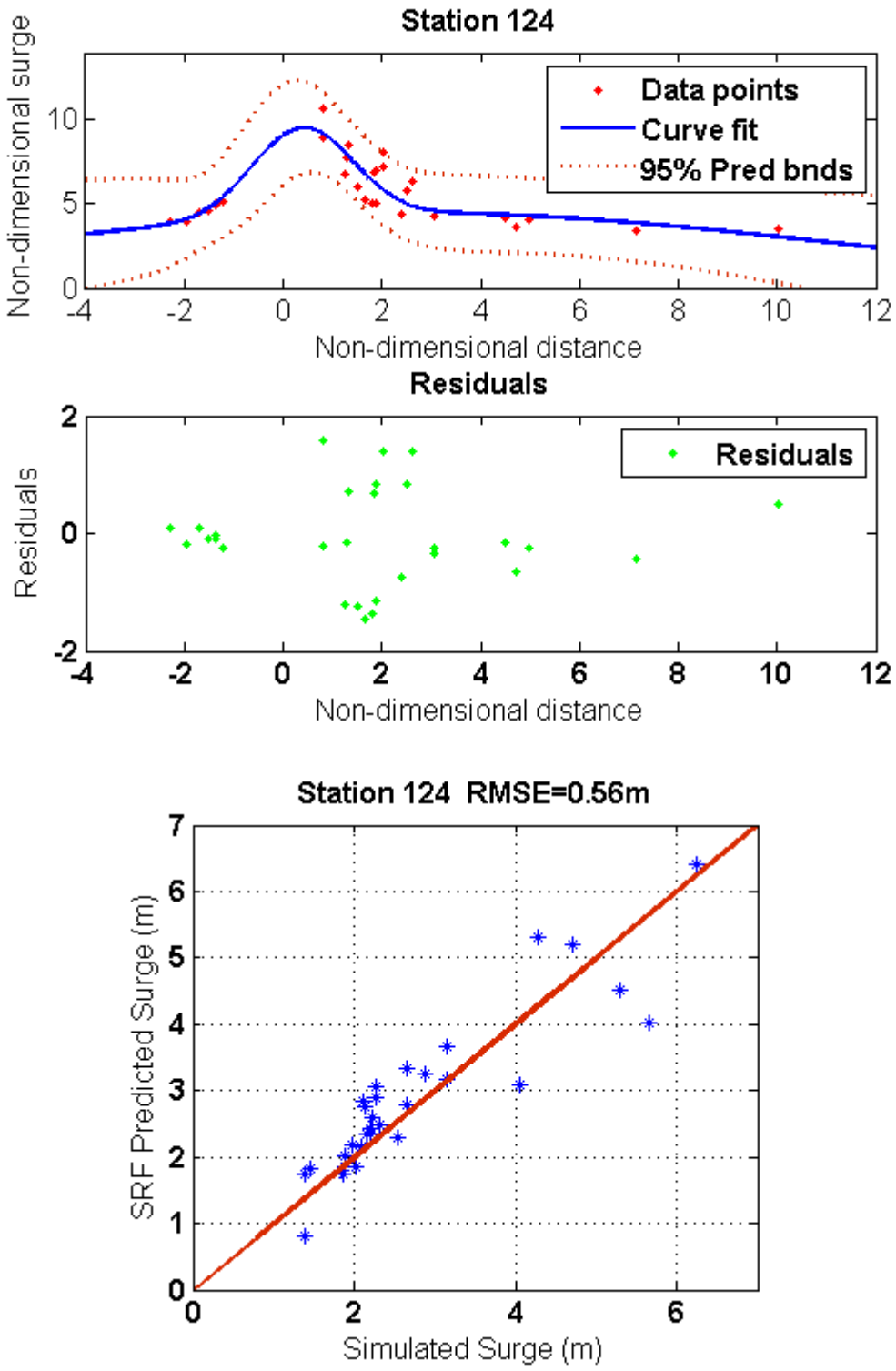

Figure A- 20 SRF at station 124 inside Galveston Bay

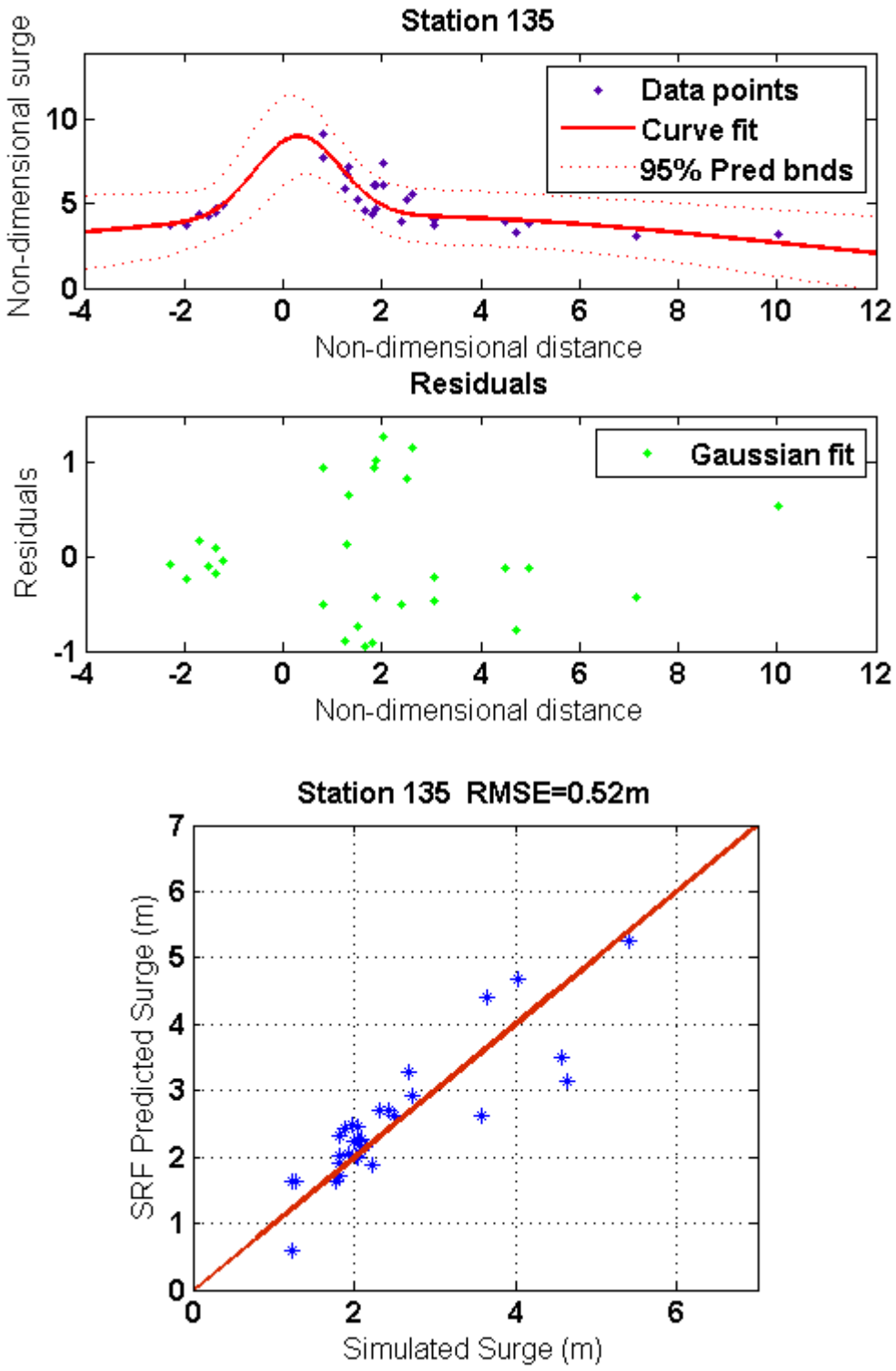

Figure A- 21 SRF at station 135 inside Galveston Bay

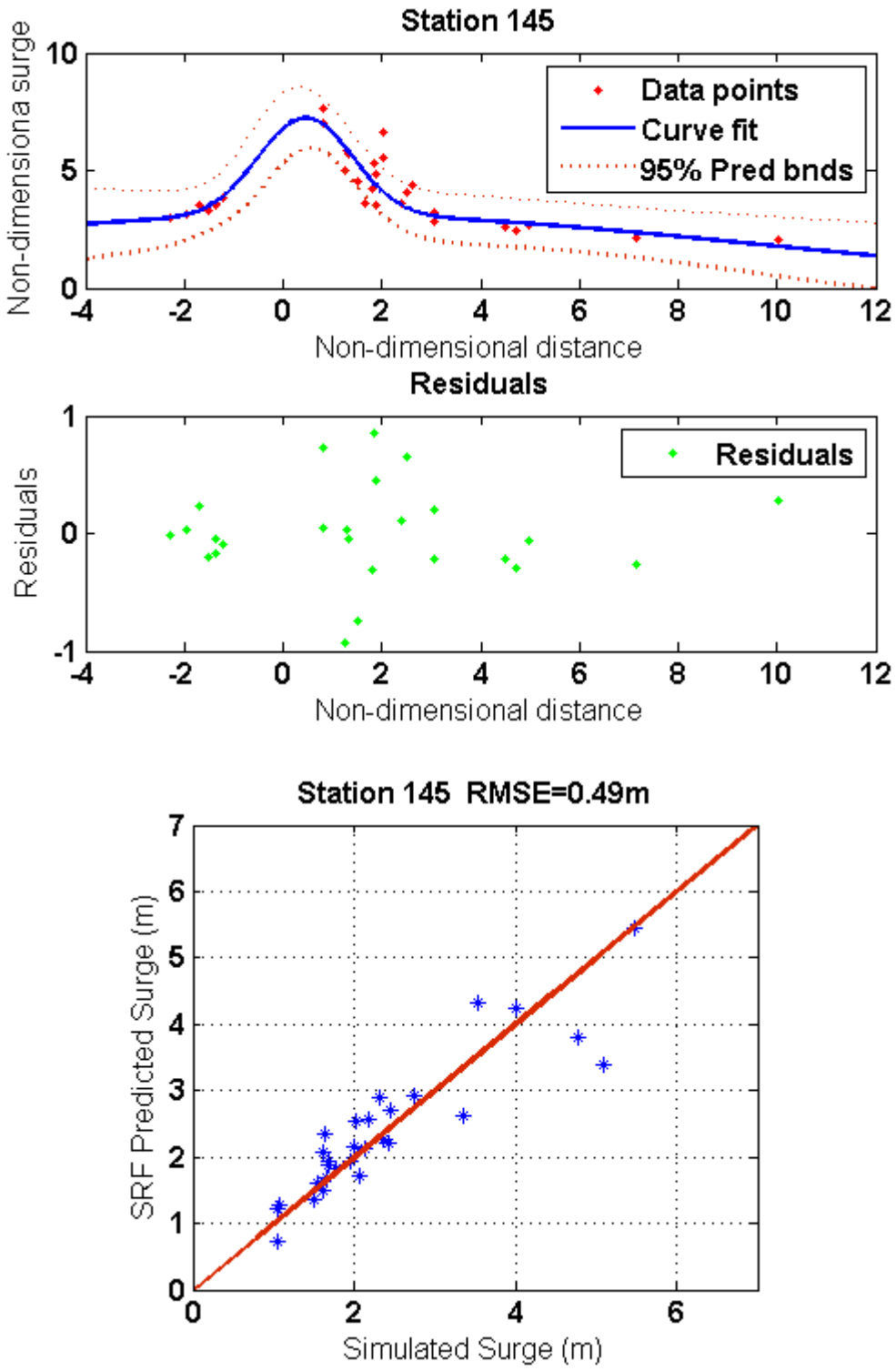

Figure A- 22 SRF at station 145 inside Galveston Bay

Table A-3 Stations Location inside Corpus Christi Bay

Station No.	Lon	Lat
1	-97.2052	27.6093
2	-97.2002	27.6202
3	-97.1943	27.6336
4	-97.1851	27.6453
5	-97.1751	27.6612
6	-97.1667	27.6771
7	-97.1609	27.6913
8	-97.1500	27.7072
9	-97.1391	27.7147
10	-97.1358	27.7264
11	-97.1291	27.7373
12	-97.1216	27.7432
13	-97.1115	27.7557
14	-97.1040	27.7674
15	-97.0965	27.7808
16	-97.0856	27.7892
17	-97.0773	27.8025
18	-97.0714	27.8134
19	-97.0580	27.8243
20	-97.0505	27.8301
21	-97.0430	27.8494
22	-97.0388	27.8636
23	-97.0313	27.8703
24	-97.0262	27.8812
25	-97.0154	27.8912
26	-97.2169	27.6369
27	-97.2069	27.6470
28	-97.2052	27.6645
29	-97.2002	27.6821
30	-97.1960	27.6972
31	-97.1843	27.7105
32	-97.1701	27.7281
33	-97.1559	27.7356
34	-97.1433	27.7499
35	-97.1366	27.7616
36	-97.1283	27.7724

Table A-3 Continued

Station No.	Lon	Lat
37	-97.1141	27.7892
38	-97.1065	27.8025
39	-97.0990	27.8092
40	-97.1090	27.8218
41	-97.1074	27.8469
42	-97.0940	27.8536
43	-97.0547	27.8619
44	-97.0463	27.8770
45	-97.2922	27.6169
46	-97.2813	27.6369
47	-97.2730	27.6587
48	-97.2679	27.6771
49	-97.2596	27.6888
50	-97.2629	27.7039
51	-97.2847	27.7097
52	-97.2989	27.7114
53	-97.3048	27.6988
54	-97.3064	27.6855
55	-97.3240	27.7005
56	-97.3357	27.7256
57	-97.3524	27.7390
58	-97.3758	27.7532
59	-97.3834	27.7674
60	-97.3942	27.7883
61	-97.3959	27.8051
62	-97.3901	27.8209
63	-97.3834	27.8327
64	-97.4009	27.8393
65	-97.4193	27.8335
66	-97.4277	27.8310
67	-97.4469	27.8318
68	-97.4687	27.8318
69	-97.4837	27.8377
70	-97.5005	27.8486
71	-97.5164	27.8578
72	-97.5205	27.8720
73	-97.5105	27.8862

Table A-3 Continued

Station No.	Lon	Lat
74	-97.4988	27.8828
75	-97.4896	27.8762
76	-97.4804	27.8644
77	-97.4670	27.8661
78	-97.4612	27.8787
79	-97.4503	27.8745
80	-97.4269	27.8720
81	-97.4110	27.8720
82	-97.3917	27.8720
83	-97.3733	27.8720
84	-97.3625	27.8803
85	-97.3491	27.8803
86	-97.3407	27.8795
87	-97.3441	27.8611
88	-97.3248	27.8678
89	-97.3098	27.8720
90	-97.2905	27.8745
91	-97.2771	27.8795
92	-97.2604	27.8720
93	-97.2437	27.8586
94	-97.2378	27.8519
95	-97.2303	27.8435
96	-97.2270	27.8310
97	-97.2204	27.8228
98	-97.2129	27.8216
99	-97.1938	27.8265
100	-97.1835	27.8429
101	-97.1776	27.8565
102	-97.1607	27.8709
103	-97.1463	27.8819
104	-97.1361	27.8946
105	-97.1277	27.9107
106	-97.1166	27.9293
107	-97.1090	27.9403
108	-97.0997	27.9547
109	-97.0887	27.9674

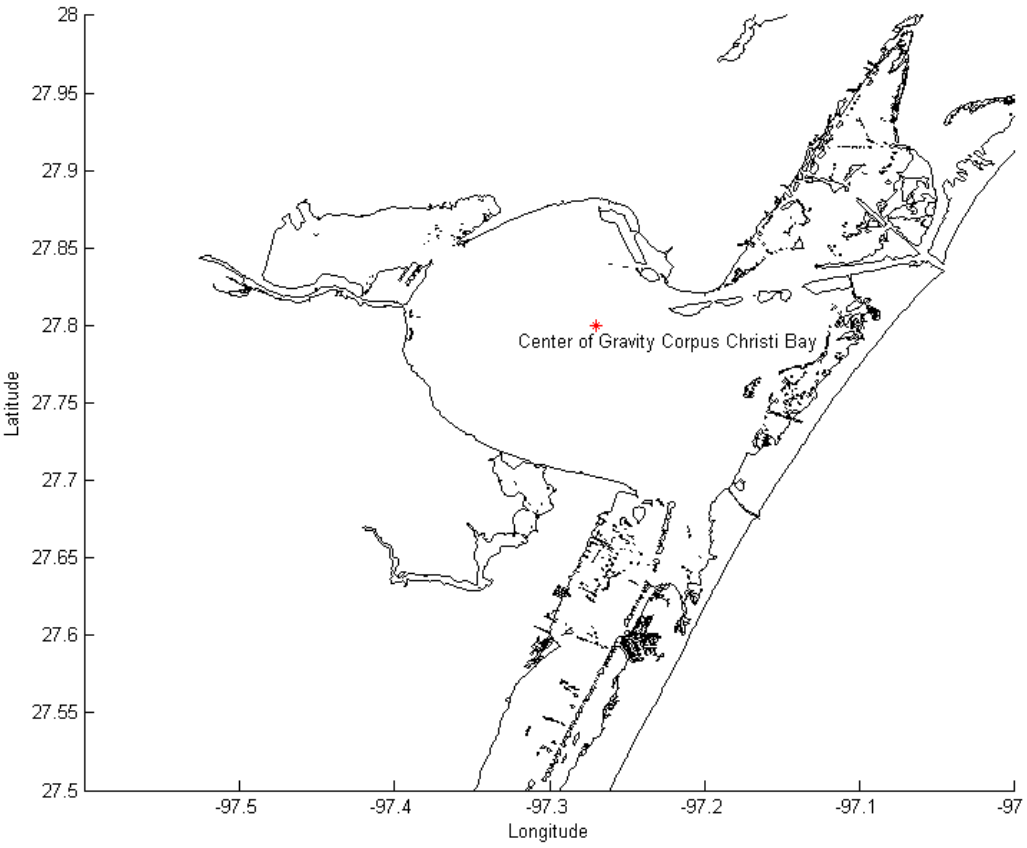

Figure A- 23 Center of gravity, Corpus Christi Bay

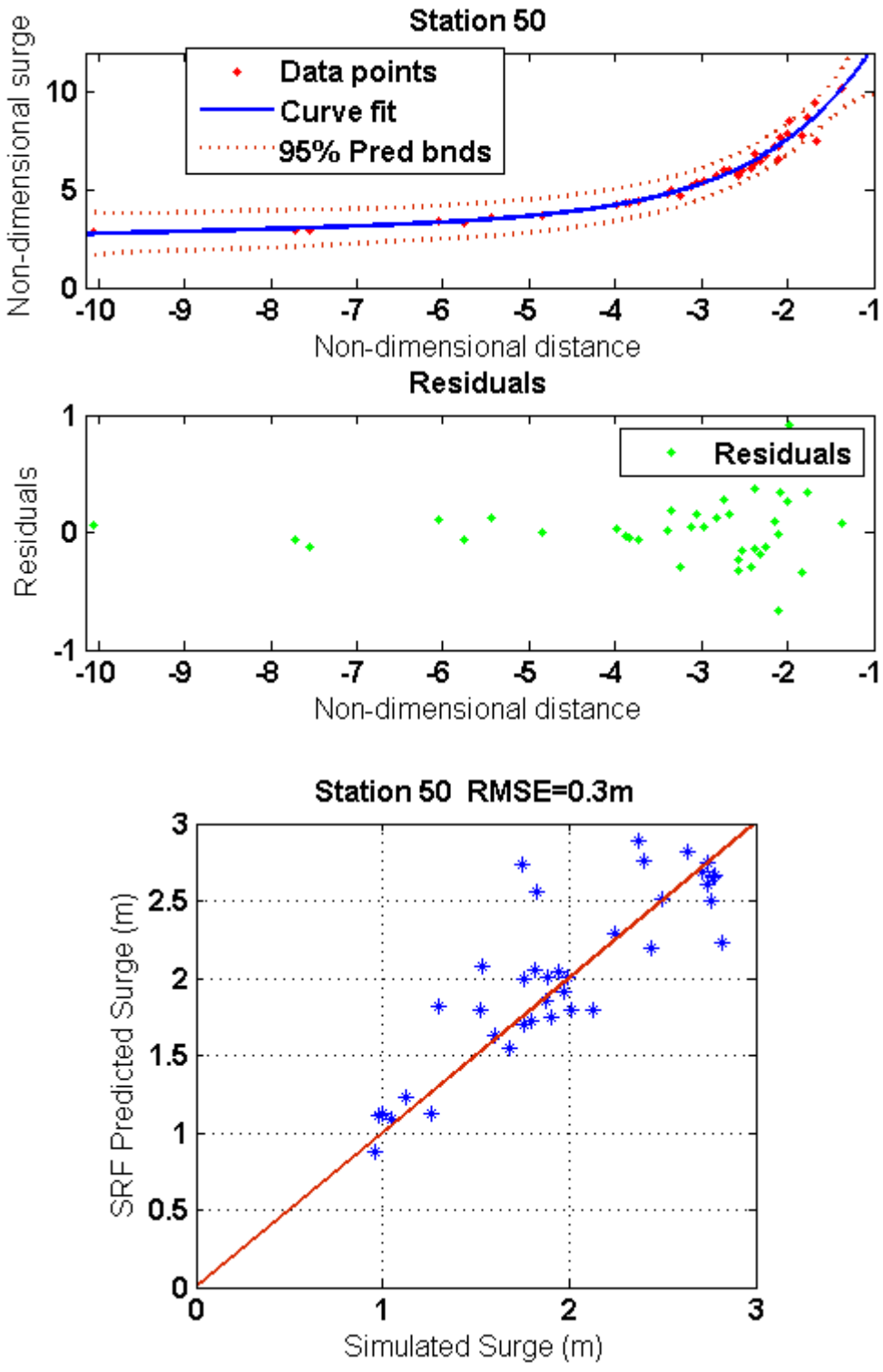

Figure A- 24 SRF at station 50 inside Corpus Christi Bay

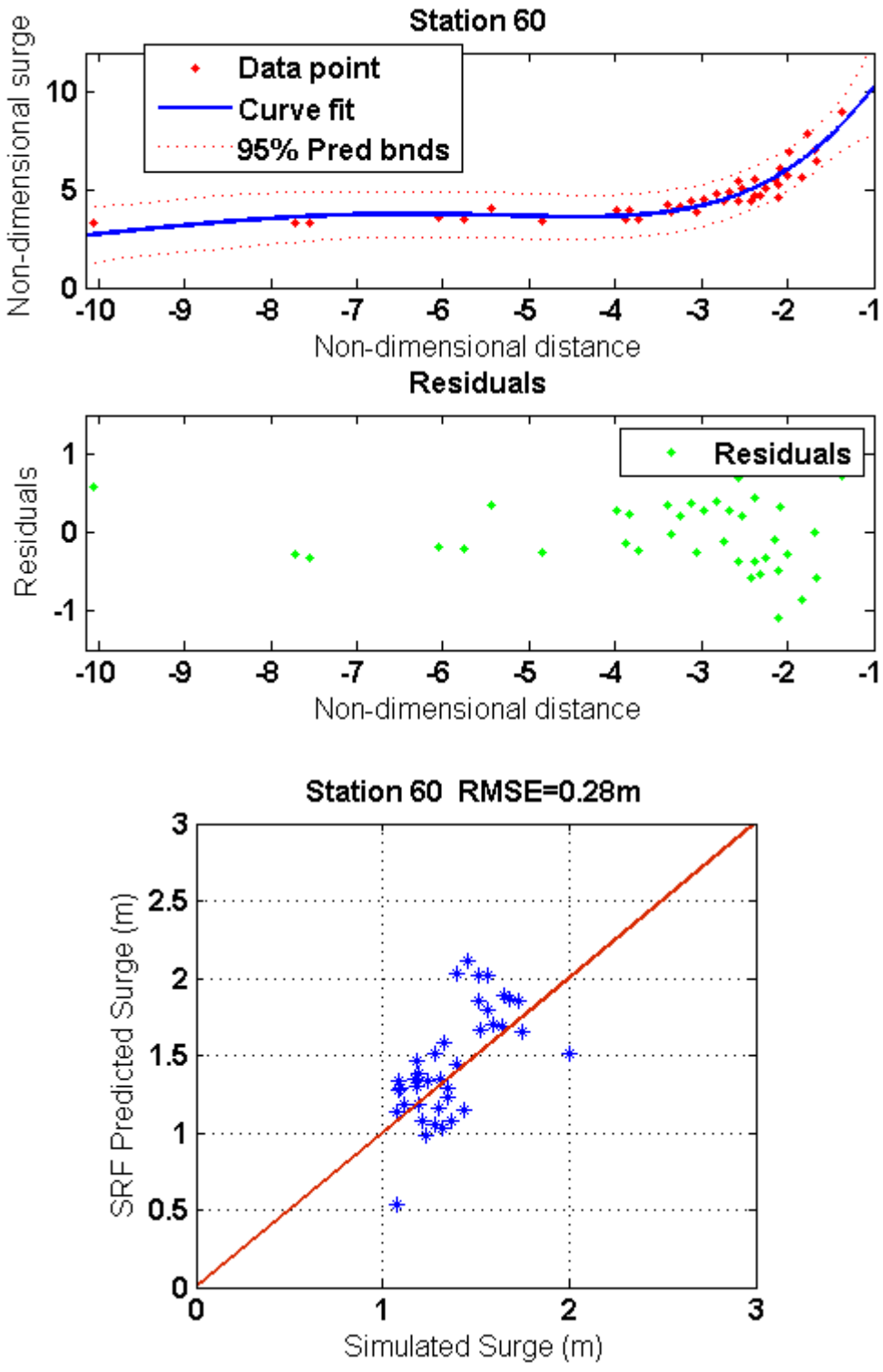

Figure A- 25 SRF at station 60 inside Corpus Christi Bay

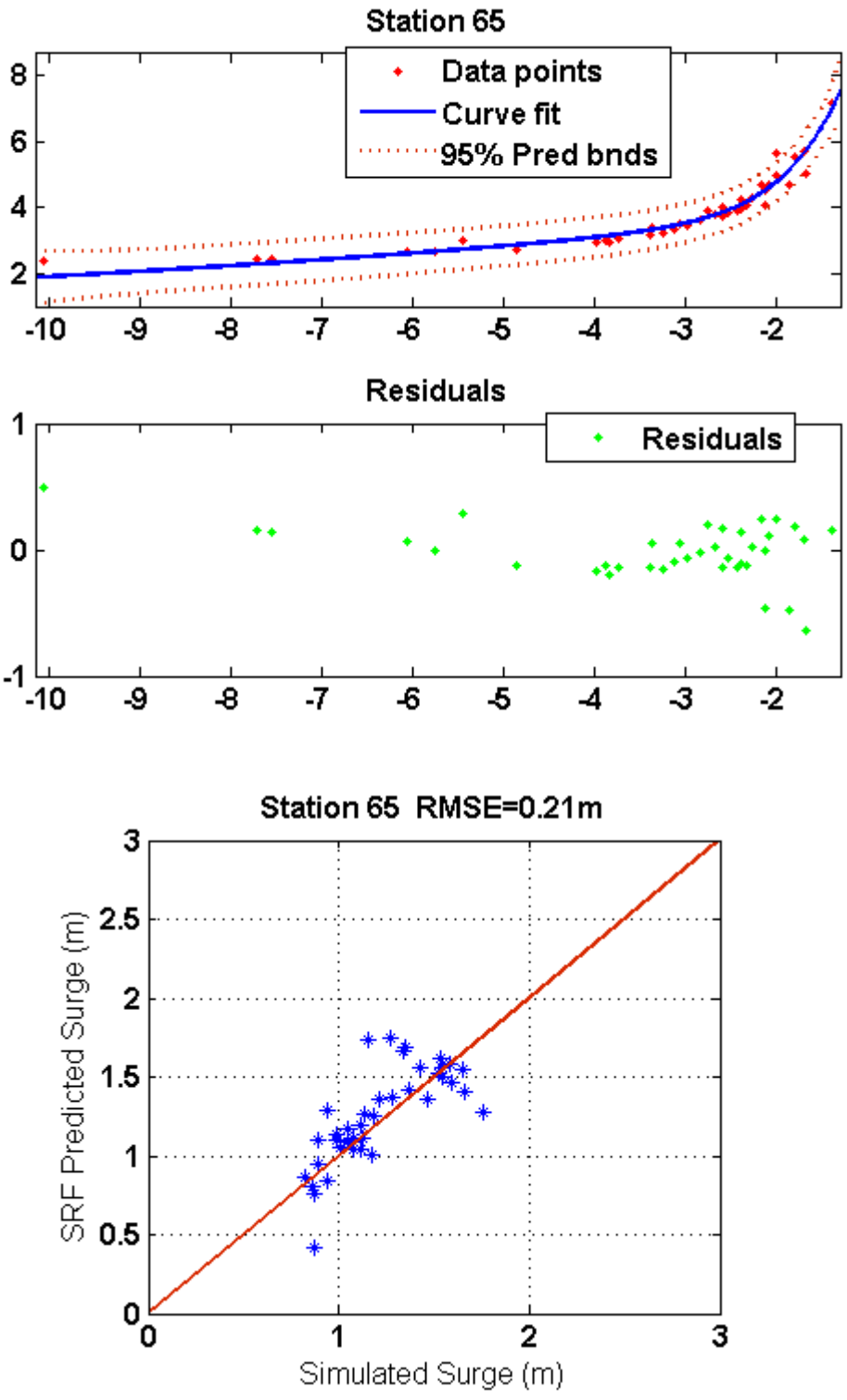

Figure A- 26 SRF at station 65 inside Corpus Christi Bay

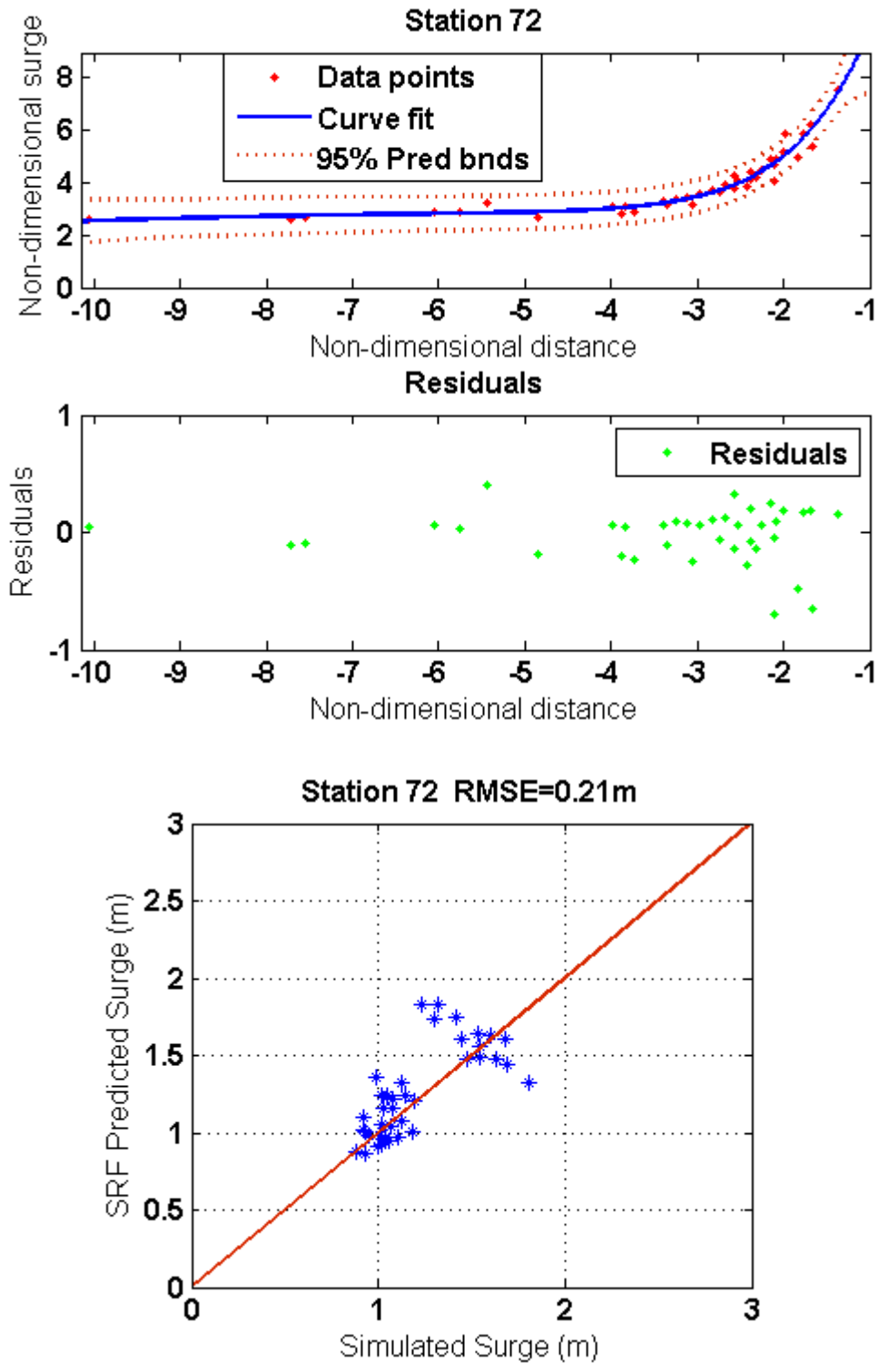

Figure A- 27 SRF at station 72 inside Corpus Christi Bay

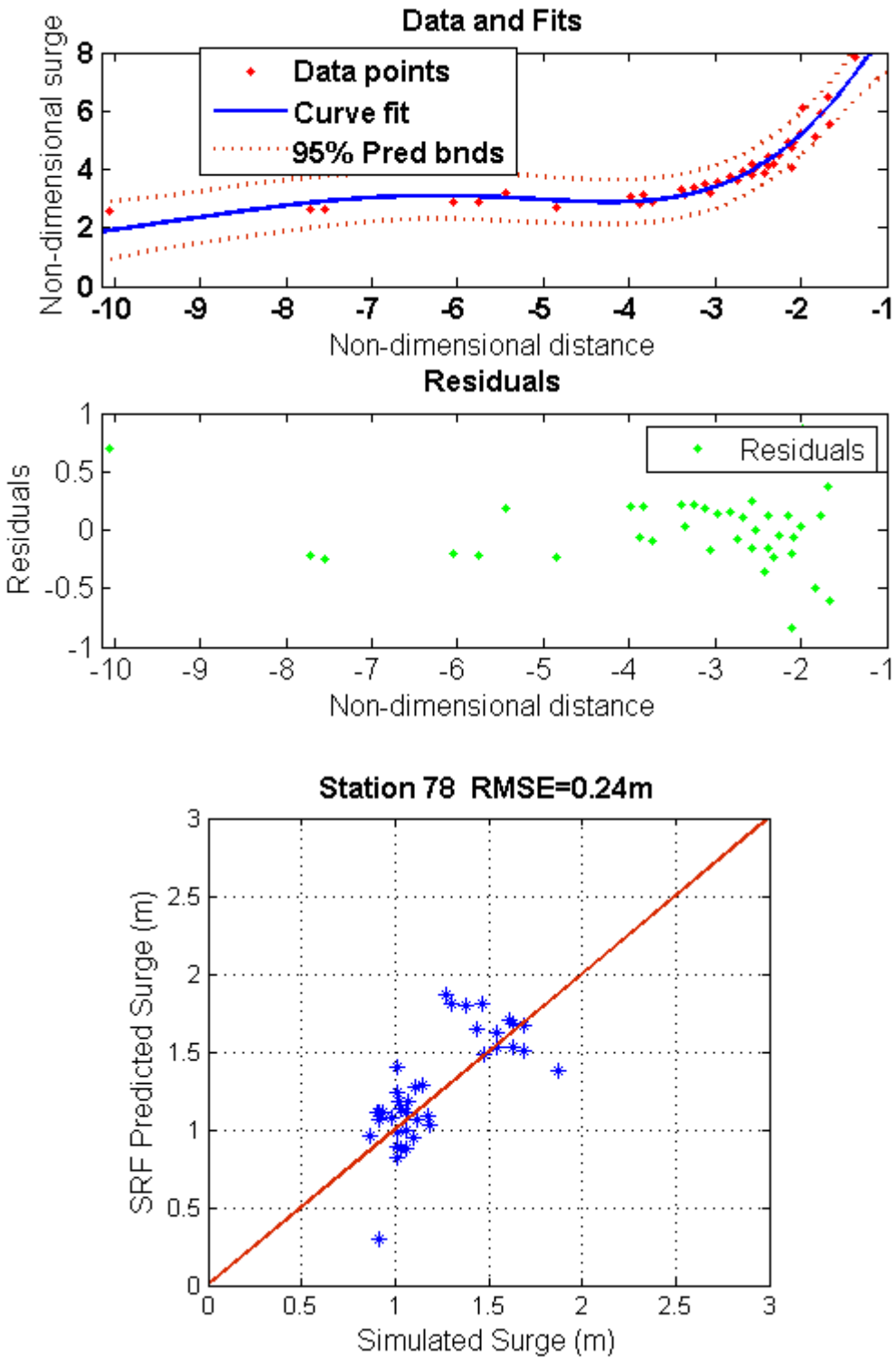

Figure A- 28 SRF at station 78 inside Corpus Christi Bay

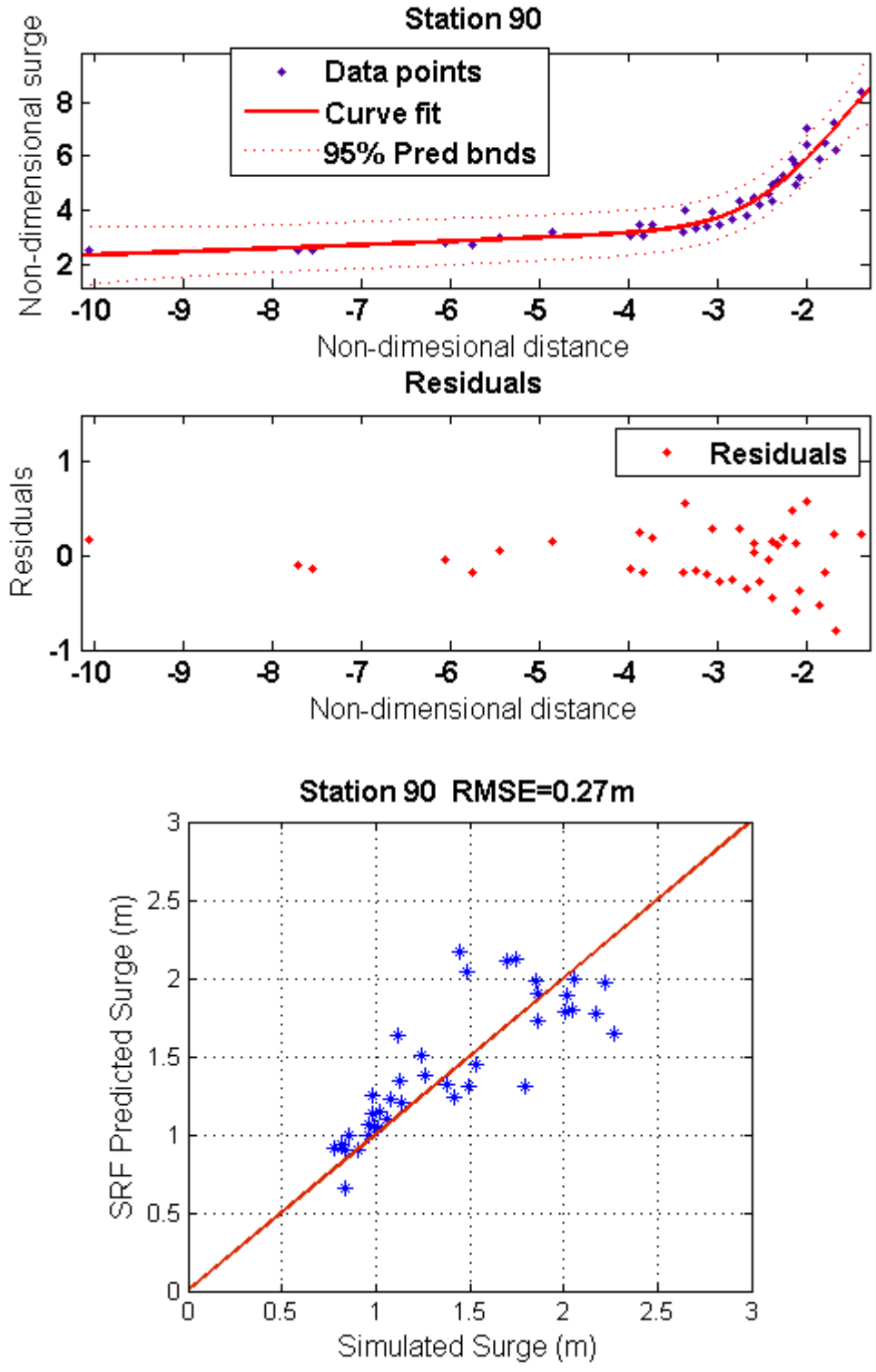

Figure A- 29 SRF at station 90 inside Corpus Christi Bay

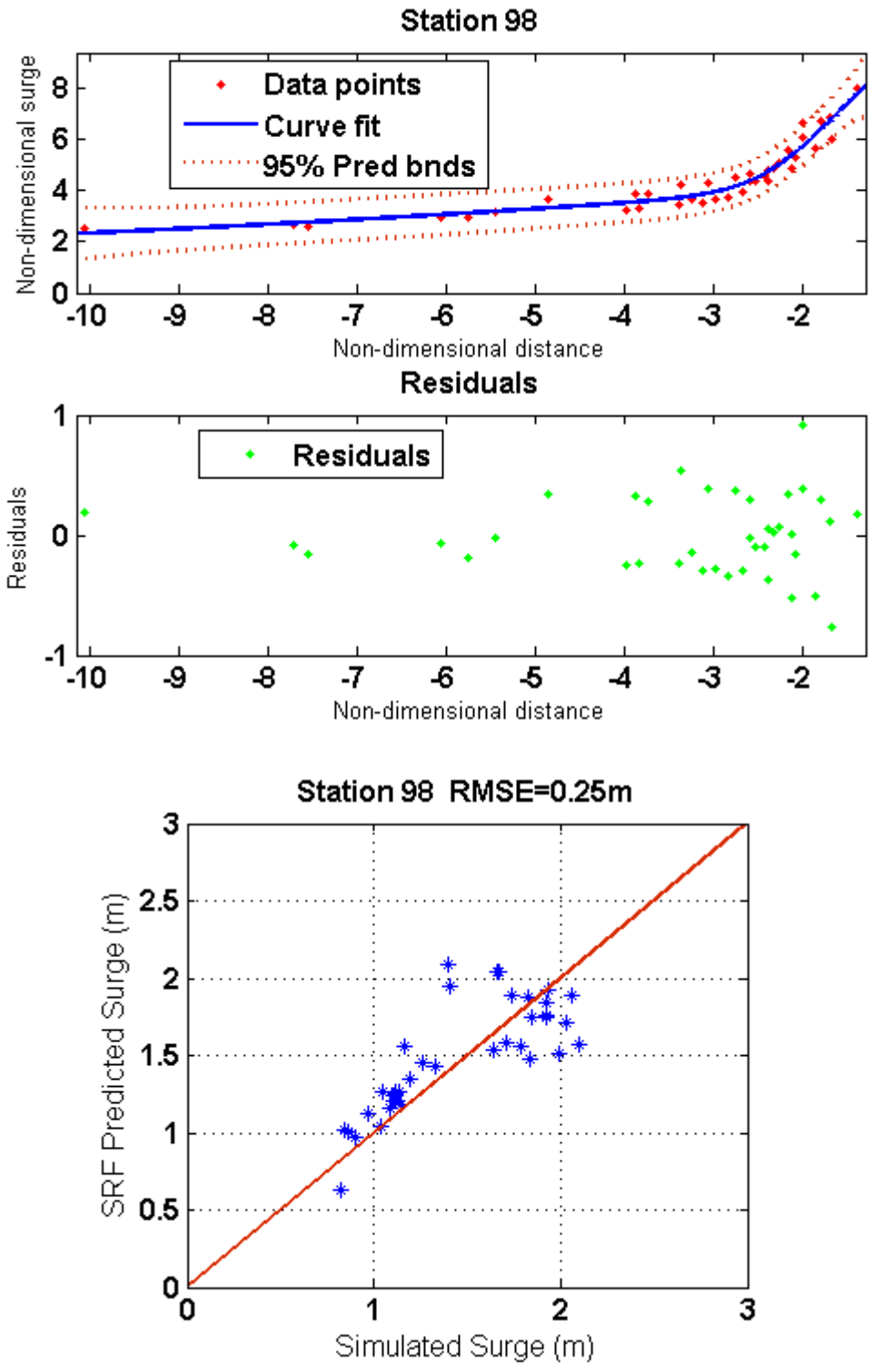

Figure A- 30 SRF at station 98 inside Corpus Christi Bay

VITA

Name: Rajat Katyal

Email Address: rajatkatyal.in@gmail.com

Education: B.E., Civil Engineering, Punjab Engineering College, 2005

M.S., Ocean Engineering, Texas A&M University, 2009

Mailing Address: Department of Ocean Engineering
c/o Dr. Jennifer Irish
Texas A&M University
College Station, TX 77843-3136